SENSORLESS VECTOR CONTROL OF INDUCTION MOTOR BASED ON
FLUX AND SPEED ESTIMATION

A THESIS SUBMITTED TO
THE GRADUATE SCHOOL OF NATURAL AND APPLIED SCIENCES
OF
MIDDLE EAST TECHNICAL UNIVERSITY

BY

BARIŞ TUĞRUL ERTUĞRUL

IN PARTIAL FULFILLMENT OF THE REQUIREMENTS
FOR
THE DEGREE OF MASTER OF SCIENCE
IN
ELECTRICAL AND ELECTRONICS ENGINEERING

DECEMBER 2008

Approval of the thesis:

SENSORLESS VECTOR CONTROL OF INDUCTION MOTOR BASED ON FLUX AND SPEED ESTIMATION

submitted by **BARIŞ TUĞRUL ERTUĞRUL** in partial fulfilment of the requirements for the degree of **Master of Science in Electrical and Electronics Engineering, Middle East Technical University** by,

Prof. Dr. Canan ÖZGEN
Dean, Graduate School of **Natural and Applied Sciences**   _____

Prof. Dr. İsmet ERKMEN
Head of Department, **Electrical and Electronics Engineering**   _____

Prof. Dr. Aydın ERSAK
Supervisor, **Electrical and Electronics Engineering, METU**   _____

Examining Committee Members:

Prof. Dr. Muammer ERMİŞ
Electrical and Electronics Engineering, METU   _____

Prof. Dr. Aydın ERSAK
Electrical and Electronics Engineering, METU   _____

Prof. Dr. Işık ÇADIRCI
Electrical and Electronics Engineering, Hacettepe Univ.   _____

Assist. Prof. Dr. Ahmet M. HAVA
Electrical and Electronics Engineering, METU   _____

Assist. Prof. Dr. M. Timur AYDEMİR
Electrical and Electronics Engineering, Gazi University   _____

Date: 02.12.2008

I hereby declare that all information in this document has been obtained and presented in accordance with academic rules and ethical conduct. I also declare that, as required by these rules and conduct, I have fully cited and referenced all material and results that are not original to this work.

Name, Last name : Barış Tuğrul ERTUĞRUL

Signature :

ABSTRACT

**SENSORLESS VECTOR CONTROL OF INDUCTION MOTOR BASED ON
FLUX AND SPEED ESTIMATION**

ERTUĞRUL, Barış Tuğrul

M. Sc. Department of Electrical and Electronics Engineering

Supervisor: Prof. Dr. Aydın Ersak

December 2008, 148 pages

The main focus of the study is the implementation of techniques regarding flux estimation and rotor speed estimation by the use of sensorless closed-loop observers. Within this framework, the information about the mathematical representation of the induction motor, pulse width modulation technique and flux oriented vector control techniques together with speed adaptive flux estimation –a kind of sensorless closed loop estimation technique- and Kalman filters is given.

With the comparison of sensorless closed-loop speed estimation techniques, it has been attempted to identify their superiority and inferiority to each other by the use of simulation models and real-time experiments. In the experiments, the performance of the techniques developed and used in the thesis has been examined under extensively changing speed and load conditions. The real-time experiments have been carried out by the use of TI TMS320F2812 digital signal processor, XILINX XCS2S150E Field Programmable Gate Array (FPGA), control card and the

motor drive card Furthermore, Matlab "Embedded Target for the TI C2000 DSP" and "Code Composer Studio" software tools have been used.

The simulations and experiments conducted in the study have illustrated that it is possible to increase the performance at low speeds at the expense of increased computational burden on the processor. However, in order to control the motor at zero speed, high frequency signal implementation should be used as well as a different electronic hardware.

ÖZ

HIZ DUYAÇSIZ ENDÜKSİYON MOTORUNUN AKI VE HIZ KESTİRİM YÖNTEMLERİNE DAYALI VEKTÖR DENETİMİ

ERTUĞRUL, Barış Tuğrul

Yüksek Lisans, Elektrik ve Elektronik Mühendisliği Bölümü

Tez Yöneticisi: Prof. Dr. Aydın Ersak

Aralık 2008, 148 sayfa

Bu çalışma ensüksiyon motorlarını esas alan hız kontrollü motor sürücü tasarımını ve uygulamalarını kapsamaktadır. Bu çalışmanın temel olarak yoğunlaştığı alan hız-duyaçsız kapalı döngü gözleyiciler kullanılarak manyetik akı kestirimi ve rotor hızı kestirim tekniklerinin uygulanmasıdır. Bu çerçevede tezde endüksiyon motorunun matematiksel modellenmesi, darbe genliği modülasyonu tekniği ve akı yönlendirmeli vektör kontrol teknikleriyle beraber duyaçsız kapalı döngü kestirim tekniklerinden hız uyarlamalı manyetik akı kestirim metodu ile Kalman filtreler hakkında bilgi verilmiştir.

Duyaçsız kapalı döngü hız kestirim yöntemlerinin birbirlerine göre olan üstünlükleri ile zayıflıkları benzetim modelleri ve gerçek zamanlı deneylerle ortaya konmaya çalışılmıştır. Deneylerde yöntemlerin geniş bir hız bandında ve yük altındaki performansı incelenmiştir.

Gerçek zamanlı deneyler TI TMS320F2812 sayısal işaret işlemcisi, XILINX XCS2S150E alanda programlanabilir kapı dizileri (FPGA) ile birlikte çeşitli analogdan sayısala, sayısaldan analoga çevirimleri sağlayan yongalar ve çevre elemanlardan oluşan kontrol kartı ile birlikte temel olarak güç anahtarlama, işaret arayüz uyumlama, gerilim ve akım ölçme devrelerini içeren motor sürücü kartı vasıtasıyla yapılmıştır. Ayrıca, yazılım arayüzü olarak Matlab "Embedded Target for the TI C2000 DSP" ve "Code Composer Studio" yazılım araçları kullanılmıştır.

Çalışma süresince ortaya konan benzetim ve deneyler göstermiştir ki işlemci yükünü arttırmak suretiyle düşük hızlarda performansı arttırmak mümkün olmaktadır ancak sıfır hızda motor kontrolünü gerçekleştirmek için farklı bir elektronik donanımla birlikte yüksek frekans işaret uygulama yöntemleri kullanılmalıdır.

Anahtar Kelimeler: Endüksiyon makinelerinin hız denetimi, duyaçsız kapalı-döngü alan yönlendirmeli denetim, akı gözleyici, hız gözleyici

ACKNOWLEDGEMENTS

TABLE OF CONTENTS

LIST OF TABLES

LIST OF FIGURES

LIST OF SYMBOLS

SYMBOL

e_{md} Back emf d-axis component

e_{mq} Back emf q-axis component

i^e_{ds} d-axis stator current in synchronous frame

i^e_{qs} q-axis stator current in synchronous frame

i^s_s Stator current in stationary frame

i^s_{ds} d-axis stator current in stationary frame

i^s_{qs} q-axis stator current in stationary frame

i_{ar} Phase-a rotor current

i_{br} Phase-b rotor current

i_{cr} Phase-c rotor current

i_{as} Phase-a stator current

i_{bs} Phase-b stator current

i_{cs} Phase-c stator current

L_m Magnetizing inductance

L_{ls} Stator leakage inductance

L_{lr} Rotor leakage inductance

L_s Stator self inductance

L_r Rotor self inductance

K_k Kalman gain

P_k Kalman filter error covariance matrix

q_{md} Reactive power d-axis component

q_{mq} Reactive power q-axis component

R_s Stator resistance

R_r Referred rotor resistance

T_{em} Electromechanical torque

τ_r Rotor time-constant

V_{as}	Phase-a stator voltage
V_{bs}	Phase-b stator voltage
V_{cs}	Phase-c stator voltage
V_{ar}	Phase-a rotor voltage
V_{br}	Phase-b rotor voltage
V_{cr}	Phase-c rotor voltage
V^s_s	Stator voltage in stationary frame
V^s_{ds}	d-axis stator voltage in stationary frame
V^s_{qs}	q-axis stator voltage in stationary frame
V^e_{ds}	d-axis stator voltage in synchronous frame
V^e_{qs}	q-axis stator voltage in synchronous frame
V_{dc}	DC-link voltage
w_e	Angular synchronous speed
w_r	Angular rotor speed
w_{sl}	Angular slip speed
x_k	Kalman filter a priori state estimate
$\hat{x}_k$	Kalman filter a posteriori state estimate
z_k	Kalman filter measurement
θ_e	Angle between the synchronous frame and the stationary frame
θ_d	Angle between the synchronous frame and the stationary frame when d-axis is leading
θ_q	Angle between the synchronous frame and the stationary frame when q-axis is leading
$\theta_{\psi r}$	Rotor flux angle
ψ^s_s	Stator flux linkage in stationary frame
ψ^s_{ds}	d-axis stator flux linkage in stationary frame
ψ^s_{qs}	q-axis stator flux linkage in stationary frame
ψ^e_{ds}	d-axis stator flux linkage in synchronous frame
ψ^e_{qs}	q-axis stator flux linkage in synchronous frame
ψ_{as}	Phase-a stator flux linkage

ψ_{bs}	Phase-b stator flux linkage
ψ_{cs}	Phase-c stator flux linkage
ψ_{ar}	Phase-a rotor flux linkage
ψ_{br}	Phase-b rotor flux linkage
ψ_{cr}	Phase-c rotor flux linkage
σ	Leakage coefficient

CHAPTER 1

INTRODUCTION

1.1   Induction Machine Drives

Due to non-linear and complex mathematical model of induction motor, it requires more sophisticated control techniques compared to DC motors. The scalar V/f method is able to provide speed control, but this method cannot provide real-time control. In other words, the system response is only satisfactory at steady state and not during transient conditions. Dynamic performance of this type of control methods was unsatisfactory because of saturation effect and the electrical parameter variation with temperature. This results in excessive current and over-heating, which necessitates the drive to be oversized. This over-design no longer makes the motor cost effective due to high cost of the drive circuitry [1].

Recent improvements with reduced loss and fast switching semiconductor power switches on power electronics, fast and powerful digital signal processors on controller technology have made advanced control techniques of induction machine drives feasible and applicable. Thanks to field-oriented control (FOC) schemes [2]-[3] induction motors can be made to operate with properties similar to those of a separately excited DC motors.

1.2   The Field Oriented Control (Vector Control) of Induction Machines

Basically, field oriented control (FOC) is a method based on vector coordinates. The term "vector" refers to the control technique that controls both the amplitude and the phase of AC excitation voltage. Vector control is used for controllers that

maintain 90° spatial orientation between the two field components which are d and q co-ordinates of a time invariant system.

In a field oriented induction motor drive, the field flux and armature mmf are separately created and controlled based on the vector coordinate transformations. These projections lead to a structure similar to that of a DC machine control.

The field oriented control is used in most of the induction motor drive applications in order to obtain high control performance, but it needs motor flux position (rotor flux angle) information and utilizes AC excitation voltages for the current regulation. Current regulation is provided with advanced feedback control methods based on the current measurements taken at the output of excitation voltages supplied from voltage source inverter (VSI). The rotor flux angle can be measured by using shaft sensor and that information is utilized by field orientation scheme. However, as discussed in the current study, sensorless control algorithms eliminate the need for a shaft sensor.

The induction machine drives without the speed sensor are attractive due to low cost and high reliability. Therefore, flux and speed estimations have become particular issues of the field oriented control in the recent years. The main advantages of speed sensorless induction motor drives are lower cost, reduced size of the drive machine, elimination of sensor cable and increased reliability.

As it is stated, for implementing vector control, the determination of the rotor flux position is required. Two basic approaches to determine the rotor flux position angle have evolved. One of them is the direct field orientation which depends on direct measurement or estimation of rotor flux magnitude and angle. From the feasibility point of view, implementation of the direct method is difficult. The other one is the indirect field orientation which makes use of slip relation in computing the angle of the rotor flux relative to rotor axis.

1.3   Induction Machine Flux Observation

The rotor flux position could be estimated from the terminal quantities (stator voltages and currents). This technique requires the knowledge of the stator resistance

along with the stator-leakage, and rotor-leakage inductances and the magnetizing inductance.

The flux observation through direct integration of stator voltage is called Voltage Model Flux Observer (VMFO) which utilizes the measured stator voltage and current. Direct integration brings about errors due to the stator resistance voltage drop and integrator bias. Since the voltage drop on stator resistor at high speeds is less significant compared to stator voltage drop at lower speeds, the error at low speeds dominates. In addition, the leakage inductance can significantly affect the system performance in terms of stability and dynamic response.
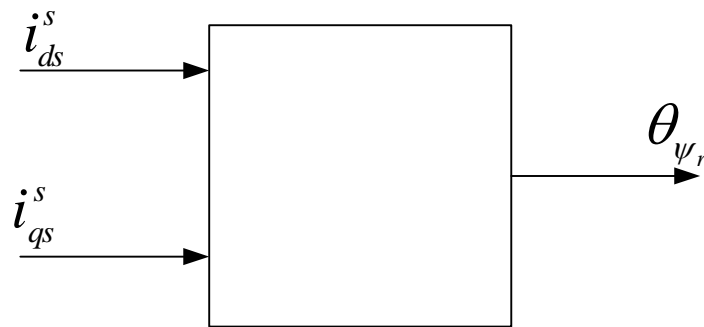
Figure 1-1 Inputs and outputs of the voltage model flux observer (VMFO)

Current Model Flux Observer (CMFO) is introduced as an alternative approach in order to overcome the problems caused by the changes in leakage inductance and stator resistance at low speed. Current model based observers use the measured stator currents and rotor velocity. The velocity dependency of the current model is a drawback since this means that even though using the estimated flux eliminates the flux sensor, position sensor is still required.

$$i_{ds}^s$$

$$i_{qs}^s$$

$$w_r$$

$$\theta_{\psi_r}$$
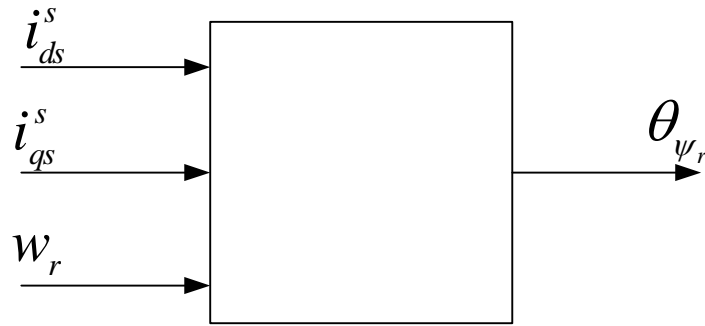
Figure 1-2 Inputs and outputs of the current model flux observer

Several methods are suggested which provide a smooth transition between current and voltage flux observer models. They combine two stator flux models via a first order lag-summing network [4]. The smooth transition between current and voltage models is governed by the rotor flux regulator which makes use of CMFO at low speeds and VMFO at high speed.

The observer structures VMFO and CMFO are open-loop schemes, based on the induction machine model and they do not use any feedback for correcting outputs. Therefore, they are quite sensitive to parameter variations.

Flux estimation through closed-loop state observers is also possible. The robustness against parameter mismatches and signal noise can be improved by employing closed-loop observers for the estimation of state variables. State observer is dependent on induction machine model and machine parameters. Basically, the observed states are rotor flux, stator currents and rotor speed. Full state observers could be utilized by using adaptive estimation techniques which makes estimation accuracy improved.

Speed adaptive flux observer is a closed-loop flux observer which is introduced by Kubota [5]. Adding an error compensator to the model establishes the closed-loop observer. The error between induction motor model current and measured current is used to generate corrective inputs to dynamic subsystem of the stator and the rotor.

The rotor speed is also required for adaptive observer; the rotor speed is obtained through a PI controller, primarily from the current error.
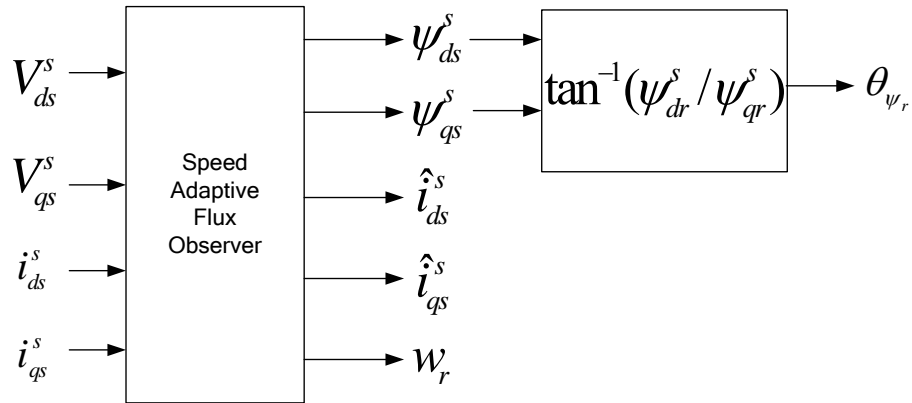
Figure 1-3 Inputs and outputs of the speed adaptive flux observer

Closed-loop Kalman filtering techniques can be based on the complete machine model. The rotor speed is considered as a state variable and induction motor model becomes non-linear, so the extended Kalman filter must be applied. The corrective inputs to the dynamic subsystems of the stator, rotor and mechanical model are derived so that the error function is minimized. The error function is evaluated on the basis of the predicted state variables, taking the noise in the measured signals and parameter deviations into account. The statistical approach reduces the error sensitivity of the observer.

1.4   Sensorless Vector Control of Induction Machine

To implement vector control, determination of the rotor flux position is required. Rotor speed or position could be measured by a shaft sensor. Moreover, rotor flux position could be taken by sensing the air-gap flux with the flux sensing coils.

The main drawbacks of using speed/position sensor are high cost, lower system reliability and special attention to noise. Such problems make sensorless drives popular. The recent trend in field-oriented control is towards avoiding the use of speed sensors and using algorithms based on the terminal quantities of the machine for the estimation of the fluxes. Different solutions for sensorless drives have been proposed in the past few years.

Saliency based fundamental or high frequency signal injection is one of the flux and speed estimation techniques. A method involving modulation of the rotor slots [6] results in a salient rotor, and the saliency can be tracked by imposing a balanced, three-phase, high-frequency set of harmonics from the inverter. An alternative method is to use saliency caused by magnetic saturation [7]. A closely related method is presented in [8]. The main benefit of the methods in [6], [7] and [8] is that the absolute rotor position can be detected. The advantage of the saliency technique is that the saliency is not sensitive to actual motor parameters. The methods in [6], [7] and [8] work also at zero rotor speed. However, extra hardware is required and high frequency signal injection may cause torque ripples, vibration and audible noise [9].

The rotor speed can be estimated through nonlinear observers, e.g. [10]-[18]. Alternatively, the rotor speed can be considered as a parameter and estimated using recursive identification, e.g. [19], [20] and [5]. The latter method can also be augmented to include machine parameter estimation (inductances, resistances, and time constants). These methods do not need to rely on harmonics or saliency, and the hardware requirements are the same as for the digital implementation of vector control, given that the estimation algorithm is not too complex. Their drawback is that the rotor speed estimate will be inaccurate if the non-estimated machine parameters are not known.

1.5   Structure of the Chapters

Chapter 2 includes mathematical model of induction machine in terms of reference frames notation. Field oriented control (FOC), space vector pulse width modulation technique are also introduced at chapter 2.

Chapter 3 covers observers for sensorless field oriented control of induction motor.

Chapter 4 includes implementation of techniques regarding magnetic flux estimation and rotor speed estimation by the use of sensorless closed loop observers. Such that adaptive magnetic flux estimators –a kind of sensorless closed loop estimation technique- and Kalman filters.

Chapter 5 concludes the overall thesis work of the closed speed loop vector controlled induction motor.

CHAPTER 2

INDUCTION MACHINE MODELING, FIELD ORIENTED

CONTROL and PWM with SPACE VECTOR THEORY

2.1   System Equations in the Stationary a,b,c Reference Frame

The induction machine has two electrically active elements: a rotor and a stator shown in Figure 2-1. In normal operation, the stator is excited by alternating voltage. The stator excitation creates a magnetic field in the form of a rotating, or traveling wave, which induces currents in the circuits of the rotor. Those currents, in turn, interact with the traveling wave to produce torque. To start the analysis of induction machine, assume that both the rotor and the stator can be described by the balanced three phase windings. The two sets are, of course, coupled by mutual inductances which are dependent on rotor position.

It is assumed that the winding configuration is as in the Figure 2-2. Stator windings are indicated as a_s, b_s and c_s. The as, b_s and c_s are supposed to have the same number of effective turns, N_s. The b_s and c_s are symmetrically displaced from the a_s by $\pm 120^o$. The subscript 's' is used to denote that these windings are stator or stationary windings. The rotor windings are similarly arranged but have N_r turns. These windings are designated by a_r, b_r and c_r in which second subscript reminds us that these three windings are rotor or rotating windings. [21]
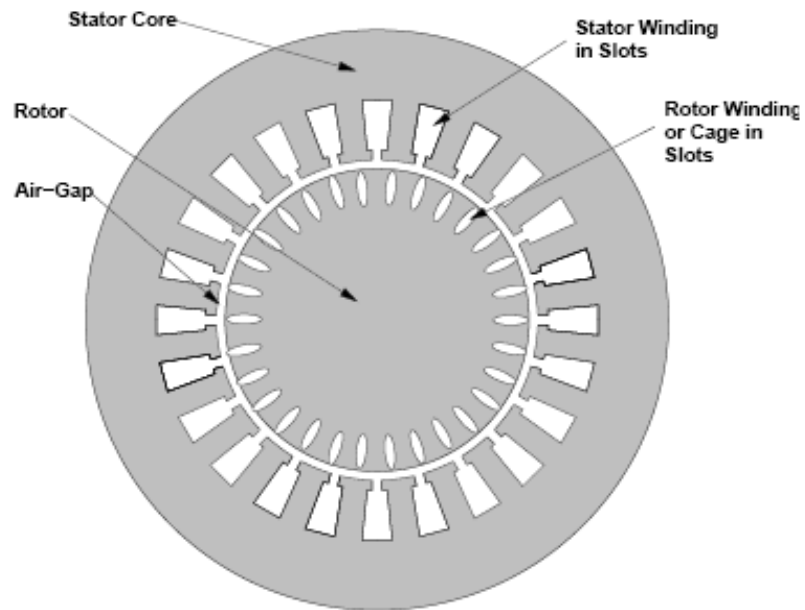
Figure 2-1 Axial view of an induction machine
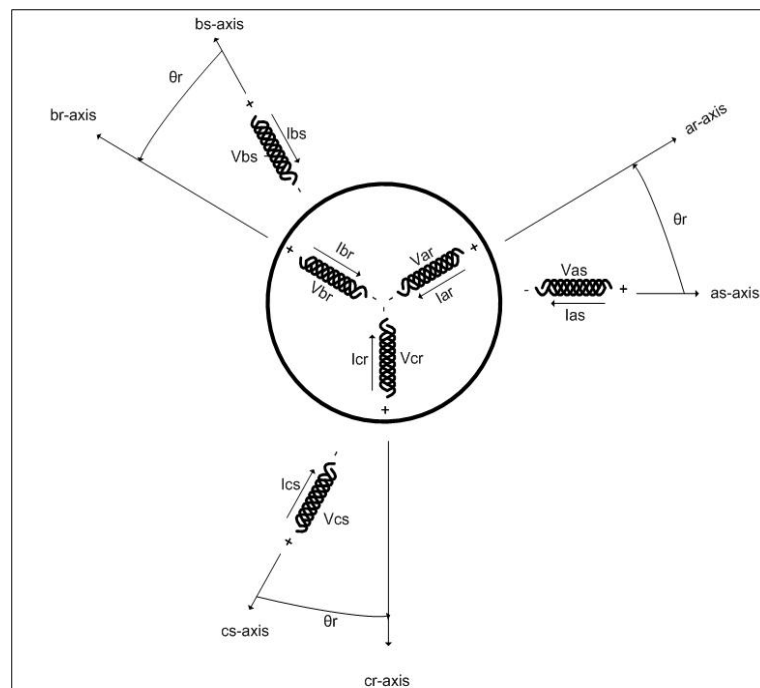
Figure 2-2 Magnetic axes of three phase induction machine

The voltage equations (2-1) - (2-8) describing the stator and rotor circuits are well known and widely referred equations in the literature [21]. Phase voltage equations can be represented in matrix form.

$$v_{abcs} = r_s i_{abcs} + \frac{d\psi_{abcs}}{dt}$$

$$v_{abcr} = r_r i_{abcr} + \frac{d\psi_{abcr}}{dt} \tag{2-1}$$

v_{abcs}, i_{abcs} and ψ_{abcs} are 3x1 column vectors defined by

$$v_{abcs} = \begin{bmatrix} v_{as} \\ v_{bs} \\ v_{cs} \end{bmatrix}; \quad i_{abcs} = \begin{bmatrix} i_{as} \\ i_{bs} \\ i_{cs} \end{bmatrix}; \quad \psi_{abcs} = \begin{bmatrix} \psi_{as} \\ \psi_{bs} \\ \psi_{cs} \end{bmatrix} \tag{2-2}$$

Similar definitions apply for the rotor variables v_{abcr}, i_{abcr} and ψ_{abcr}.

$$v_{abcr} = \begin{bmatrix} v_{ar} \\ v_{br} \\ v_{cr} \end{bmatrix}; \quad i_{abcr} = \begin{bmatrix} i_{ar} \\ i_{br} \\ i_{cr} \end{bmatrix}; \quad \psi_{abcs} = \begin{bmatrix} \psi_{ar} \\ \psi_{br} \\ \psi_{cr} \end{bmatrix} \tag{2-3}$$

Coupling between stator and rotor phases are given in matrix forms as follows. The flux linkages are, therefore, related to the machine currents.

$$\psi_{abcs} = \psi_{abcs(s)} + \psi_{abcs(r)}$$

$$\psi_{abcr} = \psi_{abcr(s)} + \psi_{abcr(r)} \tag{2-4}$$

where

$$\psi_{abcs(s)} = \begin{bmatrix} L_{as} & L_{abs} & L_{acs} \\ L_{abs} & L_{bs} & L_{bcs} \\ L_{acs} & L_{bcs} & L_{cs} \end{bmatrix} i_{abcs} \tag{2-5}$$

$$\psi_{abcs(r)} = \begin{bmatrix} L_{as,ar} & L_{as,br} & L_{as,cr} \\ L_{bs,ar} & L_{bs,br} & L_{bs,cr} \\ L_{cs,ar} & L_{cs,br} & L_{cs,cr} \end{bmatrix} i_{abcr} \qquad (2\text{-}6)$$

$$\psi_{abcr(r)} = \begin{bmatrix} L_{ar} & L_{abr} & L_{acr} \\ L_{abr} & L_{br} & L_{bcr} \\ L_{acr} & L_{bcr} & L_{cr} \end{bmatrix} i_{abcr} \qquad (2\text{-}7)$$

$$\psi_{abcr(s)} = \begin{bmatrix} L_{ar,as} & L_{ar,bs} & L_{ar,cs} \\ L_{br,as} & L_{br,bs} & L_{br,cs} \\ L_{cr,as} & L_{cr,bs} & L_{cr,cs} \end{bmatrix} i_{abcs} \qquad (2\text{-}8)$$

Note that as a result of reciprocity, the inductance matrix in (2-7), is simply the transpose of the inductance matrix of (2-6), because mutual inductances are equal. (i.e., $L_{as,br} = L_{br,as}$)

2.1.1. Determination of Induction Machine Inductances [21]

The mutual inductance between a winding x and a winding y is determined by:

$$L_{xy} = \mu_0 N_x N_y \left(\frac{rl}{g} \right) \left(\frac{\pi}{4} \right) \cos \alpha \qquad (2\text{-}9)$$

where r is the radius, l is the length of the axial length of stator and g is the length of airgap. N_x is the number of effective turns of the winding x and N_y is the number of effective turns of the winding y. Finally, let α be the angle between magnetic axes of the phases x and y.

The self inductance of stator phase as winding is obtained by simply setting $\alpha=0$, and by setting both N_x and N_y in (2-9) to N_s as

$$L_{am} = \mu_0 N_s^2 \left(\frac{rl}{g} \right) \left(\frac{\pi}{4} \right) \qquad (2\text{-}10)$$

The subscript m is used to denote the fact that this inductance is magnetizing inductance. That is, it is associated with flux lines which cross the air gap and link rotor as well as stator windings. In general, it is necessary to add a relatively smaller, but more important leakage term to (2-10) to account for leakage flux. This term accounts for flux lines which do not cross the gap but instead close to the stator slot itself (slot leakage) in the air gap (belt and harmonic leakage) and at the ends of the machine (end winding leakage). Hence, the total self inductance of phase as can be expressed.

$$L_{as} = L_{ls} + L_{am} \tag{2-11}$$

where L_{ls} represents the leakage term. Since the windings of the bs and the cs phases are identical to phase as, it is clear that the magnetizing inductances of these windings are the same as phase as so that

$$L_{bs} = L_{ls} + L_{bm}$$

$$\tag{2-12}$$

$$L_{cs} = L_{ls} + L_{cm}$$

It is apparent that L_{am}, L_{bm}, L_{cm} are equal making the self inductances also equal. It is, therefore, useful to define stator magnetizing inductance

$$L_{ms} = \mu_0 N_s^2 \left(\frac{rl}{g} \right) \left(\frac{\pi}{4} \right) \tag{2-13}$$

so that

$$L_{as} = L_{bs} = L_{cs} = L_{ls} + L_{ms} \tag{2-14}$$

The mutual inductance between phases as and bs, bs and cs, and cs and as is derived by simply setting $\alpha = 2\pi/3$ and $N_x = N_y = N_s$ in (2-9). The result is

$$L_{abs} = L_{bcs} = L_{cas} = -\mu_0 N_s^2 \left(\frac{rl}{g}\right)\left(\frac{\pi}{8}\right) \tag{2-15}$$

or, in terms of (2-13),

$$L_{abs} = L_{bcs} = L_{cas} = -\frac{L_{ms}}{2} \tag{2-16}$$

The flux linkages of phases as, bs and cs resulting from currents flowing in the stator windings can be now expressed in matrix form as

$$\psi_{abcs(s)} = \begin{bmatrix} L_{ls} + L_{ms} & -\dfrac{L_{ms}}{2} & -\dfrac{L_{ms}}{2} \\ -\dfrac{L_{ms}}{2} & L_{ls} + L_{ms} & -\dfrac{L_{ms}}{2} \\ -\dfrac{L_{ms}}{2} & -\dfrac{L_{ms}}{2} & L_{ls} + L_{ms} \end{bmatrix} i_{abcs} \tag{2-17}$$

Let us now turn our attention to the mutual coupling between the stator and rotor windings. Referring to Figure 2-2, we can see that the rotor phase a_r is displaced by stator phase a_s by the electrical angle θ_r where θ_r in this case is a variable. Similarly, the rotor phases b_r and c_r are displaced from stator phases b_s and c_s by θ_r respectively. Hence, the corresponding mutual inductances can be obtained by setting $N_x = N_s$, $N_y = N_r$, and $\alpha = \theta_r$ in (2-9).

$$\begin{aligned} L_{as,ar} = L_{bs,br} = L_{cs,cr} &= \mu_0 N_s N_r \left(\frac{rl}{g}\right)\left(\frac{\pi}{4}\right)\cos\theta_r \\ &= \frac{N_r}{N_s} L_{ms} \cos\theta_r \end{aligned} \tag{2-18}$$

The angle between the as and br phases is $\theta_r + 2\pi/3$, so that

$$L_{as,br} = L_{bs,cr} = L_{cs,ar} = \frac{N_r}{N_s} L_{ms} \cos(\theta_r + 2\pi/3) \tag{2-19}$$

Finally, the stator phase as is displaced from the rotor cr phase by angle $\theta_r - 2\pi/3$. Therefore,

$$L_{as,cr} = L_{bs,ar} = L_{cs,br} = \frac{N_r}{N_s} L_{ms} \cos(\theta_r - 2\pi/3) \qquad (2\text{-}20)$$

The above inductances can now be used to establish the flux linking the stator phases due to currents in the rotor circuits. In matrix form,

$$\psi_{abcs(r)} = \frac{N_r}{N_s} L_{ms} \begin{bmatrix} \cos\theta_r & \cos(\theta_r + 2\pi/3) & \cos(\theta_r - 2\pi/3) \\ \cos(\theta_r - 2\pi/3) & \cos\theta_r & \cos(\theta_r + 2\pi/3) \\ \cos(\theta_r + 2\pi/3) & \cos(\theta_r - 2\pi/3) & \cos\theta_r \end{bmatrix} i_{abcr} \qquad (2\text{-}21)$$

The total flux linking the stator windings is clearly the sum of the contributions from the stator and the rotor circuits, (2-17) and (2-21),

$$\psi_{abcs} = \psi_{abcs(s)} + \psi_{abcs(r)} \qquad (2\text{-}22)$$

It is not difficult to continue the process to determine the rotor flux linkages. In terms of previously defined quantities, the flux linking the rotor circuit due to rotor currents is

$$\psi_{abcr(r)} = \begin{bmatrix} L_{lr} + \left(\frac{N_r}{N_s}\right)^2 L_{ms} & -\frac{1}{2}\left(\frac{N_r}{N_s}\right)^2 L_{ms} & -\frac{1}{2}\left(\frac{N_r}{N_s}\right)^2 L_{ms} \\ -\frac{1}{2}\left(\frac{N_r}{N_s}\right)^2 L_{ms} & L_{lr} + \left(\frac{N_r}{N_s}\right)^2 L_{ms} & -\frac{1}{2}\left(\frac{N_r}{N_s}\right)^2 L_{ms} \\ -\frac{1}{2}\left(\frac{N_r}{N_s}\right)^2 L_{ms} & -\frac{1}{2}\left(\frac{N_r}{N_s}\right)^2 L_{ms} & L_{lr} + \left(\frac{N_r}{N_s}\right)^2 L_{ms} \end{bmatrix} i_{abcr} \qquad (2\text{-}23)$$

where L_{lr} is the rotor leakage inductance. The flux linking the rotor windings due to currents in the stator circuit is

$$\psi_{abcr(s)} = \frac{N_r}{N_s} L_{ms} \begin{bmatrix} \cos\theta_r & \cos(\theta_r - 2\pi/3) & \cos(\theta_r + 2\pi/3) \\ \cos(\theta_r + 2\pi/3) & \cos\theta_r & \cos(\theta_r - 2\pi/3) \\ \cos(\theta_r - 2\pi/3) & \cos(\theta_r + 2\pi/3) & \cos\theta_r \end{bmatrix} i_{abcs} \quad (2\text{-}24)$$

Note that the matrix of (2-24) is the transpose of (2-21).The total flux linkages of the rotor windings are again the sum of the two components defined by (2-23) and (2-24), that is

$$\psi_{abcr} = \psi_{abcr(r)} + \psi_{abcr(s)} \quad\quad\quad (2\text{-}25)$$

2.1.2.   Three-Phase to Two-Phase Transformations

The performance of three-phase AC machines is described by their voltage equations and flux linkages. Some machine inductances are also functions of rotor position. The coefficients of the differential equations, which describe the behavior of these machines, are time-varying except when the rotor is stalled. A change of variables is often used to reduce the complexity of these differential equations. Using transformations, many properties of electric machines can be studied without complexities in the voltage equations. These transformations make it possible for control algorithms to be implemented on the DSP. For this purpose, the method of symmetrical components uses a complex transformation to decouple the abc phase variables. By this approach, many of the basic concepts and interpretations of this general transformation are concisely established.

2.1.2.1.   The Clarke Transformation [1]

The transformation of stationary circuits to a stationary reference frame was developed by E. Clarke [22]. The stationary two-phase variables of Clarke's transformation are denoted as α and β. As shown in Figure 2-3, α-axis and β-axis are orthogonal.
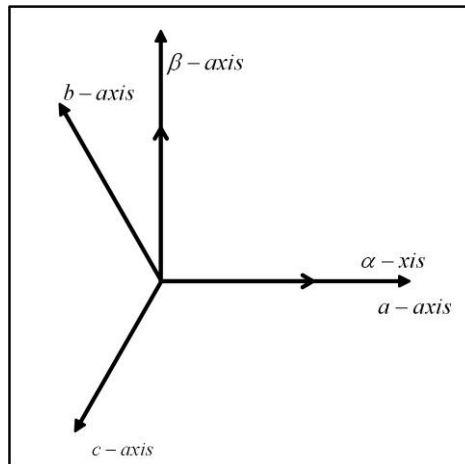
Figure 2-3 Relationship between the α, β and the abc quantities [23]

The symbol f is used to represent any of the three phase stator circuit variables such as voltage, current or flux linkage, variables along a, b and c axes (f_a, f_b and f_c) can be reffered to the stationary two-phase variables α, β and zero sequence (f_α, f_β and f_0) by,

$$[f_{\alpha\beta 0}] = [T_{\alpha\beta 0}][f_{abc}] \tag{2-26}$$

where

$$[f_{\alpha\beta 0}] = [f_\alpha \; f_\beta \; f_0]^T$$

$$[f_{abc}] = [f_a \; f_b \; f_c]^T$$

The transformation matrix is defined as

$$[T_{\alpha\beta0}] = \frac{2}{3}\begin{bmatrix} 1 & -\frac{1}{2} & -\frac{1}{2} \\ 0 & \sqrt{\frac{3}{2}} & -\sqrt{\frac{3}{2}} \\ \frac{1}{2} & \frac{1}{2} & \frac{1}{2} \end{bmatrix} \qquad (2\text{-}27)$$

And inverse transformation matrix is presented by

$$[T_{\alpha\beta0}]^{-1} = \begin{bmatrix} 1 & 0 & 1 \\ -\frac{1}{2} & \sqrt{\frac{3}{2}} & 1 \\ -\frac{1}{2} & -\sqrt{\frac{3}{2}} & 1 \end{bmatrix} \qquad (2\text{-}28)$$

2.1.2.2.   The Park Transformation [1]

In the late 1920s, R.H. Park [24] introduced a new approach to electric machine analysis. He formulated a change of variables which replaced variables such as voltages, currents, and flux linkages associated with fictitious windings rotating with the rotor. He referred the stator and rotor variables to a reference frame fixed on the rotor. From the rotor point of view, all the variables can be observed as constant values. Park's transformation, a revolution in machine analysis, has the unique property of eliminating all time varying inductances from the voltage equations of three-phase ac machines due to the rotor spinning.

Although changes of variables are used in the analysis of AC machines to eliminate time-varying inductances, changes of variables are also employed in the analysis of various static and constant parameters in power system components. Fortunately, all known real transformations for these components are also contained in the transformation to the arbitrary reference frame. The same general transformation used for the stator variables of ac machines serves as the rotor

variables of induction machines. Park's transformation is a well-known three-phase to two-phase transformation in machine analysis.

Park's transformation presented in Figure 2-4 transforms three-phase quantities f_{abc} into two-phase quantities developed on a rotating dq0 axes system, whose speed is w.
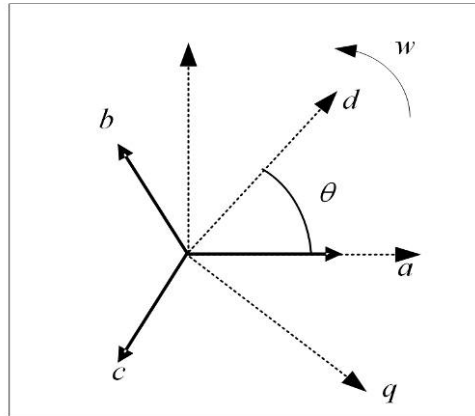
Figure 2-4 Relationship between the dq and the abc quantities [23]

$$[f_{dq0}] = [T_{dq0}(\theta)][f_{abc}] \tag{2-29}$$

where

$$[f_{dq0}] = [f_d \ f_q \ f_0]^T$$

$$[f_{abc}] = [f_a \ f_b \ f_c]^T$$

where the dq0 transformation matrix is defined as:

$$[T_{dq0}(\theta)] = \frac{2}{3} \begin{bmatrix} \cos\theta & \cos\left(\theta - \frac{2\pi}{3}\right) & \cos\left(\theta + \frac{2\pi}{3}\right) \\ -\sin\theta & -\sin\left(\theta - \frac{2\pi}{3}\right) & -\sin\left(\theta + \frac{2\pi}{3}\right) \\ \frac{1}{2} & \frac{1}{2} & \frac{1}{2} \end{bmatrix} \qquad (2\text{-}30)$$

and the inverse is given by:

$$[T_{dq0}(\theta)]^{-1} = \begin{bmatrix} \cos\theta & -\sin\theta & 1 \\ \cos\left(\theta - \frac{2\pi}{3}\right) & -\sin\left(\theta - \frac{2\pi}{3}\right) & 1 \\ \cos\left(\theta + \frac{2\pi}{3}\right) & -\sin\left(\theta + \frac{2\pi}{3}\right) & 1 \end{bmatrix} \qquad (2\text{-}31)$$

where θ is the angle between the phase a- axis and d - axis. and can be calculated by

$$\theta = \int_0^t w(\tau)d\tau + \theta(0) \qquad (2\text{-}32)$$

where τ is the dummy variable of integration.

2.2 Reference Frames

2.2.1. Induction Motor Model in the Arbitrary dq0 Reference Frame

The coupling between the stator and rotor circuits can be eliminated if the stator and the rotor equations are referred to a common frame of reference. The reference frames are usually selected on the basis of conveniences or computational reduction. A common frame of reference can be non-rotating (i.e. w = 0) which it is associated with the stator and it is, therefore, called as the stator or stationary reference frame

19

with a frame notation $d^s q^s$. Alternatively, dq0 axes (i.e. the common frame) can be taken to rotate with the same angular velocity (i.e. $w = w_s$, synchronous speed), as the rotor circuits, and is termed as the rotor reference frame with a frame notation $d^e q^e$. It may even be useful to select these axes synchronously rotating at w with one of the complex vectors denoting stator or rotor voltage, current or even flux as arbitrary reference frame. Each reference frame has appealing advantages. For example, stationary reference frame, the $d^s q^s$ variables of the machine are in the same frame as those normally used for the supply network. Furthermore, at the synchronously rotating frame, the $d^e q^e$ variables are DC in steady state.

Once the equations of the induction machine are derived in the arbitrary reference frame, which is rotating at a speed w, in the direction of the rotor rotation, the transformation between reference frames could be obtained easily. When the induction machine runs in the stationary frame, these equations of the induction machine can then be achieved by setting $w = 0$. These equations can also be obtained in the synchronously rotating frame by setting $w = w_e$.

In matrix notation, the stator winding abc voltage equations can be expressed as:

$$v_{abcs} = r_s i_{abcs} + \frac{d\psi_{abcs}}{dt} \tag{2-33}$$

Applying transformation to the stator windings abc voltages, the stator winding qd0 voltages in arbitrary reference frame are obtained.

$$v_{dq0s} = w \begin{bmatrix} 0 & 1 & 0 \\ -1 & 0 & 0 \\ 0 & 0 & 0 \end{bmatrix} \psi_{dq0s} + \frac{d\psi_{dq0s}}{dt} + r_{dq0s} i_{dq0s} \tag{2-34}$$

where

$$w = \frac{d\theta}{dt} \quad and \quad r_{dq0s} = r_s \begin{bmatrix} 1 & 0 & 0 \\ 0 & 1 & 0 \\ 0 & 0 & 1 \end{bmatrix} \tag{2-35}$$

Likewise, the rotor voltage equation becomes:

$$v_{dq0r} = (w - w_r) \begin{bmatrix} 0 & 1 & 0 \\ -1 & 0 & 0 \\ 0 & 0 & 0 \end{bmatrix} \psi_{dq0r} + \frac{d\psi_{dq0r}}{dt} + r_{dq0r} i_{dq0r} \tag{2-36}$$

Stator and rotor flux linkage equations are given as;

$$\begin{bmatrix} \psi_{qs} \\ \psi_{ds} \\ \psi_{0s} \\ \psi'_{qr} \\ \psi'_{dr} \\ \psi'_{0r} \end{bmatrix} = \begin{bmatrix} L_s & 0 & 0 & L_m & 0 & 0 \\ 0 & L_s & 0 & 0 & L_m & 0 \\ 0 & 0 & L_{ls} & 0 & 0 & 0 \\ L_m & 0 & 0 & L'_r & 0 & 0 \\ 0 & L_m & 0 & 0 & L'_r & 0 \\ 0 & 0 & 0 & 0 & 0 & L'_{lr} \end{bmatrix} \begin{bmatrix} i_{qs} \\ i_{ds} \\ i_{0s} \\ i'_{qr} \\ i'_{dr} \\ i'_{0r} \end{bmatrix} \tag{2-37}$$

where primed quantities denote referred values to the stator side.

$$L_s = L_{ls} + L_m$$
$$\tag{2-38}$$
$$L'_r = L'_{lr} + L_m$$

And

$$L_m = \frac{3}{2} L_{ms} = \frac{3}{2} N_s^2 \left(\mu_0 \frac{rl}{g} \right) \frac{\pi}{4} \quad , L'_{lr} = (\frac{N_s}{N_r})^2 L_{lr} \tag{2-39}$$

Electromagnetic torque, T_{em} equation is given as,

$$T_{em} = \frac{3}{2} \frac{p}{2w_r} \left[w(\psi_{ds} i_{qs} - \psi_{qs} i_{ds}) + (w - w_r)(\psi'_{dr} i'_{qr} - \psi'_{qr} i'_{dr}) \right] \quad Nm \tag{2-40}$$

Using the flux linkage relationships from (2.37), (2-40) can be simplified as,

$$T_{em} = \frac{3}{2}\frac{p}{2}(\psi'_{qr}i'_{dr} - \psi'_{dr}i'_{qr}) \quad Nm$$

$$= \frac{3}{2}\frac{p}{2}(\psi_{ds}i_{qs} - \psi_{qs}i_{ds}) \quad Nm \tag{2-41}$$

$$= \frac{3}{2}\frac{p}{2}L_m(i'_{dr}i_{qs} - i'_{qr}i_{ds}) \quad Nm$$

2.2.2. Induction Motor Model in dq0 Stationary and Synchronous Reference Frames

Once the induction motor model in the arbitrary dq0 reference frame is established, dq0 stationary (denoted as $d^s q^s$) and synchronous (denoted as $d^e q^e$) reference frame equations can be derived. To distinguish these two frames from each other, an additional superscript will be used, s for stationary frame variables and e for synchronously rotating frame variables.

i. dq0 stationary frame induction motor equations are given as (2-42) - (2-45).

Stator $q^s d^s$ voltage equations:

$$v^s{}_{qs} = \frac{d\psi^s{}_{qs}}{dt} + r_s i^s{}_{qs}$$

$$\tag{2-42}$$

$$v^s{}_{ds} = \frac{d\psi^s{}_{ds}}{dt} + r_s i^s{}_{ds}$$

Rotor $q^s d^s$ voltage equations:

$$v'^s_{qr} = \frac{d\psi'^s_{qr}}{dt} + (-w_r)\psi'^s_{dr} + r'_r i'^s_{qr}$$

<div align="right">(2-43)</div>

$$v'^s_{dr} = \frac{d\psi'^s_{dr}}{dt} + (w_r)\psi'^s_{qr} + r'_r i'^s_{dr}$$

where

$$
\begin{bmatrix} \psi^s_{qs} \\ \psi^s_{ds} \\ \psi'^s_{qr} \\ \psi'^s_{dr} \end{bmatrix} = \begin{bmatrix} L_s & 0 & L_m & 0 \\ 0 & L_s & 0 & L_m \\ L_m & 0 & L'_r & 0 \\ 0 & L_m & 0 & L'_r \end{bmatrix} \begin{bmatrix} i^s_{qs} \\ i^s_{ds} \\ i'^s_{qr} \\ i'^s_{dr} \end{bmatrix}
$$

<div align="right">(2-44)</div>

Torque Equations:

$$T_{em} = \frac{3}{2}\frac{p}{2}(\psi'^s_{qr}i'^s_{dr} - \psi'^s_{dr}i'^s_{qr})\ Nm$$

$$= \frac{3}{2}\frac{p}{2}(\psi^s_{ds}i^s_{qs} - \psi^s_{qs}i^s_{ds})\quad Nm$$

<div align="right">(2-45)</div>

$$= \frac{3}{2}\frac{p}{2}L_m(i'^s_{dr}i^s_{qs} - i'^s_{qr}i^s_{ds})\ Nm$$

ii. dq0 synchronous frame induction motor equations are given as (2-46) - (2-49).
Stator $q^e d^e$ voltage equations:

$$v^e_{qs} = \frac{d\psi^e_{qs}}{dt} + w_e \psi^e_{ds} + r_s i^e_{qs}$$

$$(2\text{-}46)$$

$$v^e_{ds} = \frac{d\psi^e_{ds}}{dt} - w_e \psi^e_{qs} + r_s i^e_{ds}$$

Rotor $q^e d^e$ voltage equations:

$$v'^e_{qr} = \frac{d\psi'^e_{qr}}{dt} + (w_e - w_r)\psi'^e_{dr} + r'_r i'^e_{qr}$$

$$(2\text{-}47)$$

$$v'^e_{dr} = \frac{d\psi'^e_{dr}}{dt} - (w_e - w_r)\psi'^e_{qr} + r'_r i'^e_{dr}$$

where

$$\begin{bmatrix} \psi^e_{qs} \\ \psi^e_{ds} \\ \psi'^e_{qr} \\ \psi'^e_{dr} \end{bmatrix} = \begin{bmatrix} L_s & 0 & L_m & 0 \\ 0 & L_s & 0 & L_m \\ L_m & 0 & L'_r & 0 \\ 0 & L_m & 0 & L'_r \end{bmatrix} \begin{bmatrix} i^e_{qs} \\ i^e_{ds} \\ i'^e_{qr} \\ i'^e_{dr} \end{bmatrix}$$

$$(2\text{-}48)$$

Torque Equations:

$$T_{em} = \frac{3}{2}\frac{p}{2}(\psi'^e_{qr} i'^e_{dr} - \psi'^e_{dr} i'^e_{qr}) \qquad Nm$$

$$(2\text{-}49)$$

$$= \frac{3}{2}\frac{p}{2}(\psi^e_{ds} i^e_{qs} - \psi^e_{qs} i^e_{ds}) \qquad Nm$$

2.3 Field Oriented Control (FOC)

Following the concepts outlined for the DC machine, the requirements are for torque and flux control which has to be also satisfied for ac machines in order to implement successful field orientation control [21]. They can be basically stated as:

• Independent control of the armature current to overcome the effects of armature winding resistance, leakage inductance and induced voltage.

• Independent control of flux at a constant value.

• Independent control of orthogonality between the flux and magnetomotive force (MMF) axes to avoid interaction of MMF and flux.

If all of these three requirements are met at all times, the torque will follow the current, which will allow an instantaneous torque control and decoupled flux and torque regulation.

In the DC machine, first and second requirements are assured by the presence of the commutator and the separate field excitation system. In AC machines, these two requirements are achieved by external controls.

Next, a two phase dq model of an induction machine rotating at the synchronous speed is introduced which will help to carry out this decoupled control concept to the induction machine. This model can be summarized by the following equations:

$$v^e_{ds} = \frac{d\psi^e_{ds}}{dt} - w_e\psi^e_{qs} + r_s i^e_{ds} \qquad (2\text{-}50)$$

$$v^e_{qs} = \frac{d\psi^e_{qs}}{dt} + w_e\psi^e_{ds} + r_s i^e_{qs} \qquad (2\text{-}51)$$

$$0 = \frac{d\psi^e_{qr}}{dt} + (w_e - w_r)\psi^e_{dr} + r_r i^e_{qr} \qquad (2\text{-}52)$$

$$0 = \frac{d\psi^e_{dr}}{dt} - (w_e - w_r)\psi^e_{qr} + r_r i^e_{dr} \qquad (2\text{-}53)$$

$$\psi^e_{qs} = L_s i^e_{qs} + L_m i'^e_{qr} \tag{2-54}$$

$$\psi^e_{ds} = L_s i^e_{ds} + L_m i'^e_{dr} \tag{2-55}$$

$$\psi'^e_{qr} = L_m i^e_{qs} + L'_r i'^e_{qr} \tag{2-56}$$

$$\psi'^e_{dr} = L_m i^e_{ds} + L'_r i'^e_{dr} \tag{2-57}$$

$$T_{em} = \frac{3p}{2}\frac{L_m}{L_r}\left(\psi'^e_{dr} i^e_{qs} - \psi'^e_{qr} i^e_{ds}\right) \tag{2-58}$$

$$T_{em} = J\frac{dw_r}{dt} + Bw_r + T_L \tag{2-59}$$

In this model, it can be seen from the torque expression (2-58) that if the rotor flux along the q-axis is zero, then all the flux is aligned along the d-axis and therefore, the torque can be instantaneously controlled by controlling the current along q-axis. The q^e-axis is set perpendicular to the d^e-axis. The flux along the q^e-axis in that case will obviously be zero. The phasor diagram Figure 2-7 shows these axes. The angle θ_e keeps changing as the machine input currents change. The angle θ_e accurately known, d-axis of the $d^e q^e$ frame can be locked to the flux vector. The Park and the Clarke transformations at the machine side is represented in Figure 2-5.
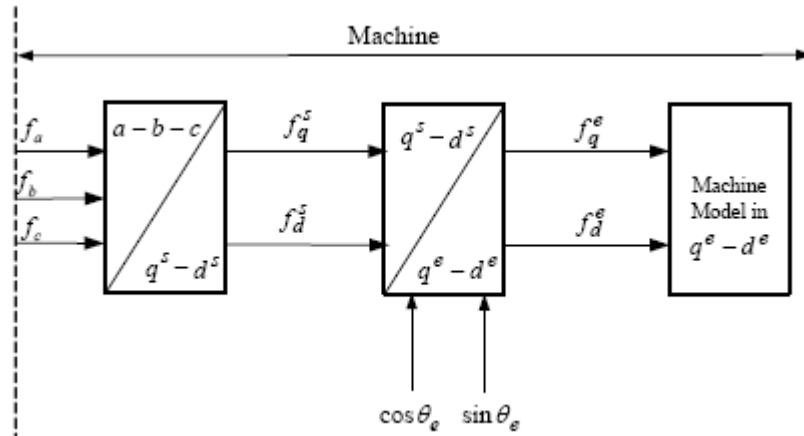
Figure 2-5 The Park and the Clarke transformations at the machine side [1]

The control inputs at field oriented control can be specified in terms of two-phase synchronous frame i^e_{ds} and i^e_{qs} variables. i^e_{ds} is aligned along the d^e-axis i.e. the flux vector, so does i^e_{qs} with the q^e-axis. These two-phase synchronous control inputs are first converted into two-phase stationary ones and then to three-phase stationary control inputs. This can be achieved by taking the inverse transformation of variables from the arbitrary rotating reference frame to the stationary reference frame and then to the abc system. To accomplish this, the flux angle θ_e must be known precisely. The block diagram of this procedure is shown in Figure 2-6. In this block diagram, * is a representation of commanded or desired values of variables.

The angle θ_e can be found either by Indirect Field Oriented Control (IFOC) or by Direct Field Oriented Control (DFOC). The controller implemented in this fashion that can achieve a decoupled control of the flux and the torque is known as field oriented controller. The block diagram is as in Figure 2-10.
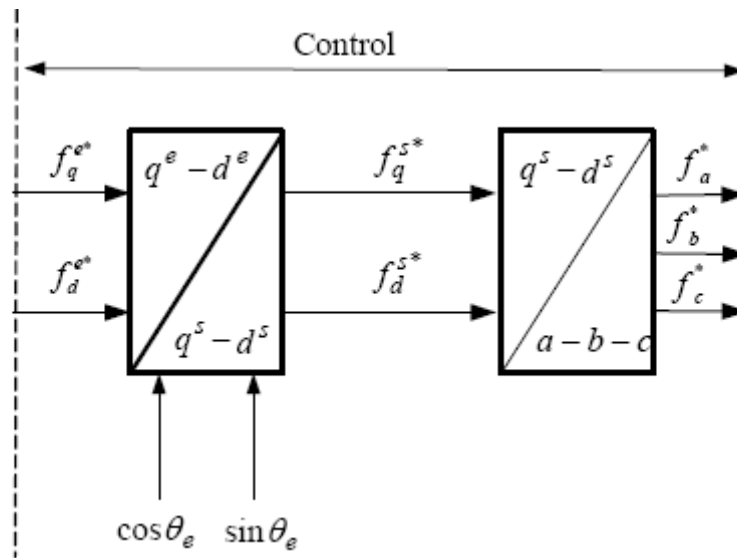
Figure 2-6 Variable transformation in the field oriented control [1]

The absence of the field angle sensors, along with the ease of operation at low speeds, has increased the popularity of the indirect vector control strategy. While the direct method is inherently the most desirable scheme, it suffers from the unreliability in measuring the flux. Although the indirect method can approach the performance of the direct measurement scheme, its major weakness is the accuracy of the control gain, which heavily depends on the motor parameters. The block diagrams of indirect field oriented control and direct field oriented control are illustrated at Figure 2-8 and Figure 2-9 respectively.
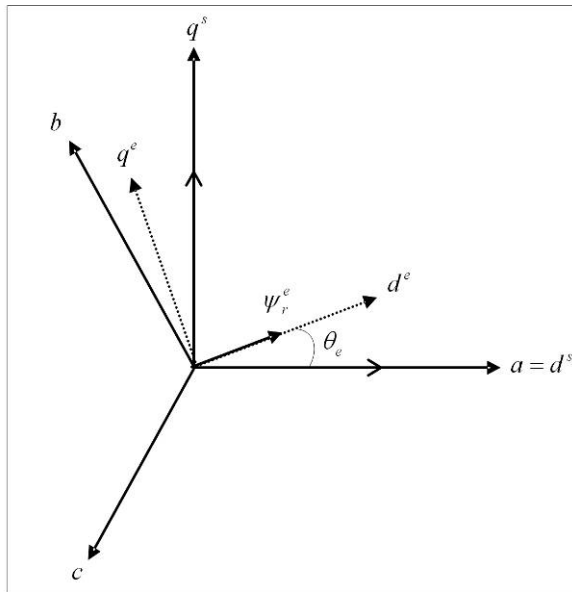
Figure 2-7 Phasor diagram of the field oriented drive system
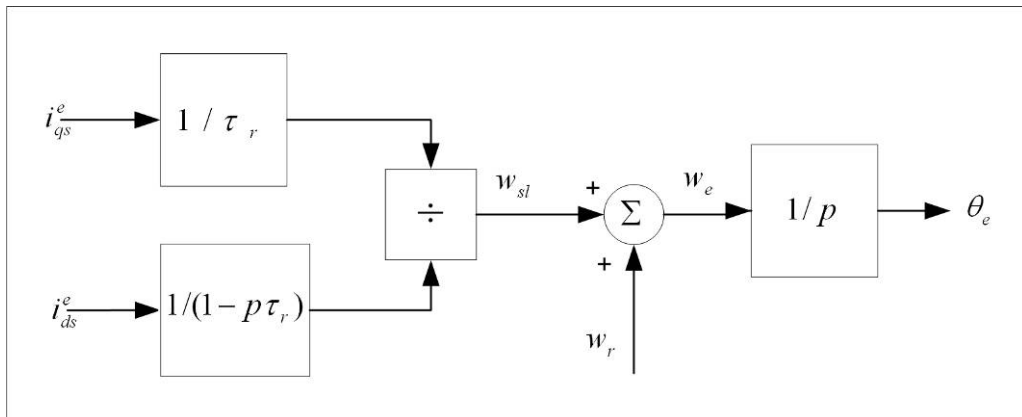
Figure 2-8 Indirect field oriented drive system

As it can be seen from Figure 2-8, indirect field orientation drive system needs the rotor resistance or rotor time-constant as a parameter. Accurate knowledge of the rotor resistance is essential to achieve the highest possible efficiency from the control structure. Lack of this knowledge results in detuning of the FOC.

Figure 2-9 Direct field oriented drive system

Figure 2-10 shows the block diagram of indirect field orientation control strategy with sensor in which speed regulation is possible using a control loop.

Figure 2-10 Indirect field oriented induction motor drive system with sensor [1]

As shown in Figure 2-10, two-phase current feeds the Clarke transformation block. These projection outputs are indicated as i^s_{ds} and i^s_{qs}. These two components of the current provide the inputs to Park's transformation, which gives the currents in qds^e the excitation reference frame. The i^e_{ds} and i^e_{qs} components, which are outputs of the Park transformation block, are compared to their reference values i^{e*}_{ds}, the flux reference, and i^{e*}_{qs}, the torque reference. The torque command, i^{e*}_{qs}, comes from the output of the speed controller. The flux command, i^{e*}_{ds} , is the output of the flux controller which indicates the right rotor flux command for every speed reference. Magnetizing current i^{e*}_{ds} is usually between 40 and 60% of the nominal current [2]. For operating in speeds above the nominal speed, a field weakening section should be used in the flux controller section. The current regulator outputs, v^{e*}_{ds} and v^{e*}_{qs} are applied to the inverse Park transformation. The outputs of this projection are v^s_{ds} and v^s_{qs}, which are the components of the stator voltage vector in $d^s q^s$ the orthogonal reference frame. They form the inputs of the SVPWM block. The outputs of this block are the signals that drive the inverter.

2.4   Space Vector Pulse Width Modulation (SVPWM)

2.4.1.   Voltage Fed Inverter (VSI)

The voltage source inverters (VSI) are the most common power electronics converters. The block diagram of the voltage source inverter supplied form the uncontrolled rectifier is shown in Figure 2-11. The DC link capacitor constitutes the actual voltage source, since voltage across it cannot change instantly. Since the output voltage of the diode bridge rectifier is not a pure DC, a filter inductor is included to absorb ripple component.
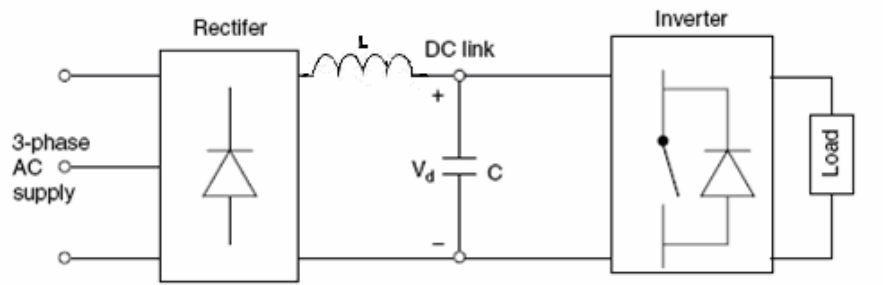
Figure 2-11 The block diagram of VSI supplied from a diode rectifier

A diagram of a three phase VSI is shown in the Figure 2-12.
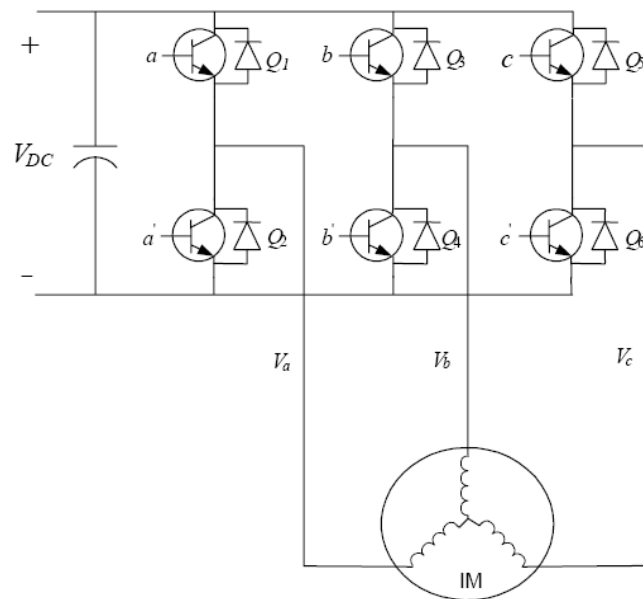
Figure 2-12 Three phase voltage source inverter supplying induction motor [1]

As it can be seen from Figure 2-11 and Figure 2-12, voltage source inverter has bridge topology with three branches (phases), each consisting of two power switches

and two freewheeling diodes. The inverter here is supplied from an uncontrolled, diode-based rectifier, via DC link which contains an LC filter in the inverted configuration. The uncontrolled rectifier allows the power flow from the supply to the load only.

2.4.2. Voltage Space Vectors

In terms of the desired phase voltages, the voltage space vector can be written by multiplying phase voltages by their phase orientations.

$$V_s(t) = \bar{V}_{an} \cdot e^{j0} + \bar{V}_{bn} \cdot e^{j2\pi/3} + \bar{V}_{cn} \cdot e^{j4\pi/3} \qquad (2\text{-}60)$$

A switch in a VSI is either "up" or "down", with the instantaneous output voltage either 1 or 0 times of Vdc . With three branch, eight switch-status combinations are possible.The voltage space vector can instantly take on one of the following seven distinct instantaneous values as shown in Table 2-1.

Table 2-1 Instantaneous Basic Voltage Vectors [25]

Switching State			Basic Vector	Value
S5	S3	S1		
0	0	0	$\bar{v}_0(000)$	0
0	0	1	$\bar{v}_1(001)$	$V_{dc} \cdot e^{j0}$
0	1	0	$\bar{v}_2(010)$	$V_{dc} \cdot e^{j2\pi/3}$
0	1	1	$\bar{v}_3(011)$	$V_{dc} \cdot e^{j\pi/3}$

Table 2-1 (Cont'd)

1	0	0	$\overline{v}_4(100)$	$V_{dc} \cdot e^{j4\pi/3}$
1	0	1	$\overline{v}_5(101)$	$V_{dc} \cdot e^{j5\pi/3}$
1	1		$\overline{v}_6(110)$	$V_{dc} \cdot e^{j\pi}$
1	1	1	$\overline{v}_7(111)$	0

In Table 2-1, $\overline{v}_1$ and $\overline{v}_7$ are the zero vectors. The resulting instantaneous voltage vectors, which are called the "basic vectors", are shown in Figure 2-13. The basic vectors form six sectors in Figure 2-13.
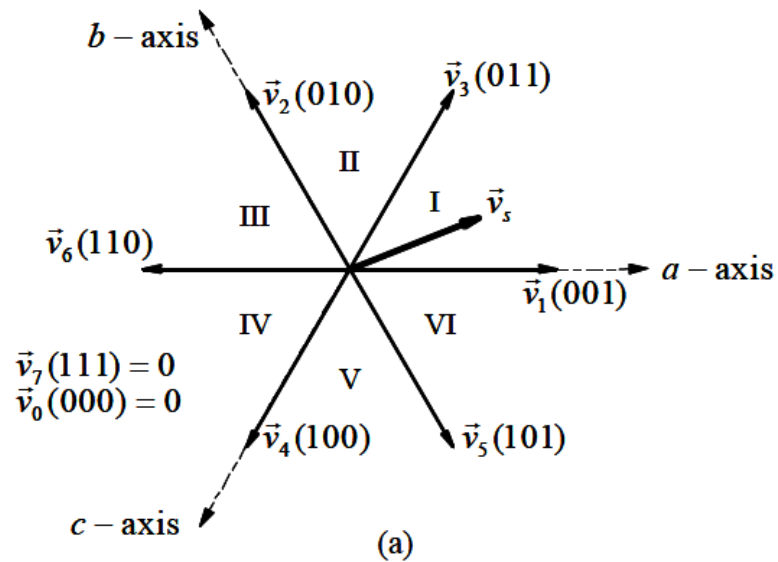
Figure 2-13 Basic space vectors [25]

2.4.3. SVPWM Application to the Static Power Bridge

Space Vector PWM (SVPWM) refers to a special technique of determining the switching sequence of the upper three power transistors of a three-phase voltage source inverter (VSI). It has been shown to generate less harmonic distortion in the output voltages or current in the windings of the motor. SVPWM provides more efficient use of the DC bus voltage compared to the direct sinusoidal modulation technique.

In AC drive applications, voltage sources are not sinusoidal. Instead, they are replaced by 6 power switches which act as on/off to the rectified DC bus voltage. The aim is to create sinusoidal current in the windings to generate rotating field. Owing to the inductive nature of the phases, a pseudo sinusoidal current is created by modulating the duty-cycle of the power switches. The switches shown in the Figure 2-12 are activated by signals a, b, c and their complement values. Eight different combinations are available with this three phase voltage source inverter including two zero states. It is possible to express each phase to neutral voltages in terms of DC supply voltage Vdc, for each switching combination of switches as listed in Table 2-2.

The voltages, V_{an}, V_{bn}, and V_{cn} are the output voltages applied to the windings of a motor. The six power transistors which are controlled by a, a', b, b', c and c' gating signals and shape the output voltages. When an upper transistor is switched on, i.e., when a, b, and c are 1, the corresponding lower transistor is switched off, i.e., the corresponding a', b' or c' is 0. The on and off states of the upper transistors S_1, S_3, and S_5, or the states of a, b, and c are sufficient to evaluate the output voltage.

Table 2-2 Power bridge output voltages (V_{an}, V_{bn}, V_{cn})

Switch Positions			Phase Voltages		
S_5	S_3	S_1	V_{an}	V_{bn}	V_{cn}
0	0	0	0	0	0

Table 2-2 (Cont'd)

0	0	1	2Vdc/3	-Vdc/3	-Vdc/3
0	1	0	-Vdc/3	2Vdc/3	-Vdc/3
0	1	1	Vdc/3	Vdc/3	-2Vdc/3
1	0	0	-Vdc/3	-Vdc/3	2Vdc/3
1	0	1	Vdc/3	-2Vdc/3	Vdc/3
1	1	0	-2Vdc/3	Vdc/3	Vdc/3
1	1	1	0	0	0

Since only 8 combinations are possible for the power switches, V^s_{ds}, V^s_{qs} can also take finite number of values in the (d^sq^s) frame. According to the command signals a, b, c Table 2-3 includes stator voltages in (d^sq^s) frame.

Table 2-3 Stator voltages in (d^sq^s) frame and related voltage vector

Switch Positions			(d^sq^s) frame Voltages		
S_5	S_3	S_1	V^s_{ds}	V^s_{qs}	Vectors
0	0	0	0	0	$\bar{v}_0(000)$
0	0	1	2Vdc/3	0	$\bar{v}_1(001)$
0	1	0	-Vdc/3	Vdc/√3	$\bar{v}_2(010)$
0	1	1	Vdc/3	Vdc/√3	$\bar{v}_3(011)$
1	0	0	-Vdc/3	-Vdc/√3	$\bar{v}_4(100)$
1	0	1	Vdc/3	-Vdc/√3	$\bar{v}_5(101)$

36

Table 2-3 (Cont'd)

1	1	0	-2Vdc/3	0	$\bar{v}_6(110)$
1	1	1	0	0	$\bar{v}_7(111)$

The eight voltage vectors re-defined by the combination of the switches are represented in Figure 2-14.

Given a reference voltage (derived from the inverse Park transform), the following step is used to approximate this reference voltage by the above defined eight vectors. The method used to approximate the desired stator reference voltage with only eight possible states of switches combines adjacent vectors of the reference voltage and modulates the time of application of each adjacent vector. In Figure 2-14 for a reference voltage V_{sref} is in the third sector and the application time of each adjacent vector is given by:

$$T = T_1 + T_3 + T_0$$

(2-61)

$$V_{sref} = \frac{T_1}{T}\vec{V}_1 + \frac{T_3}{T}\vec{V}_3$$

where T_1, T_3, and T_0 are respective time shares for vectors V_1 and V_3 an null vector V_0 within period T.
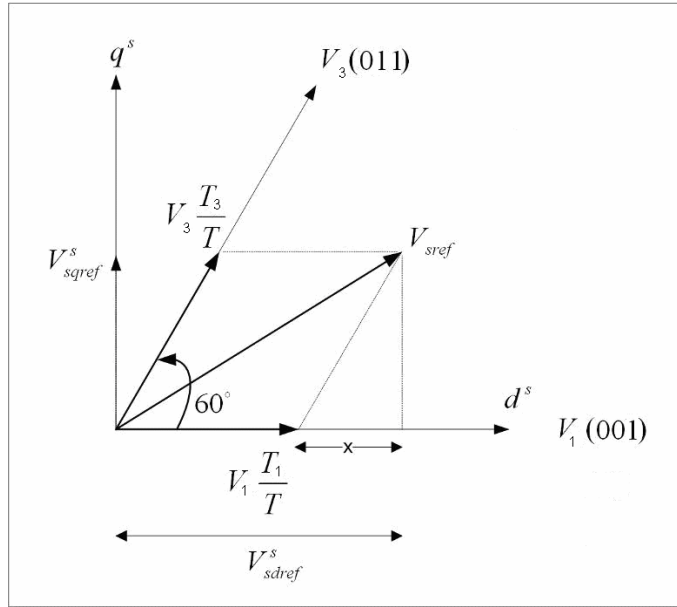
Figure 2-14 Projection of the reference voltage vector

The determination of the amount of times T_1 and T_3 are given by simple projections:

$$V_{sqref}^s = \frac{T_3}{T}\left\|\vec{V}_3\right\|\cos(30^0)$$

$$V_{sdref}^s = \frac{T_1}{T}\left\|\vec{V}_1\right\| + x \qquad\qquad (2\text{-}62)$$

$$x = \frac{V_{sqref}^s}{tg(60^0)}$$

Finally, with the ($d^s q^s$) component values of the vectors given in Table 2-3, the duration periods of application of each adjacent vector are:

$$T_1 = \frac{T}{2}(\sqrt{3}V_{sd}^s - V_{sq}^s) \qquad\qquad (2\text{-}63)$$

$$T_3 = TV_{sq}^s \qquad\qquad (2\text{-}64)$$

where the vector magnitudes are "$2V_{dc}/3$" and both sides are normalized by maximum phase to neutral voltage $V_{DC}/\sqrt{3}$.

The rest of the period spent in applying the null vector ($T_0 = T - T_1 - T_3$). For every sector, commutation duration is calculated. The amount of times of vector application can all be related to the following variables:

$$X = V_{sq}^s$$

$$Y = \frac{1}{2}V_{sq}^s + \frac{\sqrt{3}}{2}V_{sd}^s \qquad\qquad (2\text{-}65)$$

$$Z = \frac{1}{2}V_{sq}^s - \frac{\sqrt{3}}{2}V_{sd}^s$$

In the previous example for sector 3, $T_1 = -TZ$ and $T_3 = TX$. Extending this logic, one can easily calculate the sector number belonging to the related reference voltage vector. Then, three phase quantities are calculated by inverse Clarke transform to get sector information. The following basic algorithm helps to determine the sector number systematically.

If $V_{ref1} = V_{sq}^s > 0$ then set A=1   else A=0

If $V_{ref2} = \frac{1}{2}(\sqrt{3}V_{sd}^s - V_{sq}^s) > 0$ then set B=1 else B=0

If $V_{ref3} = \frac{1}{2}(-\sqrt{3}V_{sd}^s - V_{sq}^s) > 0$ then set C=1   else C=0

Then,

Sector = A+2B+4C

The duration of the sector boundary vectors application after normalizing with the period T can be determined as in Table 2-4.

Table 2-4 Durations of sector boundary

Sector	t_1	t_2
1:	$t_1 = Z$	$t_2 = Y$
2:	$t_1 = Y$	$t_2 = -X$
3:	$t_1 = -Z$	$t_2 = X$
4:	$t_1 = -X$	$t_2 = Z$
5:	$t_1 = X$	$t_2 = -Y$
6:	$t_1 = -Y$	$t_2 = -Z$

Saturations should be applied to the durations of t_1 and t_2 in case following saturation condition is satisfied.

If (t1+ t2) > PWM period then;

$t_{1sat} = t_1/(t_1+t_2)*$PWM period   and $t_{2sat} = t_2/(t_1+t_2)*$PWM period

The third step is to compute the three necessary duty-cycles. This is shown below:

$$t_{aon} = \frac{PWM\ period - t_1 - t_2}{2}$$

$$t_{bon} = t_{aon} + t_1 \qquad\qquad\qquad\qquad (2\text{-}66)$$

$$t_{con} = t_{bon} + t_2$$

The last step is to assign the right duty-cycle (t_{xon}) to the right motor phase (in other words, to the Ta, Tb and Tc) according to the sector. Table 2-5 depicts this determination below (i.e., the on time of the inverter switches).

Table 2-5 Assigned duty cycles to the PWM outputs

	1	2	3	4	5	6
Ta	t_{bon}	t_{aon}	t_{aon}	t_{con}	t_{bon}	t_{con}
Tb	t_{aon}	t_{con}	t_{bon}	t_{bon}	t_{con}	t_{aon}
Tc	t_{con}	t_{bon}	t_{con}	t_{aon}	t_{aon}	t_{bon}

The phase voltage of a general 3-phase motor Van, Vbn, Vcn can be calculated from the DC-bus voltage (V_{dc}), and three upper switching functions of inverter S_1, S_3, and S_5. The 3-ph windings of motor are connected either Δ or Y without a neutral return path (or 3-ph, 3-wire system).

Each phase of the motor is simply modeled as a series impedance of resistance r and inductance L and back emf e_a, e_b, e_c. Thus, three phase voltages can be computed as:

$$V_{an} = V_a - V_n = i_a r + L\frac{di_a}{dt} + e_a \qquad (2\text{-}67)$$

$$V_{bn} = V_b - V_n = i_b r + L\frac{di_b}{dt} + e_b \qquad (2\text{-}68)$$

$$V_{cn} = V_c - V_n = i_c r + L\frac{di_c}{dt} + e_c \qquad (2\text{-}69)$$

Summing these three phase voltages yields

$$V_a + V_b + V_c - 3V_n = (i_a + i_b + i_c)r + L\frac{d(i_a + i_b + i_c)}{dt} + e_a + e_b + e_c \qquad (2\text{-}70)$$

For a 3-phase system with no neutral path and balanced back emfs, $i_a+i_b+i_c=0$, and $e_a+e_b+e_c,=0$. Therefore, (2-71) becomes $V_{an}+V_{bn}+V_{cn},=0$. Furthermore, the neutral voltage can be simply derived from (2-71) as

$$V_n = \frac{1}{3}(V_a + V_b + V_c) \qquad (2\text{-}71)$$

Now three phase voltages can be calculated as:

$$V_{an} = V_a - \frac{1}{3}(V_a + V_b + V_c) = \frac{2}{3}V_a - \frac{1}{3}V_b - \frac{1}{3}V_c \qquad (2\text{-}72)$$

$$V_{bn} = V_b - \frac{1}{3}(V_a + V_b + V_c) = \frac{2}{3}V_b - \frac{1}{3}V_a - \frac{1}{3}V_c \qquad (2\text{-}73)$$

$$V_{cn} = V_c - \frac{1}{3}(V_a + V_b + V_c) = \frac{2}{3}V_c - \frac{1}{3}V_a - \frac{1}{3}V_b \tag{2-74}$$

Three voltages V_a, V_b, V_c are related to the DC-bus voltage V_{dc} and three upper switching functions S_1, S_3, and S_5 as:

$$V_a = S_1 V_{dc} \tag{2-75}$$

$$V_b = S_3 V_{dc} \tag{2-76}$$

$$V_c = S_5 V_{dc} \tag{2-77}$$

where S_1, S_3, and S_5 =either 0 or 1, and S_2=1-S_1, S_4=1-S_3, and S_6=1-S_5.

As a result, three phase voltages in (2-82) to (2-84) can also be expressed in terms of DC-bus voltage and three upper switching functions as:

$$V_{an} = V_{dc}(\frac{2}{3}S_1 - \frac{1}{3}S_3 - \frac{1}{3}S_5) \tag{2-78}$$

$$V_{bn} = V_{dc}(\frac{2}{3}S_3 - \frac{1}{3}S_1 - \frac{1}{3}S_5) \tag{2-79}$$

$$V_{cn} = V_{dc}(\frac{2}{3}S_5 - \frac{1}{3}S_1 - \frac{1}{3}S_3) \tag{2-80}$$

It is emphasized that the S_1, S_3, S_5 are defined as the upper switching functions. If the lower switching functions are available instead, then the out-of-phase correction

of switching function is required in order to get the upper switching functions as easily computed from equation ($S_2=1-S_1$, $S_4=1-S_3$, and $S_6=1-S_5$). Next the Clarke transformation is used to convert the three phase voltages V_{an}, V_{bn}, and V_{cn} to the stationary dq-axis phase voltages V^s_{ds} and V^s_{qs}. Because of the balanced system (V_{an} + V_{bn} + V_{cn}=0) V_{cn} is not used in Clarke transformation.

CHAPTER 3

OBSERVERS FOR SENSORLESS FIELD ORIENTED

CONTROL OF INDUCTION MACHINE

In general an estimator is defined as a dynamic system whose state variables are estimates of some other systems (e.g. induction motor). There are basically two forms of estimators; open-loop estimator and closed-loop estimator. The difference between them is whether a correction term is used to adjust the response of the estimator or not. A closed-loop estimator is referred as an observer.

Various open-loop flux estimators (flux models) are investigated in the literature. Different types of flux estimators could be implemented in rotor-flux-oriented reference frame or stationary reference frame. The common input to these models is monitored rotor speed or monitored rotor position. For a speed sensorless drive system, it is not possible to use such models. However, it is possible to establish a flux model which uses the monitored values of the stator voltages and stator currents. It is called improved flux model.

Open-loop flux estimators using pure integration are sensitive to parameter variations, and measurement error. These effects become more important at low stator frequencies due to the dominant effect of stator ohmic drops. An accurate compensation against ohmic voltage drops must be made prior to the integration. Due to the temperature dependency of the stator resistance value, it is difficult to have such compensation. Yet, with such an implementation, a lower frequency limit for useful operation is approximately 3 Hz with a 50 Hz supply [26].

Various open-loop rotor speed and rotor slip-frequency estimators are obtained by considering the voltage equations of the induction motor. They generally utilize the estimates of stator or rotor flux linkages. Hence, open-loop rotor speed estimators

basically rely on open-loop flux estimators. Open-loop rotor speed estimators mainly use the monitored stator voltages and currents. Some of these open-loop rotor speed estimation schemes are used in commercial speed sensorless induction motor drives. However, it is important to note that in general, the accuracy of open-loop estimators depends on machine parameters used. At low rotor speed, the accuracy of open-loop estimator is reduced, and in particular, parameter deviations from their actual values have great influence on the steady-state and transient performance of the drive system which uses an open-loop estimator.

On-line identification techniques are used in order to reduce the influence of parameter variations. Stator resistance, rotor time-constant, stator transient inductance and stator self inductance are identified during a self-commissioning stage of a vector controlled induction motor drive. It should be noted that in this self commissioning stage, the induction motor is at standstill during realization of all measurements. Moreover, adaptive on-line identification techniques are considered to track parameter variations during operation.

Closed-loop estimators (observers) can be classified according to the type of representation used for the plant to be observed. Once the plant is considered as deterministic, the observer is deterministic; or else, the observer is stochastic.

Thanks to the correction term, closed-loop estimators have generally better performance with respect to open-loop types. For that reason, closed-loop estimators are investigated throughout this study.

Various types of observers could be used in high-performance induction motor drives. Full-order state-observer (speed adaptive flux observer) and Kalman filter types are implemented in this thesis work, where full-order state observer is deterministic whereas Kalman filter types are stochastic.

This chapter focuses on both speed and flux observers.

3.1. Speed Adaptive Flux Observer for Induction Motor

In an inverter-fed electrical drive system, a speed adaptive flux observer could be used to estimate rotor flux linkage and stator current components by monitoring stator currents and the monitored (or reconstructed) stator voltages.

A state observer is a closed-loop estimator which can be used for the state (and/or parameter) estimation of a non-linear dynamic system in real time. In the calculations, the states are predicted by using a mathematical model of the observed system (the estimated states and actual states being denoted by $\hat{x}$ and x respectively), but the predicted states are continuously corrected by adding a feedback correction scheme. This correction scheme contains a weighted difference of some of the measured and estimated output signals (The difference is multiplied by the observer feedback gain, G). Based on the deviation from the estimated value, the state observer provides an optimum estimated output value ($\hat{x}$) at the next input instant. In an induction motor drive, a state observer can also be used for the real-time estimation of the rotor speed and some of the machine parameters such as stator resistance.

3.1.1. Flux Estimation Based on the Induction Motor Model

The model of the induction machine is established in the stationary reference frame as;

$$\frac{d}{dt}[x] = Ax + Bu \tag{3-1}$$

where

$$x = \begin{bmatrix} i_s^s & \psi_r^s \end{bmatrix}_{4x1}^T, \qquad A = \begin{bmatrix} A_{11} & A_{12} \\ A_{21} & A_{22} \end{bmatrix}_{4x4}, \qquad u = \begin{bmatrix} V_s^s \end{bmatrix}_{2x1}, \qquad \text{and} \qquad B = \begin{bmatrix} B_1 & 0 \end{bmatrix}_{4x2}^T$$

47

Then, the (3-1) takes the form below,

$$\frac{d}{dt}\begin{bmatrix} i_s^s \\ \psi_r^s \end{bmatrix} = \begin{bmatrix} A_{11} & A_{12} \\ A_{21} & A_{22} \end{bmatrix}\begin{bmatrix} i_s^s \\ \psi_r^s \end{bmatrix} + \begin{bmatrix} B_1 \\ 0 \end{bmatrix}V_s^s$$

(3-2)

$$= Ax + BV_s^s$$

and

$$i_s^s = C \cdot x$$ (3-3)

$$\psi_r^s = D \cdot x$$ (3-4)

where

$$i_s = \begin{bmatrix} i_{ds}^s & i_{qs}^s \end{bmatrix}^T$$

$$\psi_r^s = \begin{bmatrix} \psi_{dr}^s & \psi_{qr}^s \end{bmatrix}^T$$

$$V_s^s = \begin{bmatrix} V_{ds}^s & V_{qs}^s \end{bmatrix}^T$$

$$A_{11} = -\{R_s / (\sigma L_S) + (1-\sigma)/(\sigma\tau_r)\}I = a_{r11}I$$

$$A_{12} = L_m / (\sigma L_s L_r)\{(1/\tau_r)I - \omega_r J\} = a_{r12}I + a_{i12}J$$

$$A_{21} = (L_m / \tau_r)I = a_{r21}I$$

$$A_{22} = -(1/\tau_r)I + \omega_r J = a_{r22}I + a_{i22}J$$

48

$$B_1 = 1/(\sigma L_s)I = b_1 I$$

$$C = \begin{bmatrix} 1 & 0 & 0 & 0 \\ 0 & 1 & 0 & 0 \end{bmatrix}$$

$$D = \begin{bmatrix} 0 & 0 & 1 & 0 \\ 0 & 0 & 0 & 1 \end{bmatrix}$$

$$I = \begin{bmatrix} 1 & 0 \\ 0 & 1 \end{bmatrix} \qquad J = \begin{bmatrix} 1 & 0 \\ 0 & -1 \end{bmatrix}$$

$$\sigma = 1 - \frac{L_m^2}{(L_s L_r)}$$

$$\tau_r = \frac{L_r}{R_r}$$

By using the mathematical model of the induction motor given in (3-1) and adding a correction term, which contains the weighted difference of actual and the estimated states, a full-order state observer which estimates the stator current and the rotor flux linkages can be described as follows,

$$\frac{d}{dt}\hat{x} = \hat{A}\hat{x} + BV_s^s + G\left(i_s^s - \hat{i}_s^s\right) \tag{3-5}$$

where

$$\hat{A} = \begin{bmatrix} A_{11} & \hat{A}_{12} \\ A_{21} & \hat{A}_{22} \end{bmatrix} \tag{3-6}$$

$$\hat{i}_s^s = C\hat{x} \tag{3-7}$$

$$\hat{\psi}_r^s = D\hat{x} \tag{3-8}$$

$$\hat{A}_{12} = L_m / (\sigma L_s L_r) \{ (1/\tau_r) I - \hat{\omega}_r J \} = a_{r12} I + \hat{a}_{i12} J$$

$$\hat{A}_{22} = -(1/\tau_r) I + \hat{\omega}_r J = a_{r22} I + \hat{a}_{i22} J$$

where $\hat{x}$ denotes the estimated values and G is the observer gain matrix which is selected so that the observer can be stable.

It can be seen from (3-6), $\hat{A}$ is a function of estimated rotor speed $\hat{\omega}_r$.

3.1.1.1.   Estimation of Rotor Flux Angle

Once the equations (3-5) - (3-8) are solved, the estimated flux linkages are determined, it is then a straight process to compute the rotor flux angle estimate $\hat{\theta}_{\psi_r}$ by;

$$\hat{\theta}_{\psi_r} = \tan^{-1} \left(\frac{\hat{\psi}_{qr}^s}{\hat{\psi}_{dr}^s} \right) \tag{3-9}$$

The block diagram of rotor flux angle estimation is illustrated in Figure 3-1.
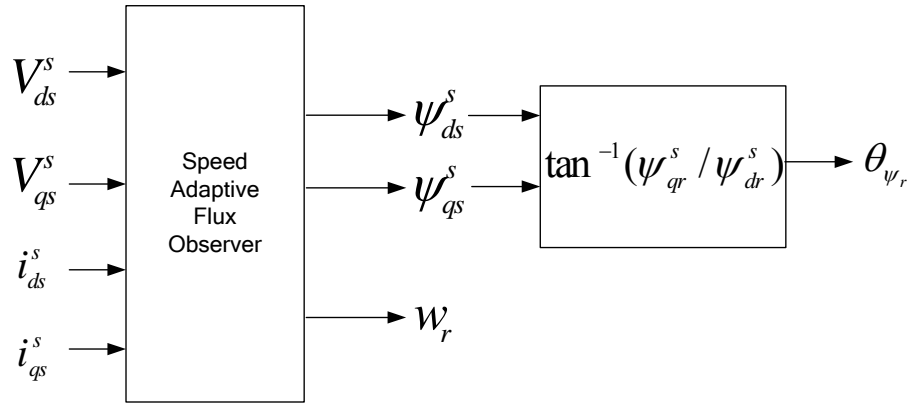
Figure 3-1 The block diagram of rotor flux angle estimation

3.1.2.   Adaptive Scheme for Speed Estimation

It can be seen that the state matrix of the observer ($\hat{A}$) (given as (3.6) is a function of the rotor speed. In a sensorless drive, the rotor speed must be estimated and fed into $\hat{A}$. The estimated rotor speed being denoted by $\hat{\omega}_r$, $\hat{A}$ becomes a function of $\hat{\omega}_r$. It is important to note that the estimated rotor speed is considered as a parameter in $\hat{A}$; however, in some other types of observers (e.g. extended Kalman filter), the estimated speed is not considered as a parameter, but it is a state variable.

A speed adaptive flux observer algorithm is implemented by Kubota [5] on the basis of an adaptive control scheme as shown in Figure 3-2. In this way, it is possible to implement a speed estimator which estimates the electrical rotor speed of an induction machine.
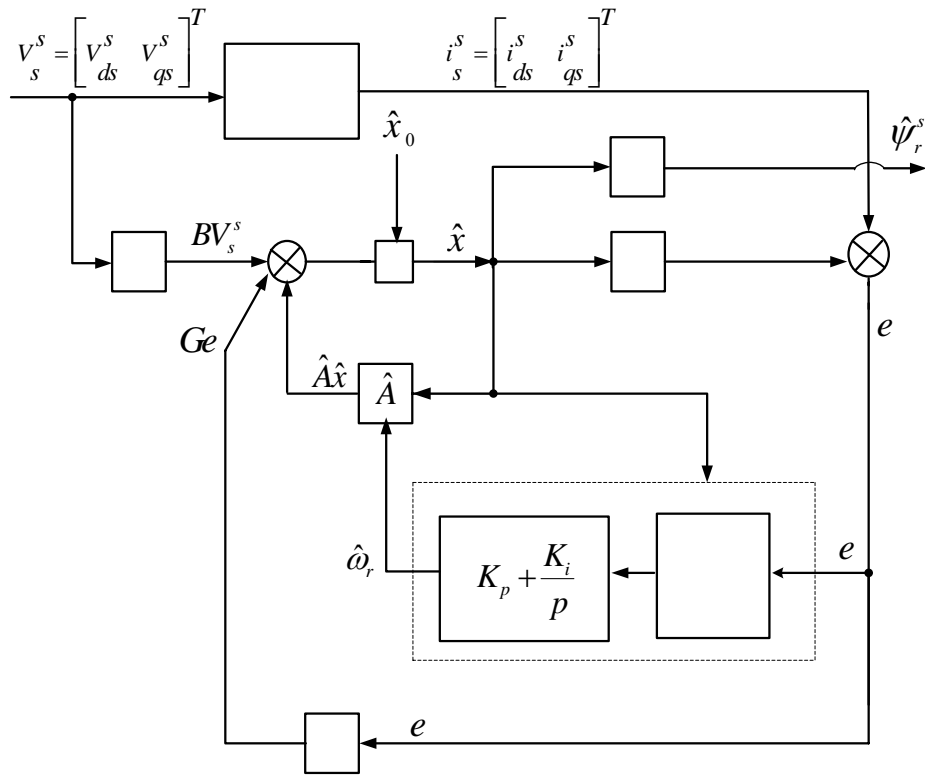
Figure 3-2 Adaptive state observer

To obtain error dynamics, (3-5) is subtracted from (3-2), yielding the following observer-error equation;

$$\frac{d}{dt}[x] - \frac{d}{dt}[\hat{x}] = [Ax + BV_s^s] - [\hat{A}\hat{x} + BV_s^s + G(i_s^s - \hat{i}_s^s)]$$

$$\frac{d}{dt}[e] = (A + GC)[e] - [\Delta A]\hat{x} \qquad (3-10)$$

where

$$e = (x - \hat{x})$$

$$[\Delta A] = \begin{bmatrix} 0 & -\Delta\omega_r J / c \\ 0 & \Delta\omega_r J \end{bmatrix}$$

$$c = \frac{(\sigma L_s L_r)}{L_m}$$

$$\Delta\omega_r = \hat{\omega}_r - \omega_r$$

It can be understood that error dynamics are described by the eigenvalues of $A + GC$ and these could also be used to design a stable observer (selecting an appropriate gain matrix, G for stability). However, in order to determine the stability of the error dynamics of the observer, it is possible to use Lyapunov stability theorem, which gives a sufficient condition for the uniform asymptotic stability of a non-linear system by using a Lyapunov function V which has to satisfy various conditions. For instance, it must be continuous, differentiable, positive semi-definite, etc. Such a function exists and the following Lyapunov function is introduced.

$$V = e^T e + (\hat{\omega}_r - \omega_r)^2 / \lambda \tag{3-11}$$

where λ is a positive constant. The time derivative of V becomes,

$$\frac{d}{dt}V = e^T \left\{ (A + GC)^T + (A + GC) \right\} e - 2\Delta\omega_r (e_{ids}^s \hat{\psi}_{qr}^s - e_{iqs}^s \hat{\psi}_{dr}^s) / c + 2\Delta\omega_r \frac{d}{dt}\hat{\omega}_r / \lambda$$

$$\tag{3-12}$$

where,

$$e_{ids}^s = i_{ds}^s - \hat{i}_{ds}^s$$
$$e_{iqs}^s = i_{qs}^s - \hat{i}_{qs}^s$$

Since a sufficiency condition for uniform asymptotic stability is that the derivative of Lyapunov function, dV/dt, is to be negative semi-definite. If observer gain matrix G is selected appropriately, the first term of (3-10) becomes always negative semi-definite, which can be satisfied by ensuring that the sum of the last two terms in (3-10) is zero, so the observer is stable. As a result, we can come up with an adaptive scheme for the speed estimation by equating the second term to the third term in (3-10).

$$\frac{d}{dt}\hat{\omega}_r = \lambda\left(e_{ids}^s \hat{\psi}_{qr}^s - e_{iqs}^s \hat{\psi}_{dr}^s\right)/c \qquad (3\text{-}13)$$

Thus, from the (3-13), the speed is estimated as;

$$\hat{\omega}_r = K_i \int\left(e_{ids}^s \hat{\psi}_{qr}^s - e_{iqs}^s \hat{\psi}_{dr}^s\right)dt \qquad (3\text{-}14)$$

However, so as to improve the performance of the speed observer, it is modified to

$$\hat{\omega}_r = K_p\left(e_{ids}^s \hat{\psi}_{qr}^s - e_{iqs}^s \hat{\psi}_{dr}^s\right) + K_i \int\left(e_{ids}^s \hat{\psi}_{qr}^s - e_{iqs}^s \hat{\psi}_{dr}^s\right)dt \qquad (3\text{-}15)$$

where K_p and K_i are arbitrary positive gains.

If the observer gain matrix G is chosen so that the A-GC term is negative semi-definite, then the speed observer is stable. To ensure the stability at all speeds, the conventional technique is to select observer poles which are proportional to motor poles [27]. Thus, by using the pole placement technique, the gain matrix is obtained as

$$G = -\begin{bmatrix} g_1 I_2 + g_2 J \\ g_3 I_2 + g_4 J \end{bmatrix} \qquad (3\text{-}16)$$

The four gains in G are obtained from the eigenvalues of the induction machine as follows,

$$
\begin{aligned}
g_1 &= (m-1)(a_{r11} + a_{r22}) \\
g_2 &= (m-1)(a_{i22}) \\
g_3 &= (m^2 - 1)(ca_{r11} + a_{r21}) - c(k-1)(a_{r11} + a_{r22}) \\
g_4 &= -c(m-1)a_{i22}
\end{aligned}
\tag{3-17}
$$

For DSP implementation the discretized form of the observer in (3-2) and the adaptation mechanism (3-15) are used. Thus the discretized observer is described by

$$
\hat{x}(m+1) = A_d \hat{x}(m) + B_d V_s^s + G_d \left(i_s^s(m) - \hat{i}_s^s(m) \right)
\tag{3-18}
$$

where A_d and B_d are discretized matrices.

$$
A_d = \exp(AT) \approx I + AT + \frac{(AT)^2}{2}
\tag{3-19}
$$

$$
B_d = \int_0^t [\exp(AT)]B dt \approx BT + \frac{ABT^2}{2}
\tag{3-20}
$$

The observer poles are chosen to be proportional to the poles of induction machine. To make the scheme insensitive to the measurement noise, the constant m in (3-17) is selected to be low. However, this pole-placement technique may have some disadvantages and may not ensure to have a good observer dynamics. It requires extensive computation time due to updating of matrix G and discretization procedure, and this is a disadvantage. The observer dynamics can be adversely affected by the fact that for small sampling time and low rotor speed, the discrete-locus being very close to the stability limit and in case there are computational errors, then an instability may arise. It is possible to overcome some of these difficulties.

For example, two different constant gain matrices G and G' are predetermined and used according to the rotor speed. (one for speed values less than a specified value and the other for speed values higher than this specific value.)

At the experimental work, for simplifying the DSP implementation, the proportionality constant k is chosen as 1.0 so G = 0 and initial value of the estimated speed is zero.

The performance of the speed adaptive flux observer is improved in [28] in terms of stability and accuracy at low speed region. In addition, in [5], adaptive stator resistance estimation is achieved together with adaptive speed estimation.

3.2. Kalman Filter for Speed Estimation

R. E. Kalman has brought a recursive solution to the problem of discrete-time filtering with his paper published in 1960. Rapid expansion and low cost of computer systems has resulted in the use of Kalman filters in numerous research and projects particularly on navigation and the modulation of servo systems.

Kalman filter consists of a number of mathematical equations which bring a recursive solution to the well-known least-square method. The filter is a strong one in the sense that it can estimate the past, present and also future states even in the situations where the mathematical model used in the design does not totally reflect the physical system.

3.2.1. Discrete Kalman Filter

Today, there are many derivatives of Kalman filter and many applications based on these derivations. Among these derivatives, adaptive Kalman filters, non-linear Kalman filters and discrete time Kalman filters are most widely-used ones. The general operating principle lying behind all these derivations can be roughly explained as the minimization of the total squares of error data. Kalman filter can

56

predict any data by the use of another data in a way to cause minimum error.Assume that the mathematical method below is a state-space expression.

$$\underline{x}_k = \underline{A}\underline{x}_{k-1} + \underline{B}\underline{u}_{k-1} + \underline{w}_{k-1}$$
$$\underline{z}_k = \underline{H}\underline{x}_k + \underline{v}_k$$

$$(3\text{-}21)$$

Here, $\underline{x}$ matrix stands for the state parameters of the system, $\underline{A}$ for system matrix, $\underline{B}$ for input matrix, $\underline{u}$ for system input, $\underline{z}$ for system output, H for output matrix, $\underline{w}$ for noise in the model (the noise affecting state parameters) and $\underline{v}$ for noise while reading signals. A subscript under any parameter shows to which instant this parameter belongs (for instance, x_k shows the x value at k instant, x_{k-1} shows the x value at k-1 instant which is just one step before k instant).

While forming discrete Kalman filter, it is assumed that $\underline{w}$ matrix, which is called as process noise and includes the reaction differences between system model and real system and the operational errors of the hardware on which the filter operates, and $\underline{v}$ matrix, which is called as measurement noise and includes the errors in signal measurement, have a mean value of zero and a normal distribution. The probability expressions of these noise matrices are given in (3-22).

$$p(\underline{w}) \approx N(0, \underline{Q})$$
$$p(\underline{v}) \approx N(0, \underline{R})$$

$$(3\text{-}22)$$

The matrices $\underline{Q}$, called as process noise covariance, and $\underline{R}$, called as measurement noise covariance are generally considered as constant although they are unsteady. By the use of the mathematical model (3-21) Kalman filter, a priori state estimate of the system output and state parameters is made (3-24) and by the use of previous estimations, $\underline{P}$ matrix, priori error covariance, is calculated (3-25). This matrix includes the data concerning how valid the filter's previous estimations are. The estimation error can be found by comparing system output taken from the system and the priori state estimate (3-23).

$$e_k = \underline{z}_k - \underline{H}\,\hat{\underline{x}}_k^-$$
(3-23)

The main goal of the filter is to correct the priori state estimate ($\hat{\underline{x}}_k^-$) by the use of these error data and approximate to the real system output as much as possible. K matrix (3-26), known as Kalman Gain, is used for this purpose. The found estimation error (3-23) is multiplied by this gain and added to the priori state estimate. In this way, state estimations are acquired (3-27). Later, posteriori estimate error covariance is calculated so as to use at the next time step (3-28).

The operating principle of Kalman filter mentioned above can be expressed by the mathematical equations given below. Priori state estimates are made.

$$\hat{\underline{x}}_k^- = \underline{A}\hat{\underline{x}}_{k-1} + \underline{B}\underline{u}_{k-1}$$
(3-24)

Priori error covariance is calculated.

$$\underline{P}_k^- = \underline{A}\underline{P}_{k-1}\underline{A}^T + \underline{Q}$$
(3-25)

Kalman Gain is calculated.

$$\underline{K}_k = \underline{P}_k^-\underline{H}^T\left(\underline{H}\underline{P}_k^-\underline{H}^T + \underline{R}\right)^{-1}$$
(3-26)

State estimations are calculated.

$$\hat{\underline{x}}_k = \hat{\underline{x}}_k^- + \underline{K}_k\left(\underline{z}_k - \underline{H}\hat{\underline{x}}_k^-\right)$$
(3-27)

Posteriori estimate error covariance is calculated.

$$\underline{P}_k = (\underline{I} - \underline{K}_k \underline{H}) \underline{P}_k^- \qquad\qquad (3\text{-}28)$$

In order for the filter to operate, the first values of $\underline{x}$ and $\underline{P}$ matrices are required. If the first values of these matrices can be measured, real values should be used. If these matrices cannot be measured, the use of approximate values won't affect the filter performance, but at the beginning, it will lead to some wrong estimations for a short time. $\underline{P}$ matrix should not be zero matrix because zero matrix means that estimations are the same with the measurements, and in this case, estimations become the same with the measurements at each time step. Generally, as the first value of $\underline{P}$ matrix, identity matrix is used.

(3-24) and (3-25) are named as Time Update equations whereas the other three are called as Measurement Update equations. By the use of these equations, the solution can be summarized as in the Figure 3-3:
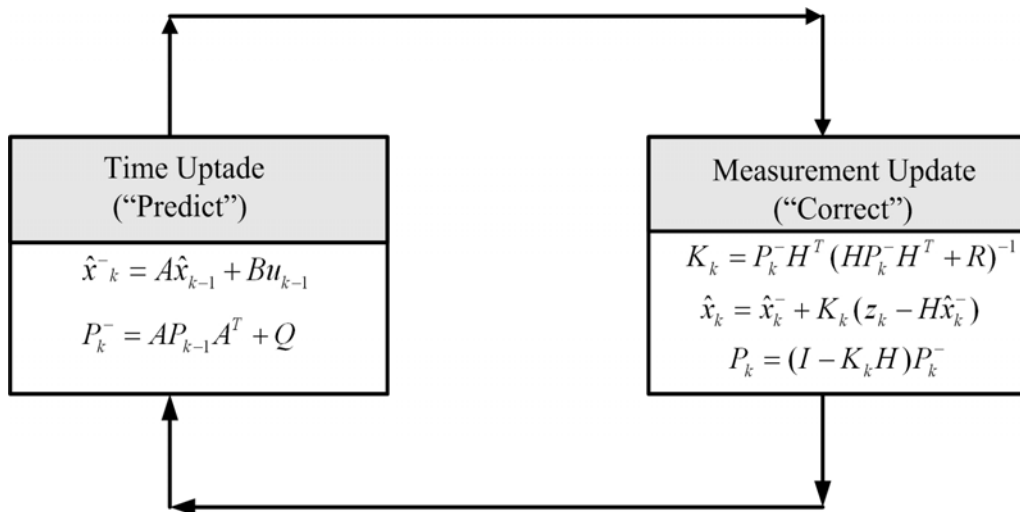
Figure 3-3 Discrete Kalman filter algorithm

The design of Kalman filter can be summarized as finding the mathematical equations defining the system, that are $\underline{Q}$ and $\underline{R}$ matrices. Although the effect of the mathematical model on filter performance is acute, very simple models may give rather satisfactory results. The important thing is to express the dominant characteristics of the system by means of the mathematical model.

$\underline{R}$ matrix can be found by measuring the noise in the measured signals. This matrix can be obtained by putting the squares of the standard deviation of the noise in the measured signals successively to the diagonal elements of $\underline{R}$ diagonal matrix (3-29).

$$\underline{R} = \begin{bmatrix} \sigma_1^2 & 0 & \cdots & 0 \\ 0 & \sigma_2^2 & \cdots & 0 \\ \vdots & \vdots & \ddots & \vdots \\ 0 & 0 & \cdots & \sigma_m^2 \end{bmatrix} \tag{3-29}$$

$\underline{Q}$ matrix includes the ambiguity assigned to the system model and it is expressed through Equation 10 for a system model with three state parameters. In this equation, σ_i is the standard deviation value of the ith state parameter, and this value includes the errors appearing upon the comparison of ith state parameter and real system and the operating errors of the hardware in which the filter is operating.

$$\underline{Q} = \begin{bmatrix} \sigma_1^2 & \sigma_1\sigma_2 & \sigma_1\sigma_3 \\ \sigma_1\sigma_2 & \sigma_2^2 & \sigma_2\sigma_3 \\ \sigma_1\sigma_3 & \sigma_2\sigma_3 & \sigma_3^2 \end{bmatrix} \tag{3-30}$$

To get $\underline{Q}$ matrix is not as easy as $\underline{R}$ matrix. Most often, state parameters cannot be measured and the operating errors to be faced in hardware cannot be predicted. Even though the general way of obtaining this matrix is to make some assumptions and

come up with mathematical conclusions, it can also be found by means of trial and error.

The smaller the values are for the values of standard deviation, the more the filter relies on the system model. Even in the situations where the system model expresses the real system quite well, giving very small values for the values of standard deviation makes the improvement of filter parameters difficult.

On the other hand, the small values in $\underline{R}$ matrix show that the measurement is reliable. Therefore, for the digital signals (in the case there is no sensor noise), this value should be chosen very small. Very small values of this parameter affect the filter performance badly by making the Kalman Gain almost constant. If it is chosen as zero, then Kalman Gain turns out to be a constant matrix. In this case, constant Kalman Gain leads $\underline{P}$ matrix, which includes estimation performance data, to be zero and give the priori state estimate of the filter as output without correction.

3.2.2. "Obtaining "Synchronous Speed, wₛ" Speed Data through the use of "Rotor Flux Angle"

It is evaluated that "Electrical synchronous speed" speed data can be attained by the use of Rotor Flux Angle. For this purpose, constant acceleration mathematical model has been used in the designed Kalman filter. Constant acceleration mathematical model can be expressed in the state-space as follows:

$$
\begin{bmatrix} \theta_k \\ \omega_k \\ \alpha_k \end{bmatrix} = \begin{bmatrix} 1 & T & T^2/2 \\ 0 & 1 & T \\ 0 & 0 & 1 \end{bmatrix} \begin{bmatrix} \theta_{k-1} \\ \omega_{k-1} \\ \alpha_{k-1} \end{bmatrix} \quad , \quad y_k = \begin{bmatrix} 1 & 0 & 0 \end{bmatrix} \begin{bmatrix} \theta_k \\ \omega_k \\ \alpha_k \end{bmatrix} \tag{3-31}
$$

Here, θ stands for "Rotor Flux Angle" angular position data, ω for "synchronous speed, wₛ" angular speed data, α for angular acceleration data, T for sampling time and y for system output. Since only θ angular position can be predicted through

"flux estimator", only this state parameter has been used as system output. Constant acceleration model does not include system dynamic. Assuming that system does not reach to high speeds and it is linear, this model has been utilized. It is due to the ignorance of the system dynamic that model shows weakness particularly at the high frequencies (above 7 Hz).

When this mathematical model and the previous equations are applied, "Synchronous speed, w_s" angular speed data can be obtained by the use of "Rotor Flux angle" θ angular position data. Due to the problems faced in the speed data estimated via "Flux estimator", the need for getting speed data from noisy position data can be met with Discrete Kalman Filter Model.

3.2.3. Extended Kalman Filter (EKF)

The extended Kalman filter (EKF) could be used for the estimation of the rotor speed of an induction machine. The EKF is suitable for use in high-performance induction motor drives, and it can provide accurate speed estimates in a wide speed-range, including very low speeds. It can also be used for joint state and parameter estimation. However, it is computationally more intensive than both speed adaptive flux observer and discrete kalman filter described in the previous sections.

The EKF is a recursive optimum stochastic state estimator which can be used for the joint state and parameter estimation of a non-linear dynamic system in real-time by using noisy monitored signals that are disturbed by random noise. This assumes that the measurement noise and disturbance noise are uncorrelated. The noise sources take account of measurement and modelling inaccuracies.

The EKF is a variant of the Kalman filter, but the extended version can deal with a non-linear system. Once the differences between speed adaptive flux observer and EKF are considered, it is noted that in the speed adaptive flux observer, the noise has not been considered. So, it is a deterministic observer in contrast to the EKF which is a stochastic observer. Furthermore, in the speed adaptive flux observer, the speed is considered as a parameter, but in the EKF it is considered as a state. Similar to the

speed-adaptive flux observer, where the state variables are adapted by the gain matrix (G), in the EKF the state variables are adapted by the Kalman gain matrix (K).

In a first stage of the calculations of the EKF, the states are predicted by using a mathematical model of the induction machine (which contains previous estimates) and in the second stage, the predicted states are continuously corrected by using a feedback correction scheme. This scheme makes use of actual measured states by adding a term to the predicted states (which are obtained in the first stage). The additional term contains the weighted difference of the measured and estimated output signals. Based on the deviation from the estimated value, the EKF provides an optimum output value at the next input instant.

In an induction motor drive, the EKF can be used for the real-time estimation of the rotor speed, but it can also be used for joint state and parameter estimation. For this purpose, the stator voltages and currents are measured (or the stator voltages are recontructed from the d.c. link voltage and the inverter switching signals) and the speed of the machine can be obtained by the EKF quickly and precisely.

The main design steps for a speed-sensorless induction motor drive implementation using the discretized EKF algorithm are as follows [26]:

1. Selection of the time-domain machine model;
2. Discretization of the induction machine model;
3. Determination of the noise and state covariance matrices Q, R, P;
4. Implementation of the discretized EKF algorithm; tuning.

These steps are now discussed.

3.2.3.1.   Selection of the Time-Domain Machine Model

For the purpose of using EKF for the estimation of rotor speed of an induction machine, it is possible to use various machine models. For example, it is possible to use the equations expressed in the rotor-flux-oriented reference frame ($\omega_g = \omega_{mr}$), or in the stationary reference frame. Due to convenience and computational reduction, induction machine model at stationary reference frame is chosen. The main advantages of using the model in the stationary reference frame are reduced

computation time (e.g. due to reduced non-linearities), smaller sampling times and more stable behaviour. [26]

The two-axis state-space equations including rotor speed of the induction machine in the stationary reference are as follows,

$$\frac{d}{dt}[x] = Ax + Bu \qquad (3\text{-}32)$$

where

$$x = \begin{bmatrix} i_{ds}^s & i_{qs}^s & \psi_{dr}^s & \psi_{qr}^s & \omega_r \end{bmatrix}^T, \quad u = \begin{bmatrix} V_{ds}^s & V_{qs}^s \end{bmatrix}^T, \quad B = \begin{bmatrix} 1/\sigma L_s & 0 \\ 0 & 1/\sigma L_s \\ 0 & 0 \\ 0 & 0 \\ 0 & 0 \end{bmatrix}^T$$

and

$$A = \begin{bmatrix} -1/T_s^* & 0 & L_m(\sigma L_s L_r T_r) & \omega_r L_m /(\sigma L_s L_r) & 0 \\ 0 & -1/T_s^* & \omega_r L_m /(\sigma L_s L_r) & L_m(\sigma L_s L_r T_r) & 0 \\ L_m /T_r & 0 & -1/T_r & -\omega_r & 0 \\ 0 & L_m /T_r & \omega_r & -1/T_r & 0 \\ 0 & 0 & 0 & 0 & 0 \end{bmatrix}$$

$$1/T_s^* = (R_s + R_r(L_m /L_r)^2)/(\sigma L_s)$$

Then, the (3-32) takes the form below,

$$\frac{d}{dt}\begin{bmatrix} i^s_{ds} \\ i^s_{qs} \\ \psi^s_{dr} \\ \psi^s_{qr} \\ \omega_r \end{bmatrix} = A \begin{bmatrix} i^s_{ds} \\ i^s_{qs} \\ \psi^s_{dr} \\ \psi^s_{qr} \\ \omega_r \end{bmatrix} + B \begin{bmatrix} V^s_{ds} \\ V^s_{qs} \end{bmatrix}$$

(3-33)

$$= Ax + BV^s_s$$

and

$$i^s_s = C \cdot x \qquad\qquad (3\text{-}34)$$

$$\psi^s_r = D \cdot x \qquad\qquad (3\text{-}35)$$

where

$$i_s = \begin{bmatrix} i^s_{ds} & i^s_{qs} \end{bmatrix}^T, \qquad\qquad \psi^s_r = \begin{bmatrix} \psi^s_{dr} & \psi^s_{qr} \end{bmatrix}^T, \qquad\qquad V^s_s = \begin{bmatrix} V^s_{ds} & V^s_{qs} \end{bmatrix}^T$$

$$C = \begin{bmatrix} 1 & 0 & 0 & 0 \\ 0 & 1 & 0 & 0 \end{bmatrix} \qquad \text{and} \qquad D = \begin{bmatrix} 0 & 0 & 1 & 0 \\ 0 & 0 & 0 & 1 \end{bmatrix}$$

Note that, the rotor speed derivative has been assumed to be negligible, $d\omega_r/dt = 0$. Although this last equation implies that the machine has infinite inertia and therefore unable to accelerate, actually this is not true. This is corrected by the operation of Kalman filter (by the system noise, which also takes account of the computational inaccuracies). Furthermore, it should be noted that the effects of saturation of the magnetic paths of the machine have been neglected. This assumption is justified since it can be shown that the EKF is not sensitive to changes in the inductances, since changes in the stator parameters are compensated by the current loop inherent in the EKF. The application of (3-32) in the EKF will give not only the rotor speed

but also the rotor flux-linkage components (and as a consequence the angle and modulus of the rotor flux-linkage space vector will also be known). This is useful for high-performance drive implementations. It is important to emphasize that the rotor-speed has been considered as a state variable and the system matrix A is non-linear – it contains the speed, A = A(x).

3.2.3.2. Discretization of the Induction Motor Model

For digital implementation of the EKF, the discretized machine equations are obtained as follows:

$$x(m+1) = A_d x(m) + B_d u(m) \tag{3-36}$$

where A_d and B_d are discretized system and input matrices respectively.

$$A_d = \exp(AT) \approx I + AT + \frac{(AT)^2}{2} \tag{3-37}$$

$$B_d = \int_0^t \left[\exp(AT)\right]Bdt \approx BT + \frac{ABT^2}{2} \tag{3-38}$$

By considering the system noise v(k) (v is the noise vector of the states), which is assumed to be zero-mean, white Gaussian, which is independent of x(k), and which has covariance matrix Q, the system model becomes:

$$x(m+1) = A_d x(m) + B_d u(m) + v(k) \tag{3-39}$$

By considering a zero-mean, white Gaussian measurement noise, w(k) (noise in the measured stator currents), which is independent of y(k) and v(k) and whose covariance matrix is R, the output equation becomes,

$$y(m) = Cx(m) + w(k) \hspace{5cm} (3\text{-}40)$$

3.2.3.3. Determination of the Noise and State Covariance Matrices Q, R, P

The goal of the Kalman filter is to obtain estimates about the unmeasurable states (e.g. rotor speed) by using measured states, and also statistics of the noise and measurements. In general, by means of the noise inputs, it is possible to take account of computational inaccuracies, modelling errors, and errors in the measurements. The filter estimation ($\hat{x}$) is obtained from the predicted values of the states (x) and this is corrected recursively by using a correction term, which is the product of the Kalman gain (K) and the deviation of the estimated measurement output vector and the actual output vector (y-$\hat{y}$). The Kalman gain is chosen to result in the best possible estimated states. Thus, the filter algorithm contains basically two main stages, a prediction stage and a filtering stage as illustrated at Figure 3-3.

During the prediction stage, the next predicted values of the states x(k+1) are obtained by using a mathematical model (state-variable equations) and also the previous values of the estimated states. Furthermore, the predicted state covariance matrix (P) is also obtained before the new measurements are made, and for this purpose, the mathematical model and also the covariance matrix of the system (Q) are used.

In the second stage, which is the filtering stage, the next estimated states, $\hat{x}$(k+1) are obtained from the predicted estimates x(k+1) by adding a correction term K(y-$\hat{y}$) to the predicted value. This correction term is a weighted difference between the actual output vector (y) and the predicted output vector ($\hat{y}$), where K is the Kalman gain. Thus, the predicted state estimate (and also its covariance matrix) is corrected through a feedback correction scheme that makes use of the actual measured quantities.

The Kalman gain is chosen to minimize the estimation-error variances of the states to be estimated. The computations are realized by using recursive relations. The

algorithm is computationally impressive, and the accuracy also depends on the model parameters used. A critical part of the design is to use correct initial values for the various covariance matrices. These can be obtained by considering the stochastic properties of the corresponding noises. Since these are usually not known, in most cases they are used as weight matrices, but it should be noted that sometimes simple qualitative rules can be set up for obtaining the covariances in the noise vectors. With the advances in DSP technology, it is possible to conveniently implement an EKF in real time.

The system noise matrix Q is a five-by-five matrix, the measurement noise matrix R is a two-by-two matrix, so in general this would require the knowledge of 29 elements. However, by assuming that the noise signals are not correlated, both Q and R are diagonal, and only 5 elements must be known in Q and 2 elements in R. However, the parameters in the direct and quadrature axes are the same, which means that the first two elements in the diagonal of Q are equal ($q_{11} = q_{22}$), the third and fourth elements in the diagonal Q are equal ($q_{33} = q_{44}$), so Q = diag(q_{11}, q_{11}, q_{33}, q_{33}, q_{55}) contains only 3 elements which have to be known. Similarly, the two diagonal elements in R are equal ($r_{11} = r_{22} = r$), thus R = diag(r, r). It follows that in total only 4 noise covariance elements must be known.

3.2.3.4.   Implementation of the Discretized EKF Algorithm; Tuning

As discussed above, the EKF algorithm contains basically two main stages, a prediction stage and a filtering stage. During the prediction stage, the next predicted values of the states x(k+1) [which will be denoted by x^* (k+1)] and the predicted state covariance matrix (P) [which will be denoted by P^*] are also obtained. For this purpose, the state-variable equations of the machine and the system covariance matrix (Q) are used. During the filtering stage, the filtered states ($\hat{x}$) are obtained from the predicted estimates by adding a correction term to the predicted value (x^*); this correction term is Ke = K(y- $\hat{y}$), where e = (y- $\hat{y}$) is an error term, and it uses

measured stator currents, $y = i^s_s$, $\hat{y} = \hat{i}^s_s$. This error is minimized in the EKF. The EKF equation is given as,

$$\frac{d}{dt}\hat{x} = \hat{A}(\hat{x})\hat{x} + BV^s_s + K\left(i^s_s - \hat{i}^s_s\right) \qquad (3\text{-}41)$$

The structure of the EKF is shown in Figure 3-4. The state estimates are obtained by the EKF algorithm in the following seven steps:

Step 1: Initialization of the state vector and covariance matrices

Starting values of the state vector $x_0 = x(t_0)$ and the starting values of the noise covariance matrices Q_0 (diagonal 5 x 5 matrix) and R_0 (diagonal 2 x 2 matrix) are set, together with the starting value of the state covariance matrix P_0 (which is a 5 x 5 matrix), where P is the covariance matrix of the state vector.
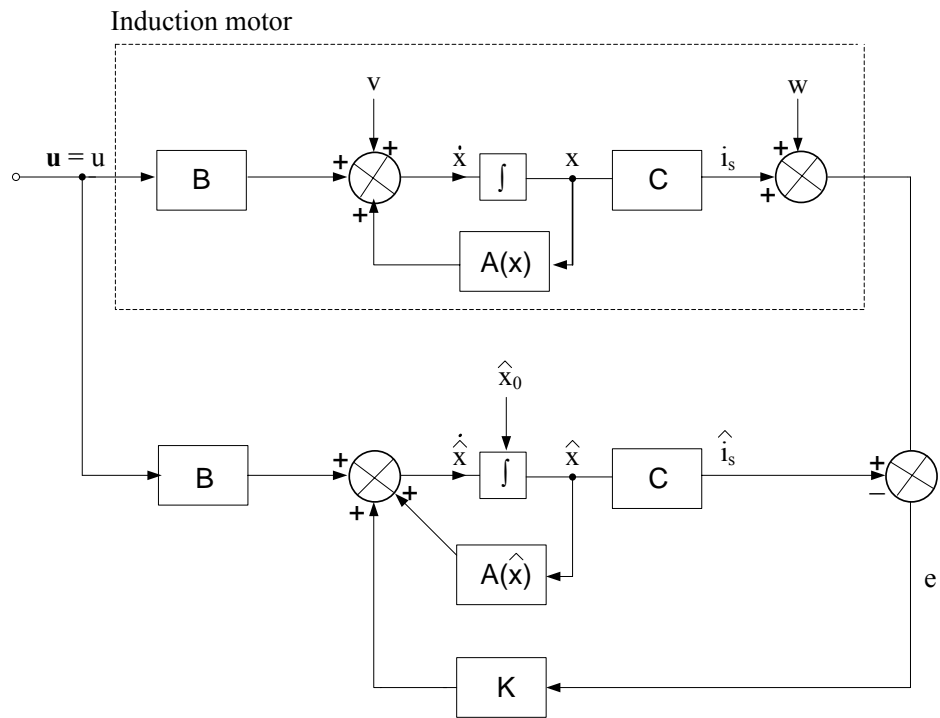
Figure 3-4 The structure of EKF algorithm

The initial-state covariance matrix can be considered as a diagonal matrix, where all the elements are equal. The initial values of the covariance matrices reflect on the degree of knowledge of the initial states. A suitable selection allows us to obtain satisfactory speed convergence, and avoids divergence problems or unwanted large oscillations.

Step 2: Prediction of the state vector

Prediction of the state vector at sampling time (k+1) from the input u(k), state vector at previous sampling time $\hat{x}$(k), by using A_d and B_d is obtained by performing

$$x^*(k+1) = A_d \hat{x}(k) + B_d u(k) \tag{3-42}$$

The notation $x^*(k+1)$ $P^*(k+1)$ and etc. mean that it is a predicted value at the (k+1)-th instant, and it is based on measurements up to the kth instant.

Step 3: Covariance estimation of prediction

The covariance matrix of prediction is estimated as,

$$P^*(k+1) = f(k+1)\hat{P}(k)f^T(k+1) + Q \tag{3-43}$$

where $\hat{P}(k)$ denotes prediction at time k based on data up to time k and f is the following gradient matrix:

$$f(k+1) = \frac{\partial}{\partial x}(A_d x + B_d u)\Big|_{x=\hat{x}(k+1)} \tag{3-44}$$

$$f(k+1) = \begin{bmatrix} 1-T/T_s^* & 0 & TL_m(\sigma L_s L_r T_r) & \omega_r TL_m/(\sigma L_s L_r) & TL_m(\sigma L_s L_r)\psi_{qr}^s \\ 0 & 1-T/T_s^* & -\omega_r TL_m/(\sigma L_s L_r) & TL_m(\sigma L_s L_r T_r) & -TL_m(\sigma L_s L_r)\psi_{dr}^s \\ TL_m/T_r & 0 & 1-T/T_r & -T\omega_r & T\psi_{qr}^s \\ 0 & TL_m/T_r & T\omega_r & 1-T/T_r & T\psi_{dr}^s \\ 0 & 0 & 0 & 0 & 1 \end{bmatrix}$$

$$\tag{3-45}$$

where $\omega_r = \hat{\omega}_r(k+1)$, $\psi_{dr}^s = \hat{\psi}_{dr}^s(k+1)$, $\psi_{qr}^s = \hat{\psi}_{qr}^s(k+1)$.

Step 4: Kalman filter gain computation

The Kalman filter gain (correction matrix) is computed as,

$$K(k+1) = P^*(k+1)h^T(k+1)\left[h(k+1)P^*(k+1)h^T(k+1) + R\right]^{-1} \tag{3-46}$$

71

where h(k+1) is a gradient matrix and defined as,

$$h(k+1) = \frac{\partial}{\partial x}(Cx)\Big|_{x=x^*(k+1)}$$

(3-47)

$$h(k+1) = \begin{bmatrix} 1 & 0 & 0 & 0 & 0 \\ 0 & 1 & 0 & 0 & 0 \end{bmatrix}$$

For the induction machine application, the Kalman gain matrix (K) contains two columns and five rows.

Step 5: State-vector estimation

The state-vector estimation (corrected state-vector estimation, filtering) at time (k+1) is performed as:

$$\hat{x}(k+1) = x^*(k+1) + K(k+1)[y(k+1) - \hat{y}(k+1)]$$

(3-48)

Where

$$\hat{y}(k+1) = Cx^*(k+1)$$

(3-49)

Step 6: Covariance matrix of estimation error

The error covariance matrix can be obtained from

$$\hat{P}(k+1) = P^*(k+1) - K(k+1)h(k+1)P^*(k+1)$$

(3-50)

Step 7: Put k = k+1, x(k) = x(k-1), P(k) = P(k-1) and go to Step 1.

The EKF described above can be used under both steady-state and transient conditions of the induction machine for the estimation of the rotor speed. By using

the EKF in the drive system, it is possible to implement a PWM inverter-fed induction motor drive without the need of an extra speed sensor. It should be noted that accurate speed sensing is obtained in a very wide speed-range, down to very low values of speed (but not zero speed). However, care must be taken in the selection of the machine parameters and covariance values used. The speed estimation scheme requires the monitored stator voltages and stator currents. Instead of using the monitored stator line voltages, the stator voltages can also be reconstructed by using the d.c. link voltage and inverter switching states, but especially at low speeds it is necessary to have an appropriate dead-time compensation, and also the voltage drops across the inverter switches (e.g. IGBTs) must be considered.

The tuning of the EKF involves an iterative modification of the machine parameters and covariances in order to yield the best estimates of the states. Changing the covariance matrices Q and R affects both the transient duration and steady-state operation of the filter. Increasing Q corresponds to stronger system noises, or larger uncertainity in the machine model used. The filter gain matrix elements will also increase and thus the measurements will be more heavily weighted and the filter transient performance will be faster. If the covariance R is increased, this corresponds to the fact that the measurements of the currents are subjected to a stronger noise, and should be weighted less by the filter. Thus the filter gain matrix elements will decrease and this results in slower transient performance. Finally, it should be noted that in general, the following qualitative tuning rules can be obtained:

Rule 1: If R is large then K is small (and the transient performance is faster).

Rule 2: If Q is large then K is large (and the transient performance is slower). However, if Q is too large or if R is too small, instability can arise.

It is possible to derive similar rules to these rules, and to implement a fuzzy-logic-assisted system for the selection of the appropriate covariance elements.

In summary it can be stated that the EKF algorithm is computationally more intensive than the algorithm for the full-order state observer described in the previous section. The EKF can also be used for joint state and parameter estimation. It should

be noted that in order to reduce the computational effort and any steady state error, it is possible to use various EKFs, which utilize reduced-order machine models and different reference frames.

CHAPTER 4

SIMULATIONS AND EXPERIMENTAL WORK

4.1 Experimental Work

4.1.1 Induction Motor Data

A squirrel cage induction motor with electrical name plate data shown in Table 4-1 has been used in experiments.

Table 4-1 Induction motor electrical data

SIEMENS 1LA7107-4AA1	
	Manufacturer Specification
Frequency	50 Hz
Nominal Voltage	400 Vrms
Nominal Current	6.4 Arms
Nominal Power	3 kW
Power Factor	0.82
Nominal Speed	1420 rpm
Nominal Torque	20 Nm
Motor Inertia	0.05 kgm^2
Number of Poles	4

Parameters of the induction motor are needed to be known in implementing the speed adaptive flux observer. These are shown in Table 4-2.

Table 4-2 Induction motor parameters

SIEMENS 1LA7107-4AA1		
	Test Result	**Manufacturer Specification**
Rotor resistance per phase (referred)	2.19 Ω	1.658 Ω
Stator resistance per phase	1.80 Ω	2.037 Ω
Stator self inductance per phase	0.192 H	0.24268 H
Rotor self inductance per phase	0.192 H	0.23379 H
Magnetizing inductance	0.184 H	0.22885 H

The per unit values related to direct on-line starting are given at Table 4-3. Manufacturer provided direct on-line starting curves for the induction motor are shown in Figure 4-1 - Figure 4-3.

Table 4-3 Direct on-line starting per unit definitions

SIEMENS 1LA7107-4AA1	
	Manufacturer Specification
Per Unit Speed	1420 rpm
Per Unit Torque	14.8 Nm
Per Unit Power	2.2 kW

Table 4-3 (Cont'd)

Moment of Inertia at Start-up	0.05 kgm^2
Input Voltage	400 V
Frequency	50 Hz

The direct on-line starting moment versus motor speed graph is illustrated at Figure 4-1.
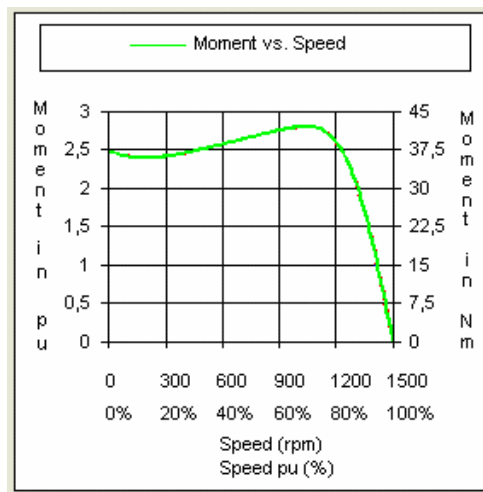
Figure 4-1 The direct on-line starting moment vs motor speed graph

The direct on-line starting motor current versus motor speed at given load condition is given at Figure 4-2.
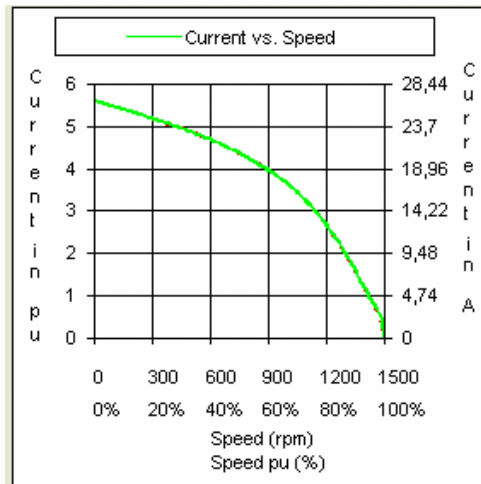
Figure 4-2 The direct on-line starting motor current vs motor speed graph

The direct on-line starting time versus motor speed at given load condition is given at Figure 4-3. The per unit valuıes related to direct on-line starting are given at Table 4-3. Manufacturer provided direct on-line starting curves for the induction motor which are shown in Figure 4-1 - Figure 4-3
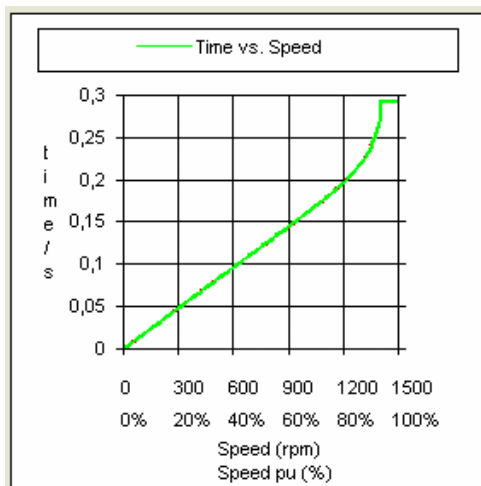
Figure 4-3 The direct on-line starting time vs motor speed graph

78

4.1.2. Experimental Set-up

The schematic block diagram of the experimental set-up is illustrated at Figure 4-4.
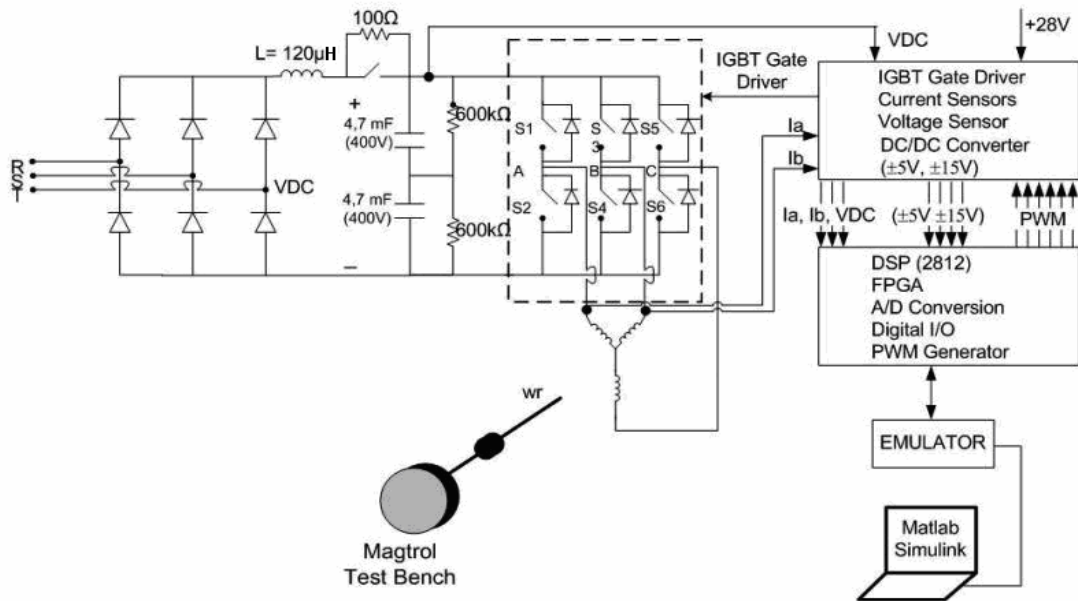
Figure 4-4 The schematic block diagrams of experimental set-up

The rectifier used in this drive is bridge rectifier which is 450V, 28A that consists of six uncontrolled diodes and produced by IXYS. The three-phase voltage is supplied over a digitally controlled three-phase supply.

The rectified output voltage is filtered by two dc-link capacitors each being 4700 μF (400V) and connected in series. 600 KΩ, 0.6 W resistors are connected across each capacitor for proper voltage sharing.

The voltage across the capacitors is raised by charging them over a 100 Ω soft start resistor to limit the in-rush current at starting. Upon the capacitors are charged to a predefined level, a relay shorts the two ends of the resistor so that the rectifier output voltage is applied directly onto the capacitors.

A motor drive electronics card is used to drive inverter circuit IGBTs. This drive circuit incorporates an IGBT voltage source inverter, an IGBT gate driver, phase current sensors, a dc-link voltage sensor, DC/DC converters which are needed by control electronics and signal interface adaptation circuits.

The inverter used in the drive system is Semikron IGBT module (SKM 40 GDL 123 D) with rated values of 1200V and 40 A. IGBTs in this module are driven by a gate drive electronic module, Concept Scale Driver (Scale Driver 6SD106E). The module provides over-current and short-circuit protection for all six IGBTs in the full bridge by real-time tracking of the collector-emitter voltage of the switches.

The dc-link voltage is measured with a voltage sensor (LEM LV25-P) at the motor drive electronics card. The magnitude of the dc-link voltage is measured to reconstruct the phase voltages in the control software with the information of PWM cycles.

The other measured variables are stator phase currents. For this purpose (LEM LA 25-NP), current transducers are used. These sensors are capable of sensing AC, DC and mixed current waveforms. The sensor has multi-range current sensing options depending on the pin connections. The sensors use hall-effect phenomena to sense the current. The output of these sensors is between ±15V and unipolar.

The PWM signals generated by DSP are amplified at the motor drive electronics card to make them compatible with the gate drive module inputs. Moreover, the errors (gate drive card errors such as short-circuit error, over-current error, and an external interrupt) are monitored in order to stop IGBT operation.

In order to verify the estimator performance of the induction motor, an incremental encoder is mounted on the rear side of the shaft to determine real rotor speed. The encoder is 1440 pulses/rev (Us Digital Corp. E2 – Optical Kit Encoder).

The real-time experiments have been carried out by the use of electronic control card including mainly TI TMS320F2812 digital signal processor, XILINX XCS2S150E Field Programmable Gate Array (FPGA), various chips which enable transformations from analog to digital or vice versa and supplementary circuits. In order to run the real-time control algorithm and create PWM signals, Texas

Instruments' TMS320 processor is used in this work. The F2812 is a member of the "C2000 DSP" platform, and is optimized specifically for motor control applications. It uses a 16-bit word length along with 32-bit registers. The F2812 has application-optimized peripheral units, coupled with the high-performance DSP core, enables the use of advanced control techniques for high-precision and high-efficiency full variable-speed control of motors. The event managers of F2812 include special pulse-width modulation (PWM) generation functions such as a programmable dead-band function and a space-vector PWM state machine for 3-phase motors that also provides a quite high efficiency in the switching of power transistors, quadrature encoder pulse circuit module to read encoder signals. F2812 also contains 16 channels, 12-bit A/Ds, enhanced controller area network (eCAN), serial communication interface (SCI) and general purpose digital I/Os (GPIO) as peripherals. XILINX XCS2S150E Field Programmable Gate Array (FPGA) is used for logical operations and external memory access.

Magtrol test bench is used for applying load torque. Magtrol test bench includes hysteresis load, torque analyser, power analyzer, signal amplifier and graphical user interfece. The load characteristics of magtrol test bench are tuned in order to ensure proper load characteristics. The tuned load response is given at Figure 4-5.
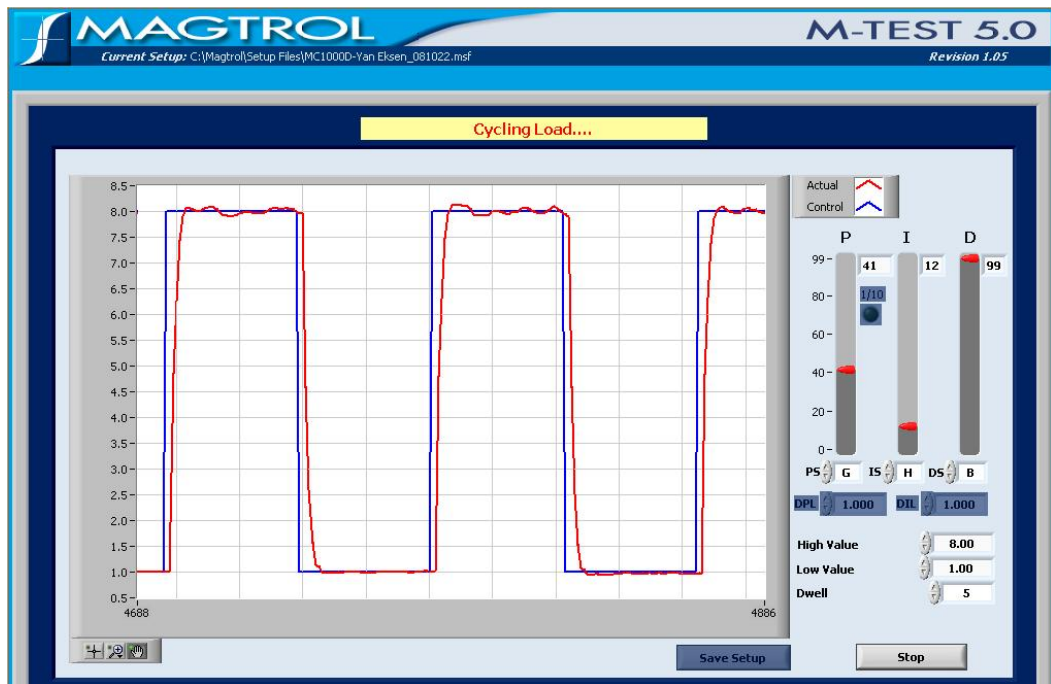
Figure 4-5 The Magtrol test bench load response

The pictures of experimental set-up are given at Figure 4-6.

Figure 4-6 The experimental set-up

4.1.3 Experimental Results of Speed Adaptive Flux Observer

The induction motor parameters at Table 4-2 are used at the experimental stage of the speed adaptive flux observer.

The speed estimator designed with speed adaptive flux observer has been tested experimentally for satisfactory operation at different speeds of motor.

The control parameters used at the speed adaptive flux observer experiments are listed at Table 4-4.

Table 4-4 Control parameters used at the speed adaptive flux observer experiments

I_{ds}^{e*} Current Regulator	K_I	194
	K_P	1
I_{qs}^{e*} Current Regulator	K_I	1
	K_P	194
ω_r Speed Requlator	K_I	0.08
	K_P	0.005
Adaptive Scheme Gain	K_I	800
	K_P	4

4.1.3.1 No-Load Experiments of Speed Adaptive Flux Observer

In these no-load experiments, motor is run in the closed- loop speed mode and the quadrature encoder coupled to the shaft of the motor is utilized in order to verify the estimated speed. Log of the mechanical rotor angle, the estimated speed, and the actual speed are taken for 50rpm, 100rpm, 500rpm, 1000rpm and 1500rpm constant speed request. The speed estimate derived from actual rotor (quadrature encoder) position is given as dotted line.

Speed command, real rotor speed and estimated rotor speed for 50rpm, 100 rpm, 500 rpm 1000 rpm and 1500 rpm cases are respectively represented at Figure 4-7 to Figure 4-11.
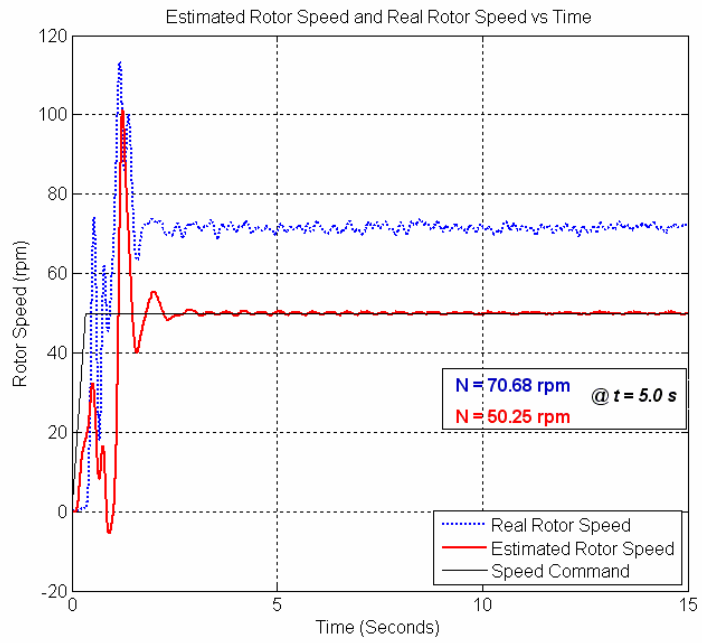
Figure 4-7 50 rpm speed reference, motor speed estimate
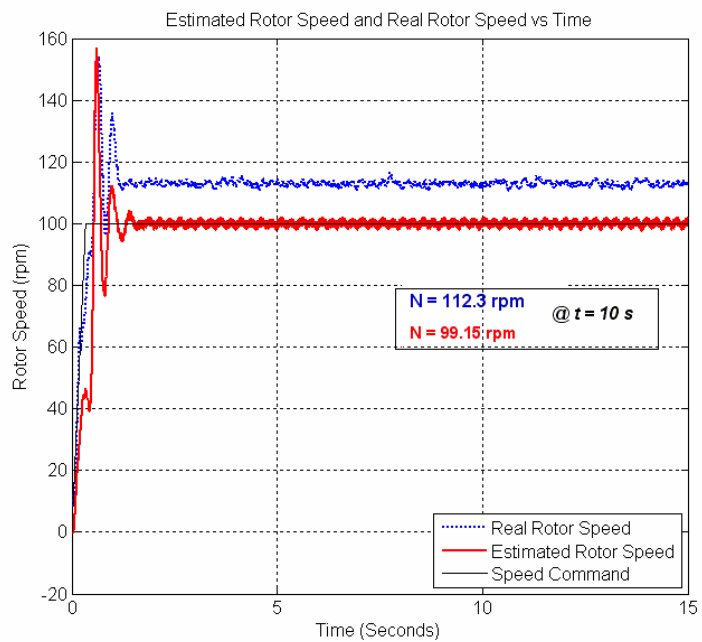
Figure 4-8 100 rpm speed reference, motor speed estimate

85

It can be seen from Figure 4-7 and Figure 4-8, no-load speed estimation performance of speed adaptive flux observer is not satisfactory at low speeds such as 50 rpm and 100 rpm. Also, it is observed that once the speed is increased to 100 rpm, speed estimation error percentage decreases from 40 % to 10%. By considering equations (2-37) and (3-15), the speed estimate of speed adaptive flux observer is derived from torque error representation. Since the torque error is very small at no-load case, the speed estimates at no-load has lower performance. This results in performance decrease due to the poor flux estimator characteristic at low speeds. In addition to that, it is particularly at lower speeds that motor parameter variations have significant influence on steady state and dynamic performance of the drive system.
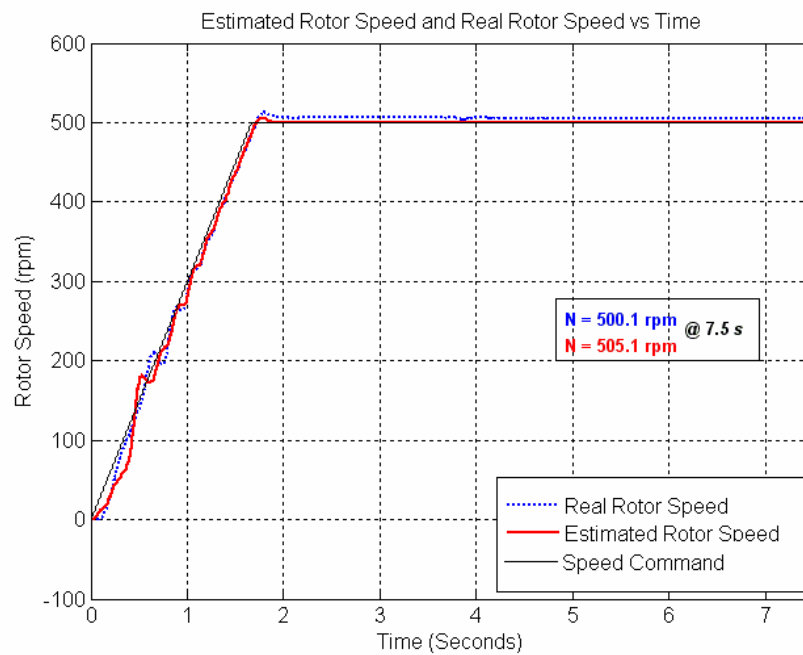
Figure 4-9 500 rpm speed reference, motor speed estimate
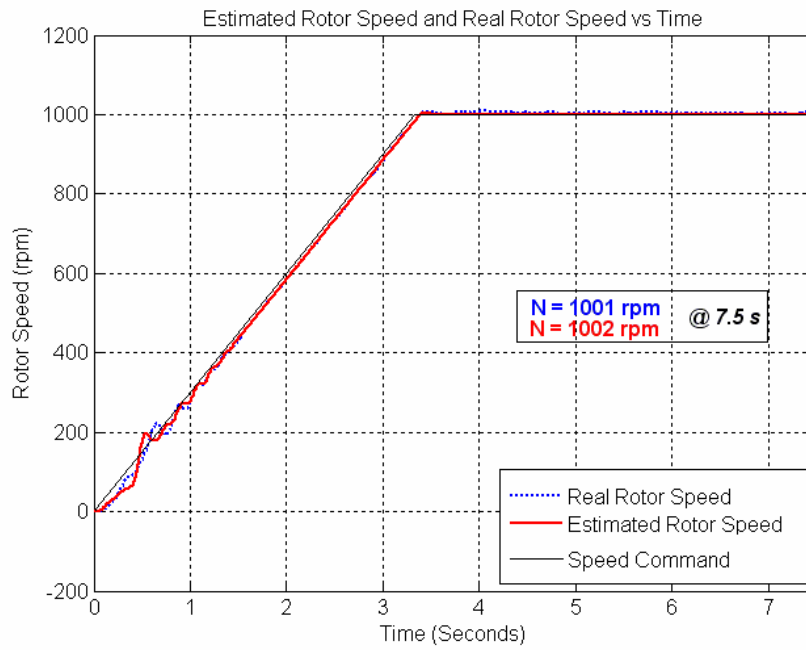
Figure 4-10 1000 rpm speed reference, motor speed estimate
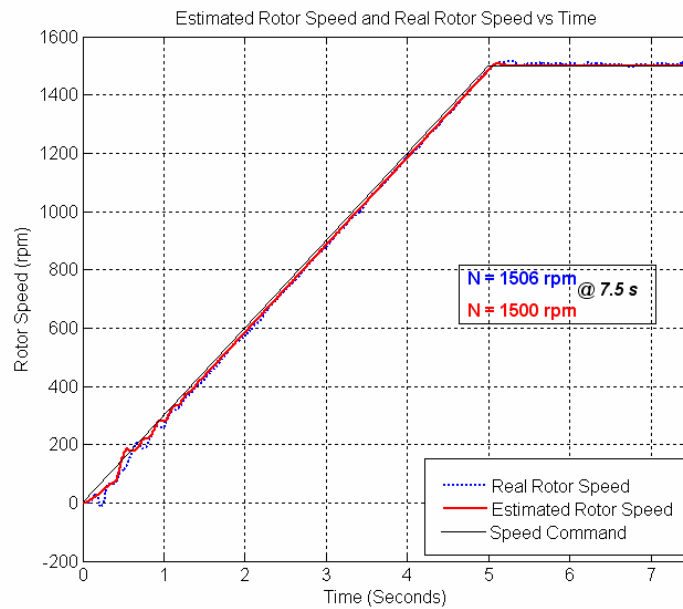
Figure 4-11 1500 rpm speed reference, motor speed estimate

It can be seen from Figure 4-9 to Figure 4-11 that no-load speed estimation performance of speed adaptive flux observer is satisfactory at speeds higher than 100 rpm. It is observed from Figure 4-9 to Figure 4-11. The observed speed estimator error is less than 1 % at at speeds higher than 100 rpm.

In Figure 4-13 to Figure 4-12, quadrature encoder position, phase currents, and voltages are given for 50rpm case.
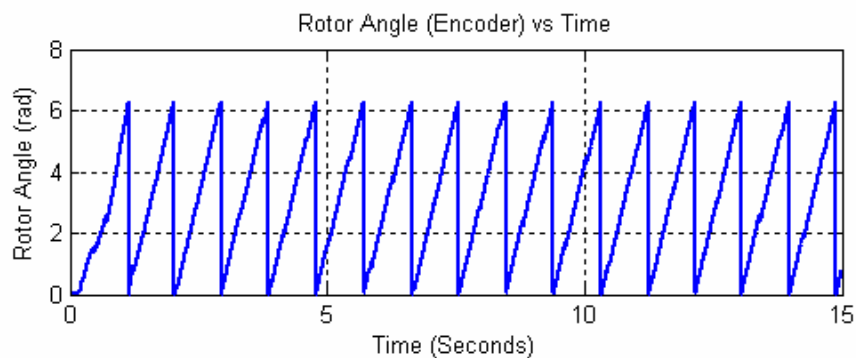
Figure 4-12 50 rpm speed reference, motor quadrature encoder position
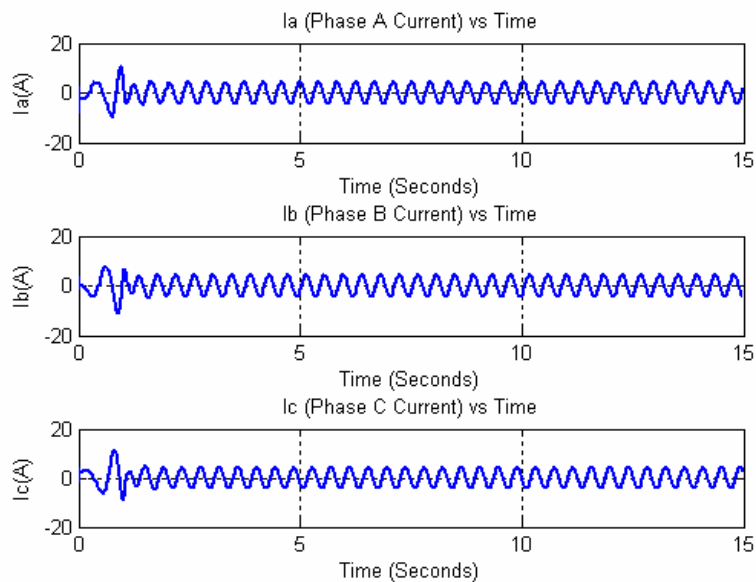
Figure 4-13 50 rpm speed reference, motor phase currents
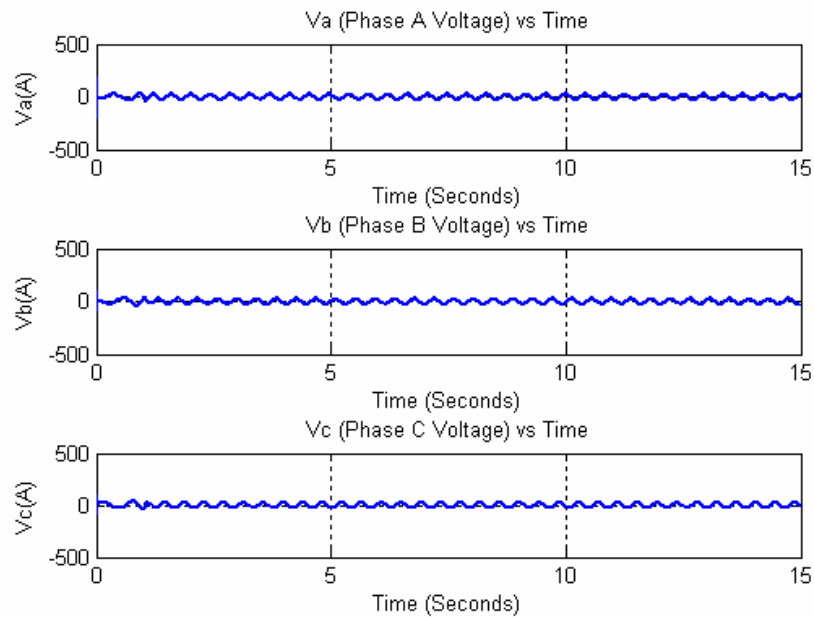
Figure 4-14 50 rpm speed reference, motor phase voltages

The figures from Figure 4-9 to Figure 4-11 demonstrate that stator phase currents and phase voltages are sinusoidal and the quadrature encoder position data are consistent with the estimated speed.

4.1.3.2. The Speed Estimator Performance under Switched Loading

In this section, the performance of the drive system is investigated under switched loading. The loading is obtained by using the Magtrol dynamometer coupled to the shaft of the induction motor.

The Magtrol load dynamometer has following properties:

T_{max} = 56 Nm,

P = 8 kW

Load experiments are at 50rpm, 100 rpm, 500rpm, 1000rpm and 1500rpm constant speed references. Load experiments are carried out with the same conditions;

however, the load is switched on and off. The Table 4-5 shows the references and corresponding measurements under loading.

Table 4-5 Loading measurements

Speed Reference (rpm)	Real Rotor Speed (rpm)	Estimated Speed (rpm)	Load T_{load}(Nm)
50	46.19	50.52	10
100	102.7	100.4	10
500	503.4	499.9	10
1000	999.8	1000	10
1500	1499	1500	8

Speed command, real rotor speed and estimated rotor speed for 50rpm, 100 rpm, 500 rpm 1000 rpm and 1500 rpm cases at Figure 4-15, Figure 4-17, Figure 4-19, Figure 4-21 and Figure 4-23 respectively. The load profiles are added to speed response at Figure 4-16, Figure 4-18, Figure 4-20, Figure 4-22 and Figure 4-24.
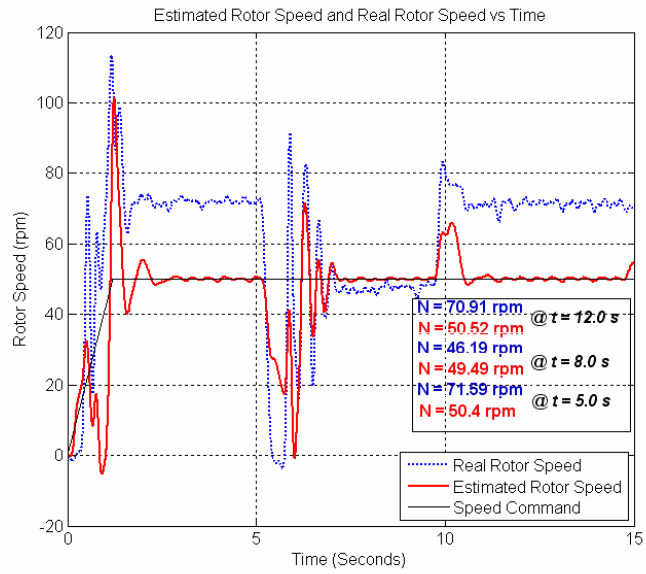
Figure 4-15 50 rpm speed reference, motor speed estimate under switched loading-1
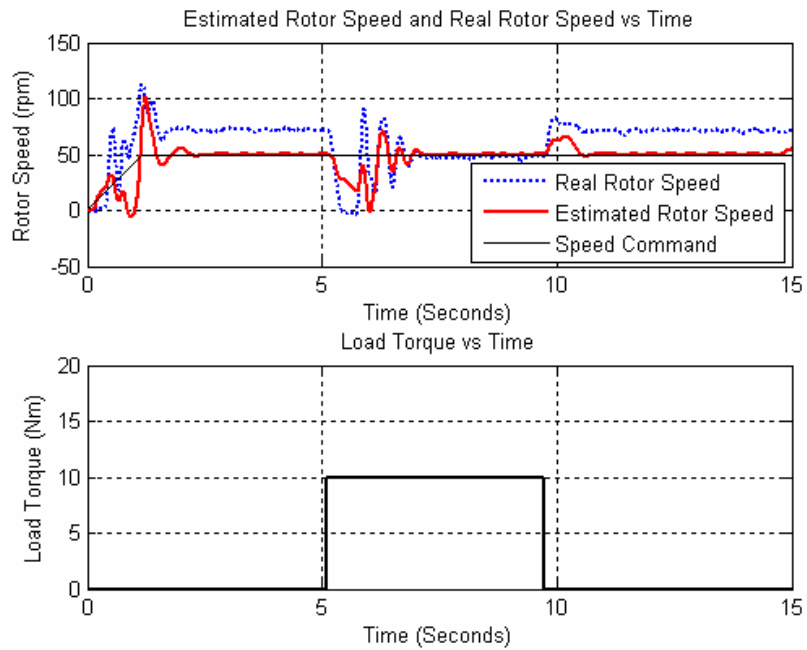
Figure 4-16 50 rpm speed reference, motor speed estimate under switched loading-2
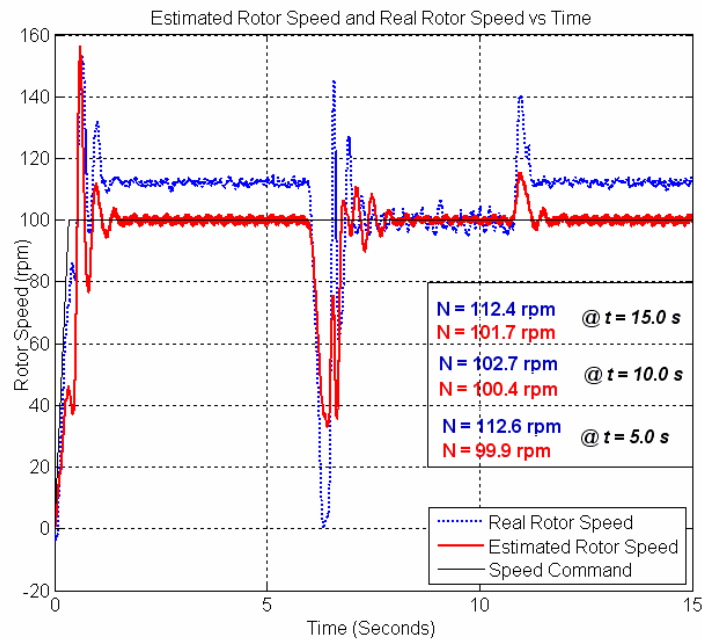
Figure 4-17 100 rpm speed reference, motor speed estimate under switched loading-1

It can be observed in Figure 4-15 and Figure 4-17 that the speed estimator performance under loading is increased when they are compared with no–load test results in Figure 4-7 and Figure 4-8. The performance increase is enabled due to significant torque error component. So, more proper speed estimation is achieved under loading at low speeds, but dynamic performance is still unsatisfactory.
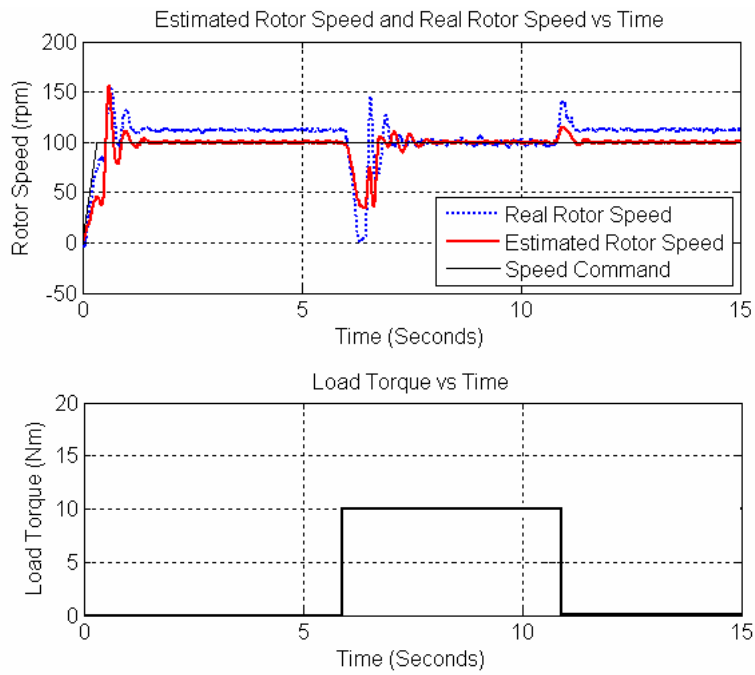
Figure 4-18 100 rpm speed reference, motor speed estimate under switched loading-2
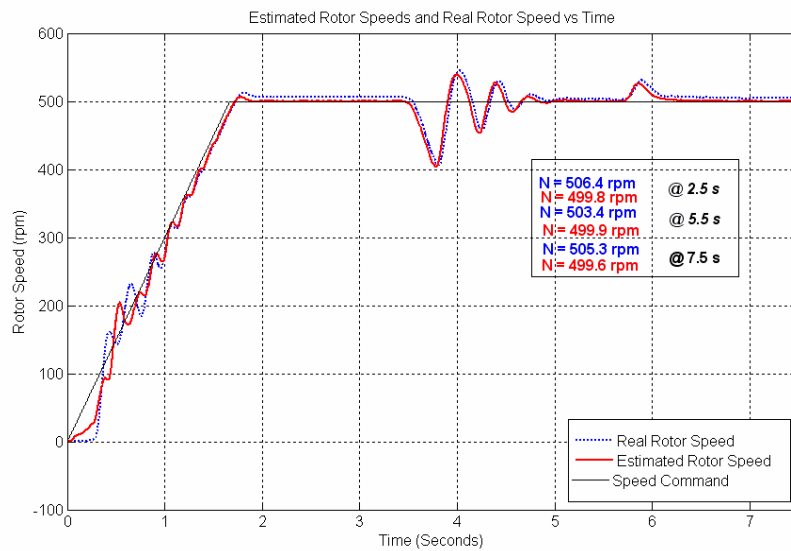
Figure 4-19 500 rpm speed reference, motor speed estimate under switched loading-1
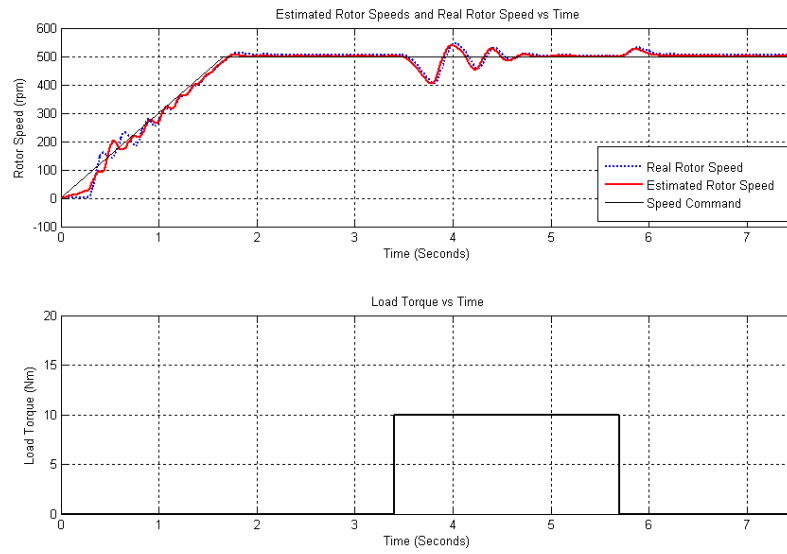
Figure 4-20 500 rpm speed reference, motor speed estimate under switched loading-2
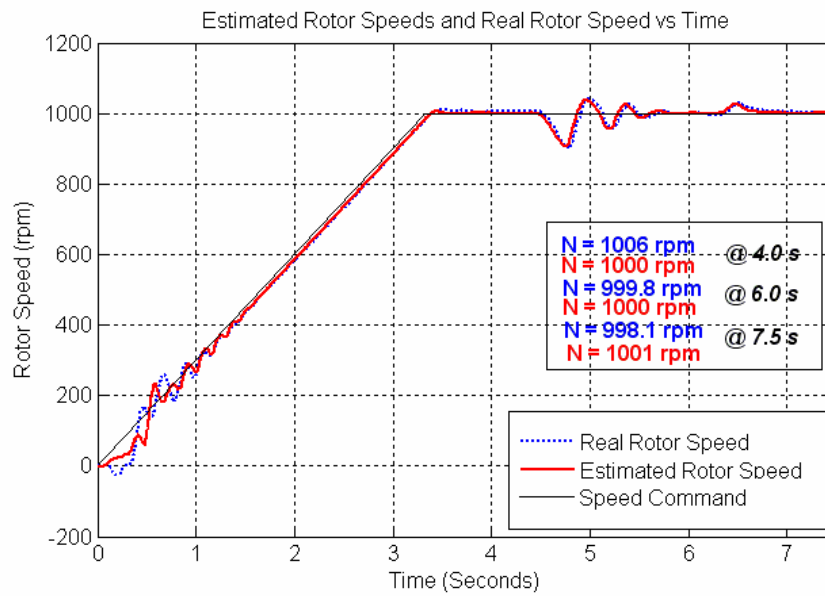
Figure 4-21 1000 rpm speed reference, motor speed estimate under switched loading-1
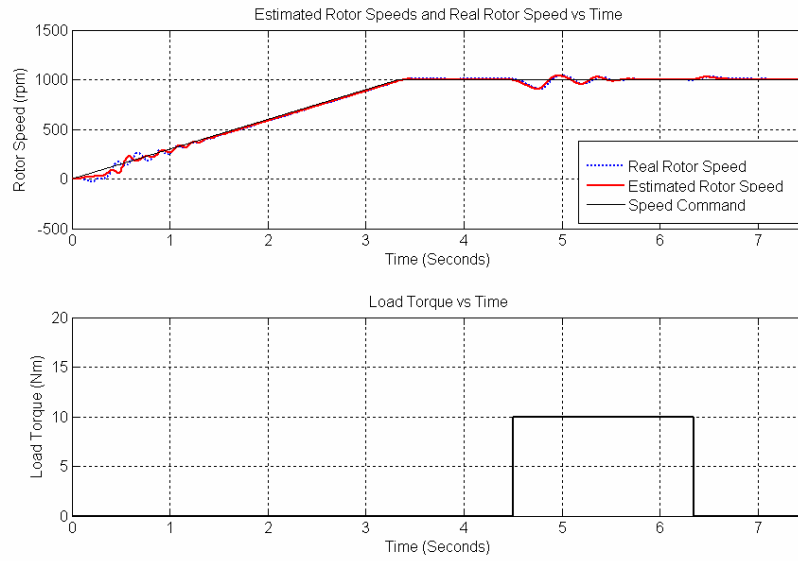
Figure 4-22 1000 rpm speed reference, motor speed estimate under switched loading-
2
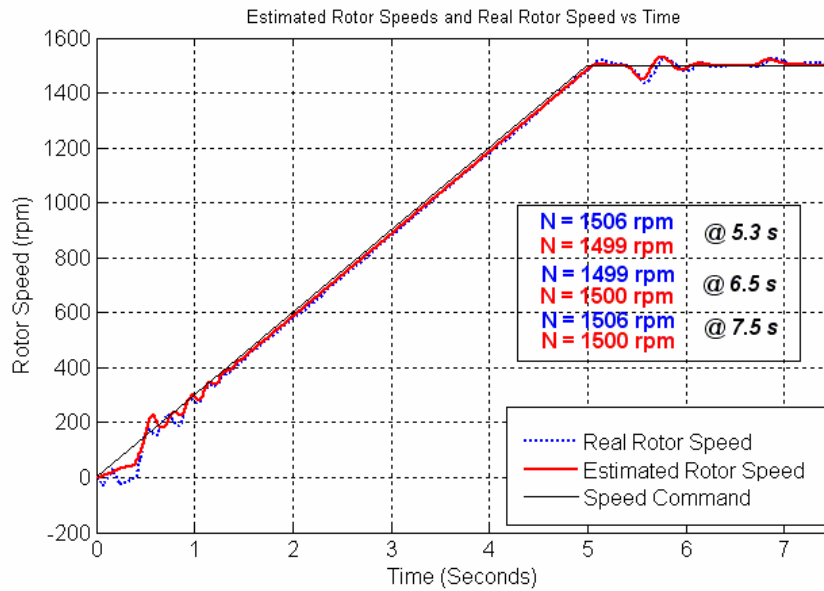
Figure 4-23 1500 rpm speed reference, motor speed estimate under switched loading-
1
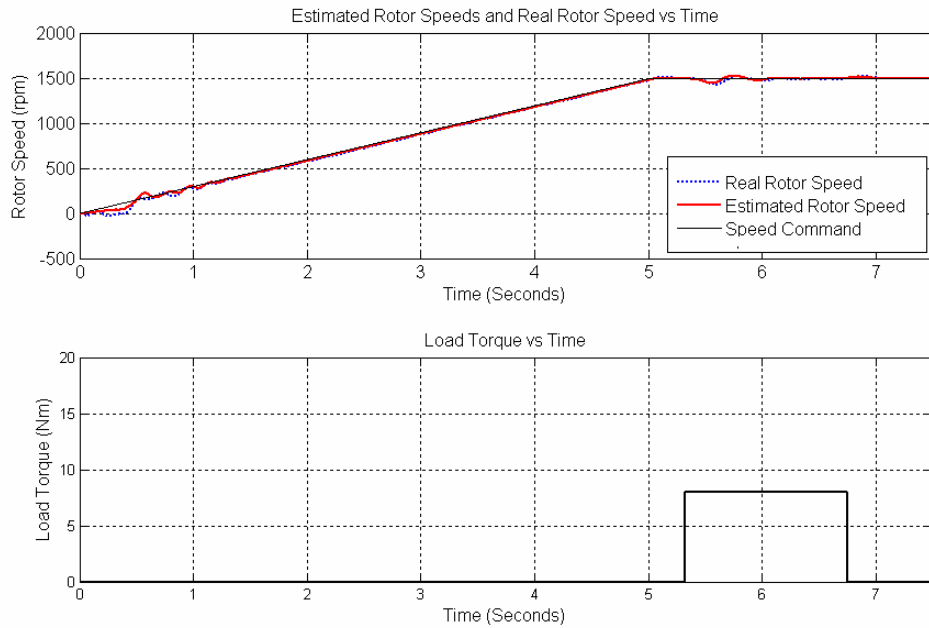
Figure 4-24 1500 rpm speed reference, motor speed estimate under switched loading-
2

At the experiments of speed adaptive flux observer, the speed variation due to switched loading is quite small and the drive system quickly reaches to the steady state. The load switching times can be seen from speed graphs for time as speed decreases.

It can be deduced from the experiments that the speed estimator performance under loading are better than no–load test results.The performance increase is enabled due to significant torque error component. Hence, more proper speed estimation is achieved under loading at low speeds.

4.1.3.3. The Speed Estimator Performance under Accelerating Load

The speed estimator performance of the speed adaptive flux observer is investigated under accelerating torque. The aim of this section is to ensure sensorless vector drive performance while accelerating load.

Speed command, real rotor speed and estimated rotor speed for 50rpm to 500rpm, 500 rpm to 750rpm and 1000 to 1250 rpm cases are represented at Figure 4-25, Figure 4-27 and Figure 4-29 respectively. The load profiles are added to speed response at Figure 4-26, Figure 4-28 and Figure 4-30.

It can be deduced from Figure 4-25 to Figure 4-30 that the acceleration under loading could be achieved by using speed adaptive flux observer algorithm.
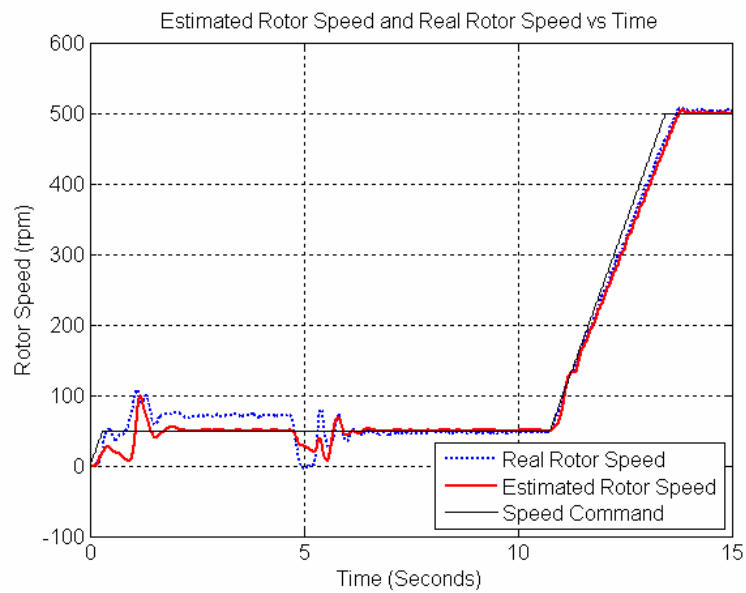
Figure 4-25 50 rpm to 500 rpm speed reference, motor speed estimate under accelerating load-1
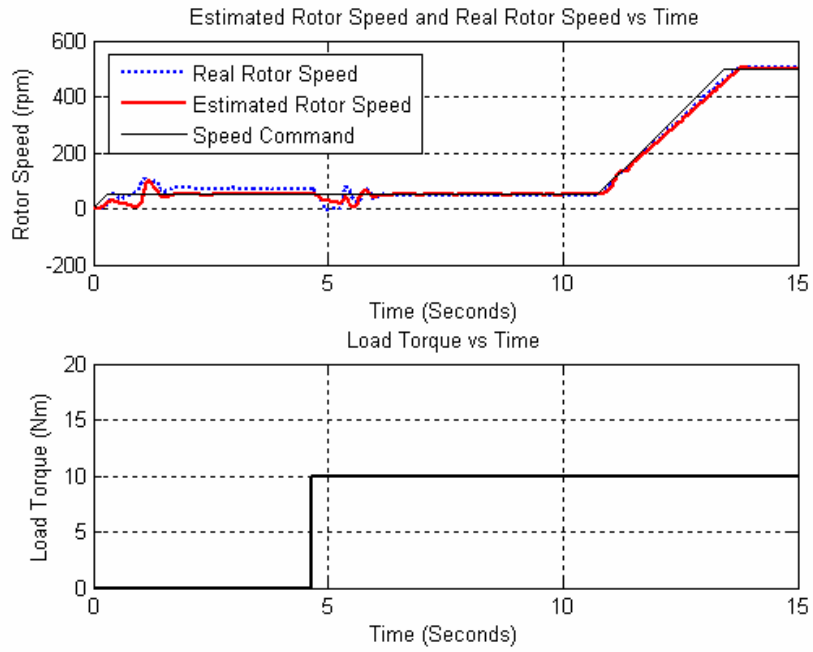
Figure 4-26 50 rpm to 500 rpm speed reference, motor speed estimate under accelerating load-2
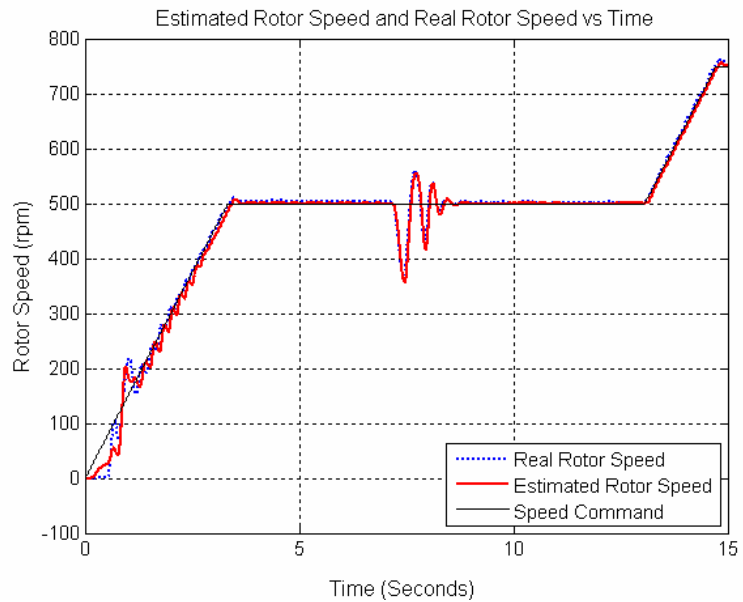
Figure 4-27 500 rpm to 750 rpm speed reference, motor speed estimate under accelerating load-1
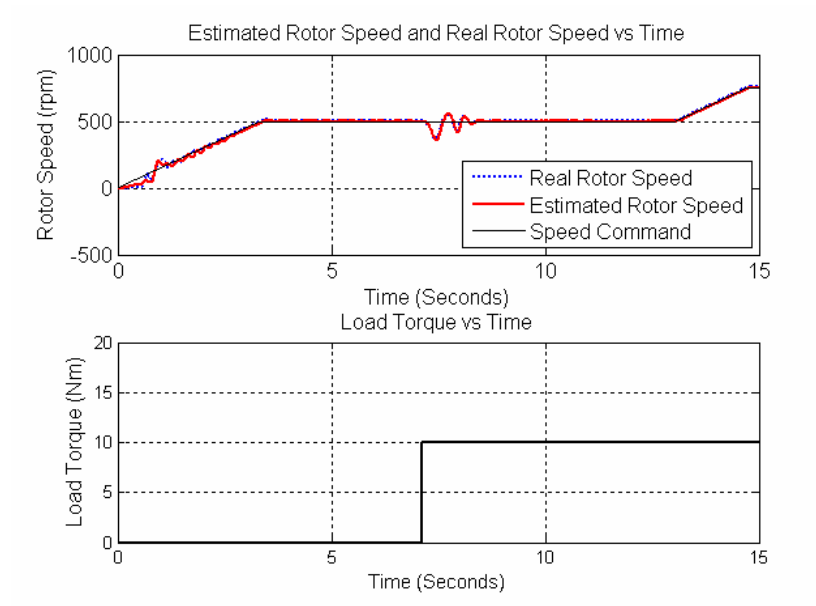
Figure 4-28 500 rpm to 750 rpm speed reference, motor speed estimate under accelerating load-2
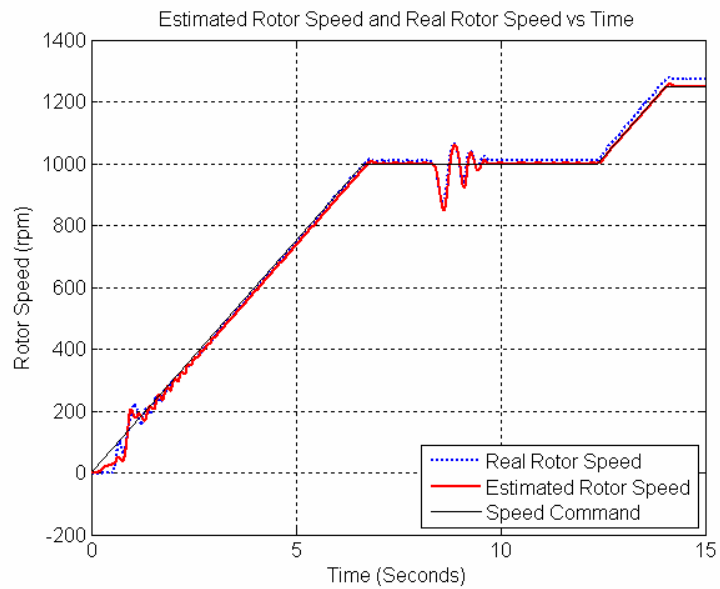
Figure 4-29 1000 rpm to 1250 rpm speed reference, motor speed estimate under accelerating load-1
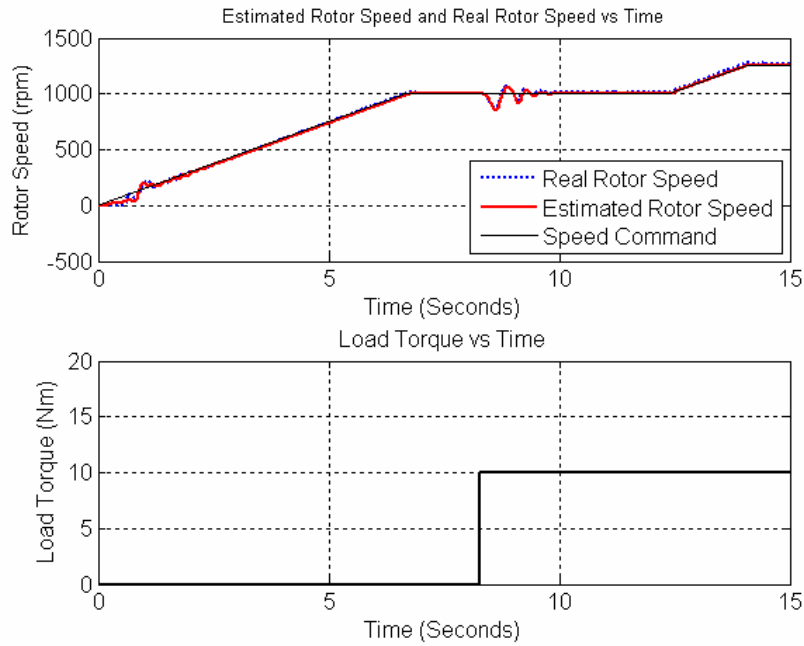
Figure 4-30 1000 rpm to 1250 rpm speed reference, motor speed estimate under accelerating load-2

4.1.3.4. The Speed Estimator Performance under No-Load Speed Reversal

The speed estimator performance of the speed adaptive flux observer is observed under no-load speed reversal. The aim of this section is to determine the performance of the speed estimator at low speeds and at zero speed while the machine is changing the direction of rotation.

Figures 4-31 – 4-33 show the speed command, real rotor speed and estimated rotor speed for different speeds. Fig.4-31 is for the operation of the machine at 50 rpm, in transition from 50 rpm to -50 rpm, and at -50 rpm.. Fig.4-32 is for the operation of the machine at 500 rpm, in transition from 500 rpm to -500 rpm, and at -500 rpm. Fig.4-33 is for the operation of the machine at 1000 rpm, in transition from 1000 rpm to -1000 rpm, and at -1000 rpm.
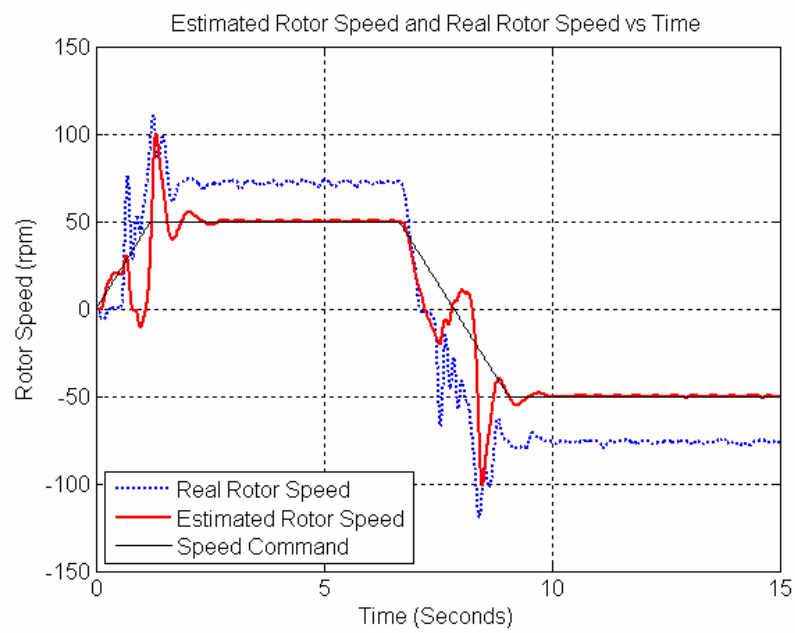
Figure 4-31 The speed reference, motor speed estimate under no-load speed reversal
for the speed range 50 rpm to -50 rpm
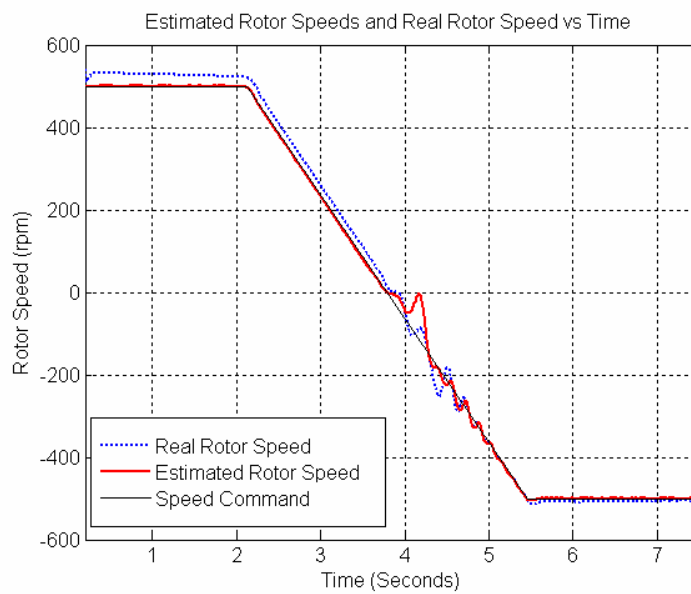
Figure 4-32 The speed reference, motor speed estimate under no-load speed reversal
for the speed range 500 rpm to -500 rpm
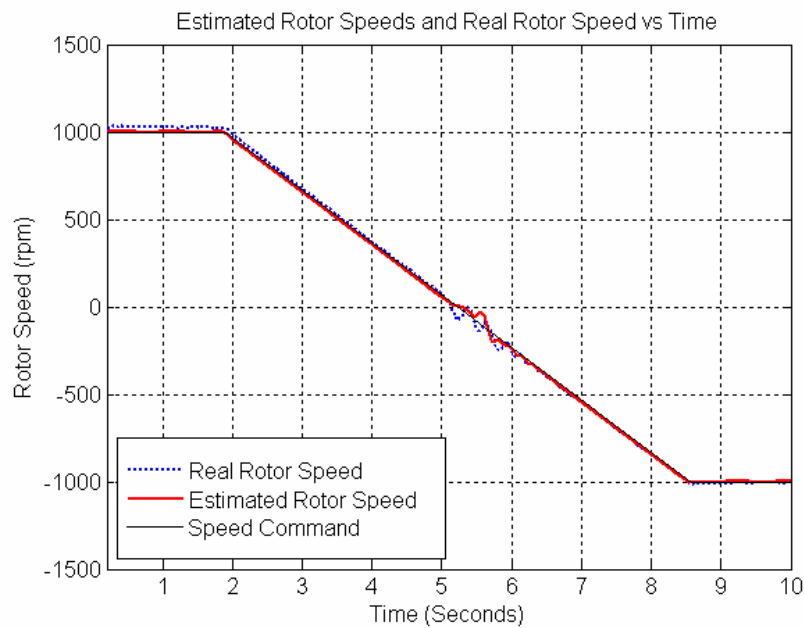
Figure 4-33 The speed reference, motor speed estimate under no-load speed reversal for the speed range 1000 rpm to -1000 rpm

As it can be seen from Figure 4-31, Figure 4-32 and Figure 4-33, both at low speeds and the zero speed crossing, speed estimator performance decreases due to the flux estimator characteristic. It should be kept in mind that phase voltages are input for speed adaptive flux estimator method and the phase voltages are almost zero at the zero speed crossing which leads the mathematical model of induction motor to be unobservable. So the speed estimation at zero speed is not possible by enabling speed adaptive flux observer.

The experiments of speed adaptive flux observer show that speed estimator based on speed adaptive flux observer has very high tracking capability for whole speed range and for no-load and with load cases. However, the speed-loop performance, the flux and the speed estimation accuracies should be improved for whole loading range and for low speeds. Improvement could be achieved by increasing the computational load of the processor. Some improvements are suggested at [28]

4.1.4 Experimental Results of Kalman Filter for Speed Estimation

The induction motor parameters at Table 4-2 are used at the experimental stage of Kalman filter for speed estimation.

The speed estimator designed with Kalman filter for speed estimation algorithm has been tested experimentally for satisfactory operation at different speeds of motor.

The control parameters used at the speed adaptive flux observer experiments are listed at Table 4-6.

Table 4-6 Control parameters used at Kalman filter for speed estimation experiments

I_{ds}^{e*} Current Regulator	K_I	49
	K_P	0.5
I_{qs}^{e*} Current Regulator	K_I	49
	K_P	0.5
ω_r Speed Regulator	K_I	0.08
	K_P	0.005
Adaptive Scheme Gain	K_I	800
	K_P	4

4.1.4.1. No-Load Experiments of Kalman Filter for Speed Estimation

In the no-load experiment, motor runs in the closed-loop speed control mode and the quadrature encoder coupled to the shaft of the motor is utilized in order to verify the estimated speed. The output of Kalman filter for speed estimation is utilized as

speed feedback. Logs of the mechanical rotor angle, the estimated and the actual speeds are kept for constant speed requests of 50rpm, 100rpm, 250 rpm, 500rpm, 1000rpm and 1500rpm. The speed estimate derived from actual rotor (quadrature encoder) position is given as dotted line.

Figure 4-34 to Figure 4-39 show the time variations of the set speed, the real and the estimated rotor speeds for 50rpm 100 rpm, 250rpm, 500 rpm 1000 rpm and 1500 rpm. .

Since Kalman filter for the speed observer requires the use of the estimated flux data derived from the speed adaptive flux estimator, the output performance of the Kalman estimator is bounded by the accuracy in the flux estimation and the accuracy of the speed observer. Since the adaptive scheme is internally corrected by speed estimation of the flux observer, there is no direct correlation between speed adaptive flux estimation scheme and Kalman filter for speed estimation. So, closed-loop adaptive scheme is not statisfied. In other words, the flux observer is independent of the closed-loop speed feedback which may lead to poorer performance of Kalman filter for speed estimation compared to the estimated speed output of the speed adaptive flux observer.
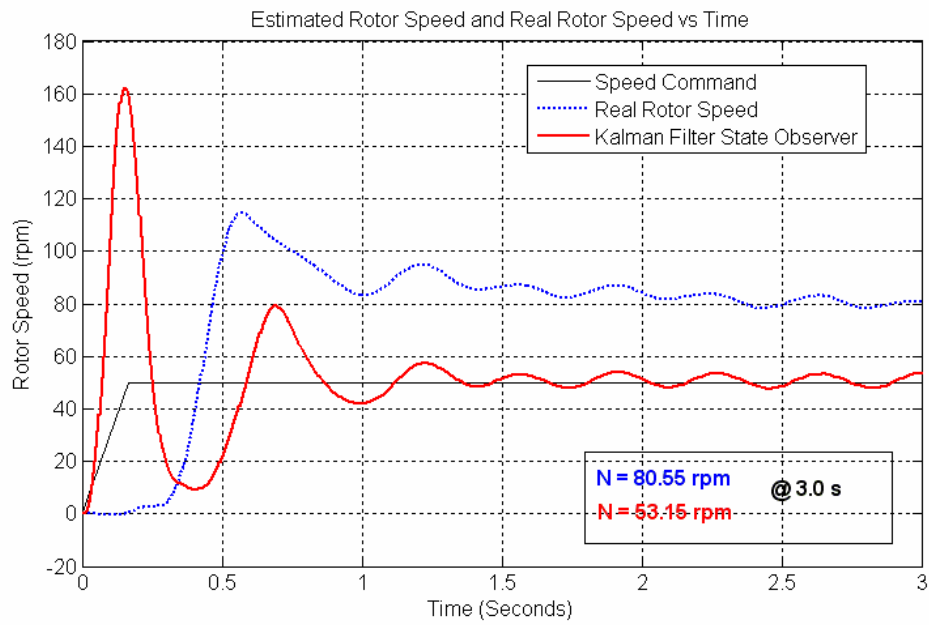
Figure 4-34 50 rpm speed reference, motor speed estimate
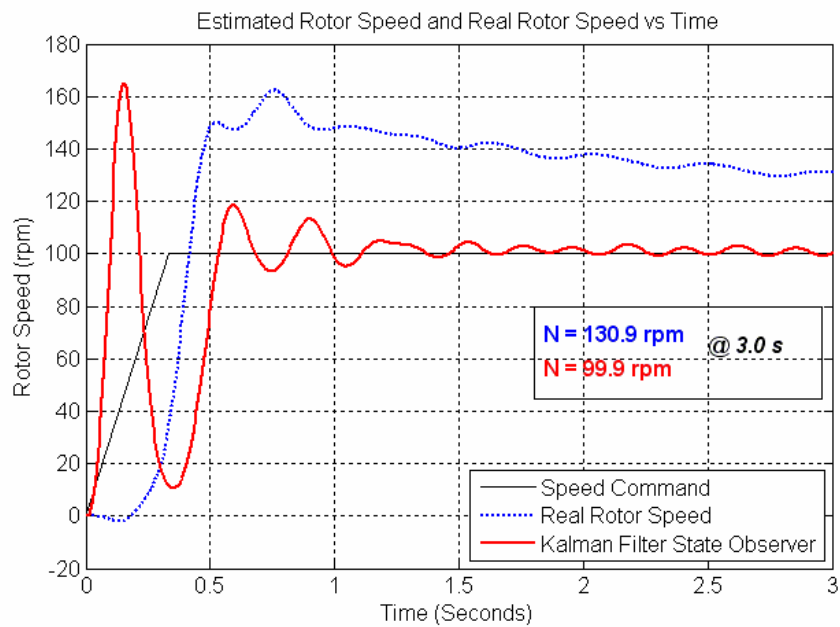
Figure 4-35 100 rpm speed reference, motor speed estimate
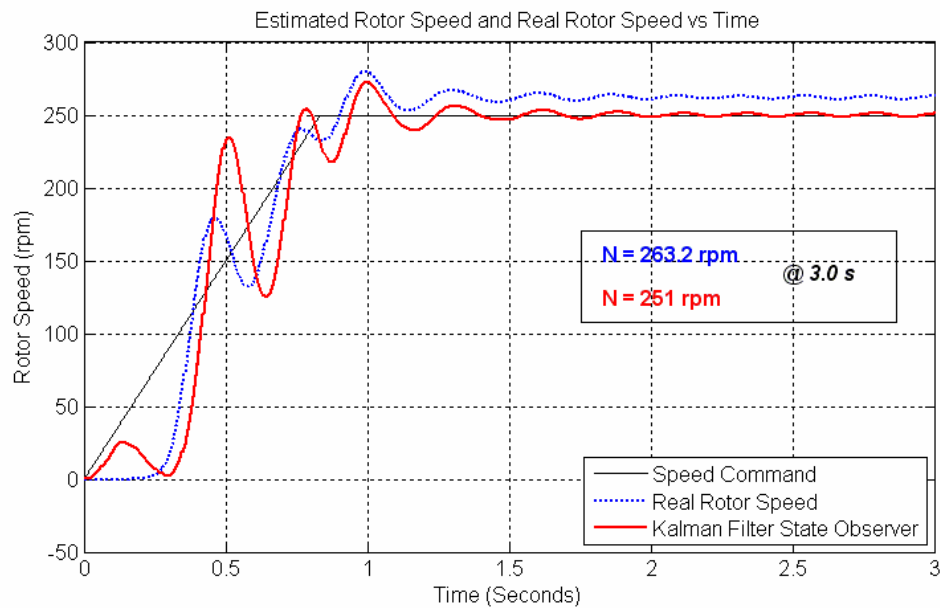
Figure 4-36 250 rpm speed reference, motor speed estimate

As it can be seen in Figure 4-34 - Figure 4-36, the no-load closed-loop speed estimation performance of the Kalman filter state observer is poorer than the performance of the speed adaptive flux observer. The speed curves at start up are more oscillatory, and the steady state offset is higher than that in the speed adaptive flux observer.

It is observed that once the speed increases the percentage error state in the speed estimation decreases at steady-state. Note that the percentage speed estimation errors at steady-state for 50 rpm and 100 rpm speed commands in Figs.4-34 and 4-35 are 60% and 31%, respectively.
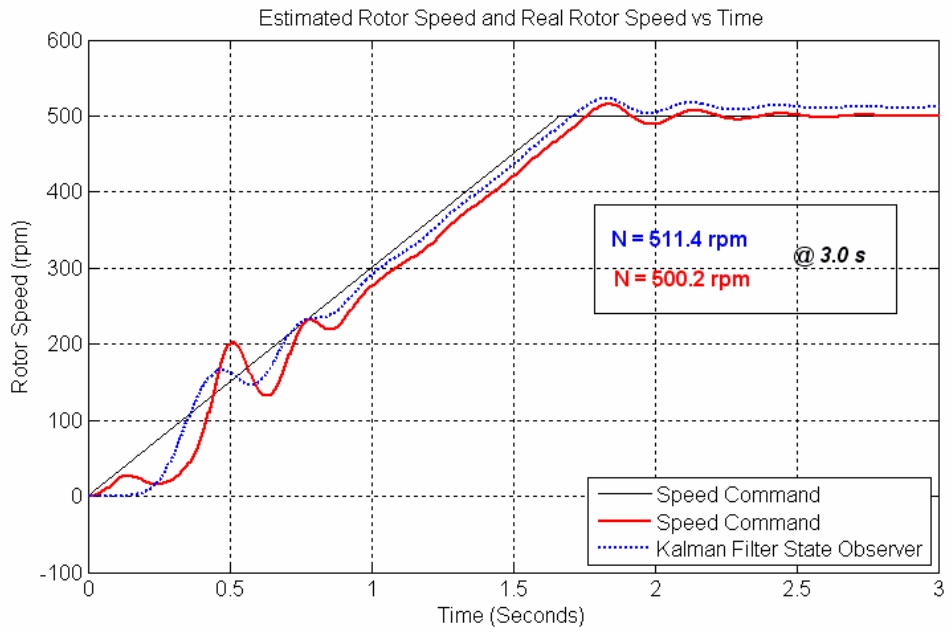
Figure 4-37 500 rpm speed reference, motor speed estimate
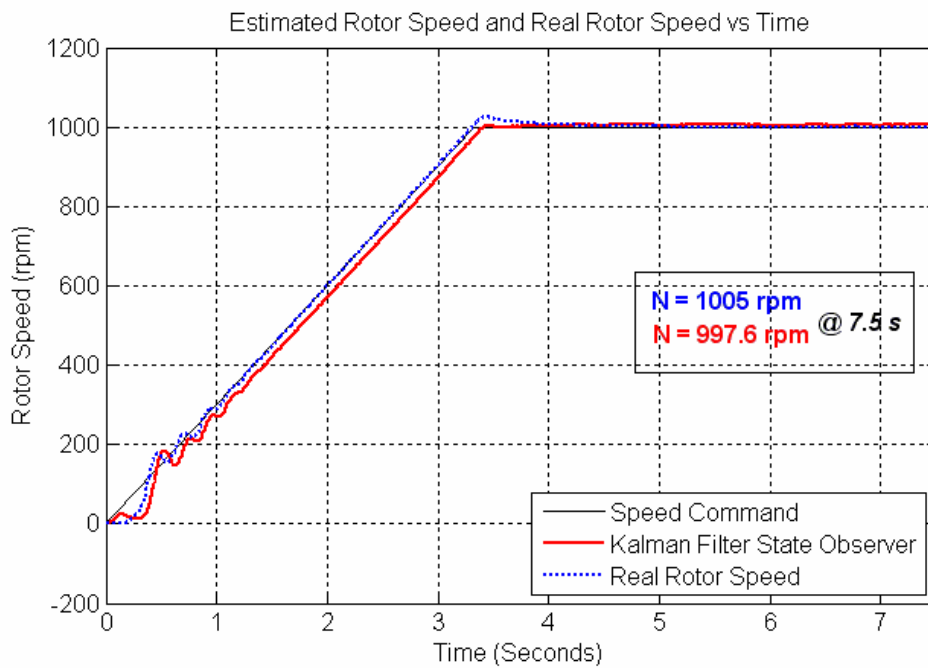
Figure 4-38 1000 rpm speed reference, motor speed estimate
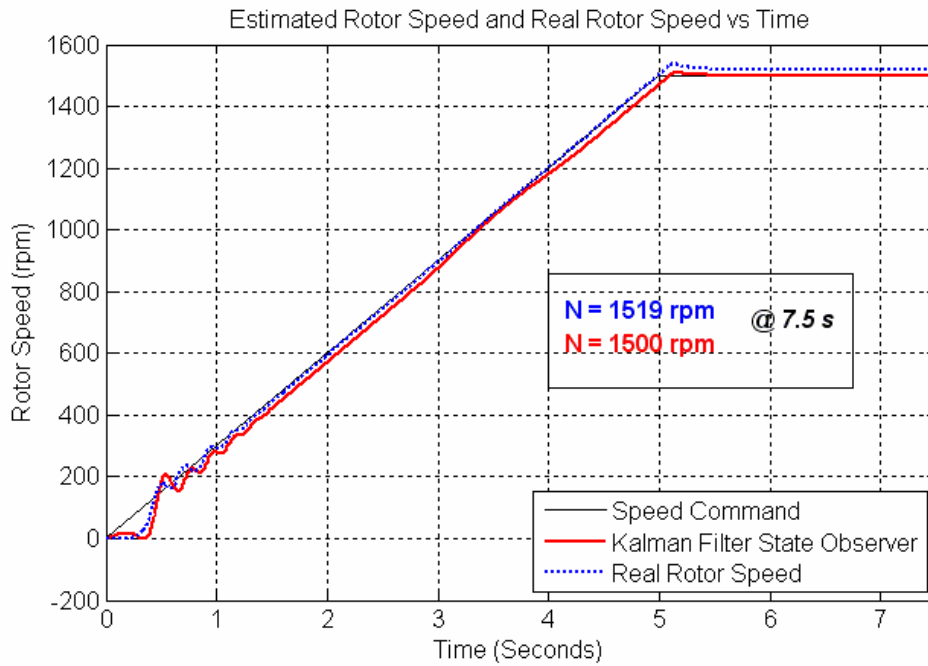
Figure 4-39 1500 rpm speed reference, motor speed estimate

It can be seen from Figure 4-37 to Figure 4-39 that no-load speed estimation performance of Kalman state observer is increased at speeds higher than 250 rpm. It is observed from Figure 4-37 to Figure 4-39 that speed estimator error percentage is less than 3 % at at speeds higher than 250 rpm.

From Figure 4-40 to Figure 4-42, quadrature encoder position, phase currents and voltages are given for 50rpm case.
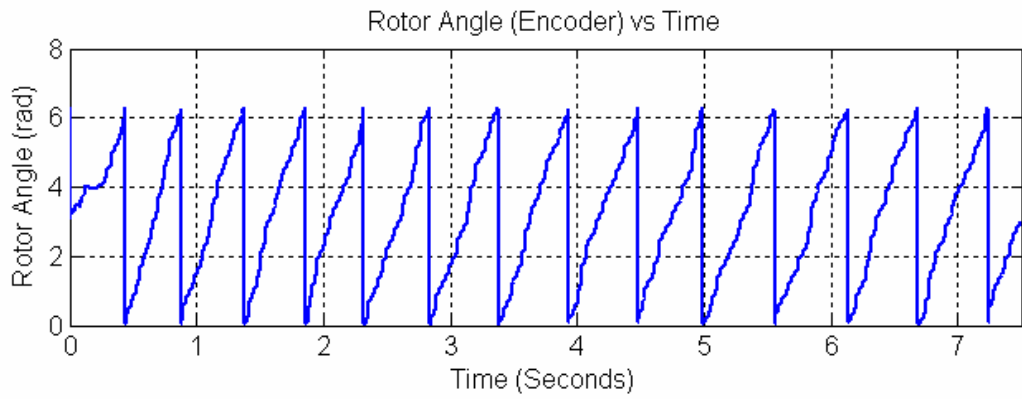
Figure 4-40 50rpm speed reference, motor quadrature encoder position
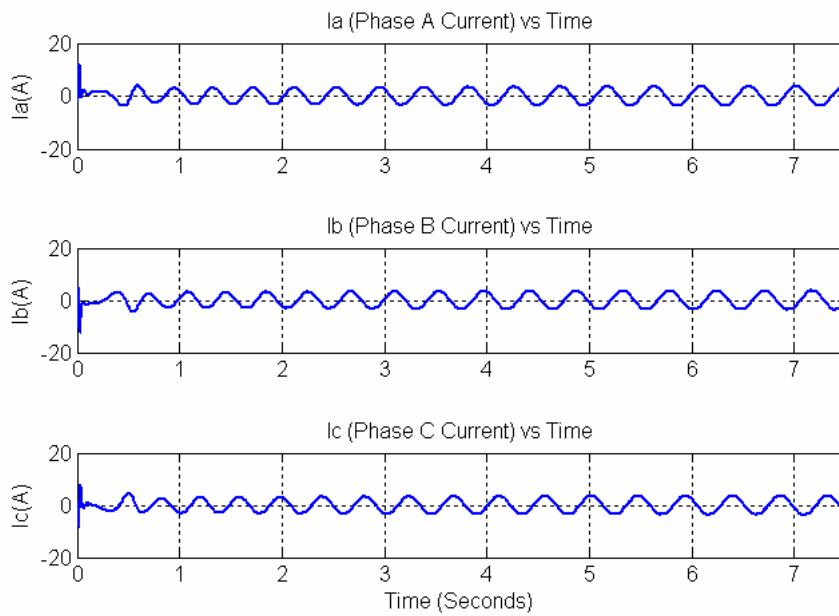
Figure 4-41 50 rpm speed reference, motor phase currents
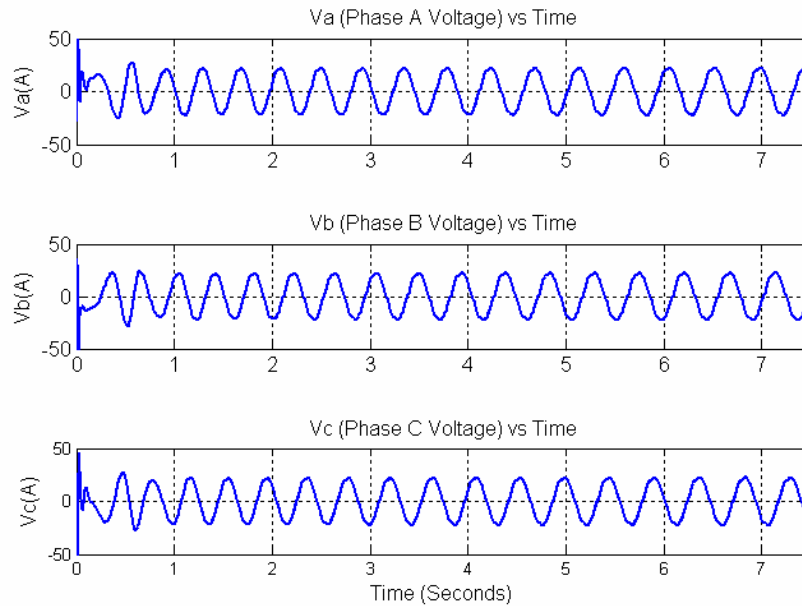
Figure 4-42 50 rpm speed reference, motor phase voltages

Figure 4-40 to Figure 4-42 demonstrate that the stator phase currents and phase voltages are sinusoidal and the quadrature encoder position data are consistent with the estimated speed.

4.1.4.2. The Kalman Filter for Speed Estimation Performance under Switched Loading

This section investigates the performance of the drive system under switched loading conditions. The loading pattern is obtained by using the Magtrol dynamometer coupled to the shaft of the induction motor.

Figures 4-43 – 4-51 show the speed command, real rotor speed and estimated rotor speed for different speeds. Figures are for the operation of the machine at 50, 100, 500, 1000, and 1500 rpm, respectively. The load profiles are added to the speed responses in Figure 4-44, Figure 4-46, Figure 4-48, Figure 4-50 and Figure 4-52.

110
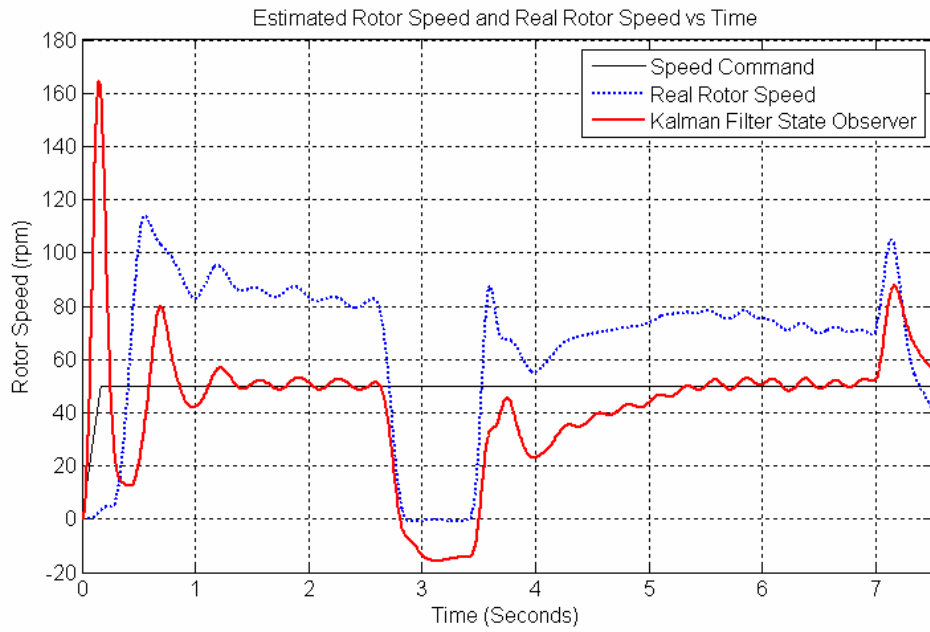
Figure 4-43 50 rpm speed reference, motor speed estimate under switched loading-1
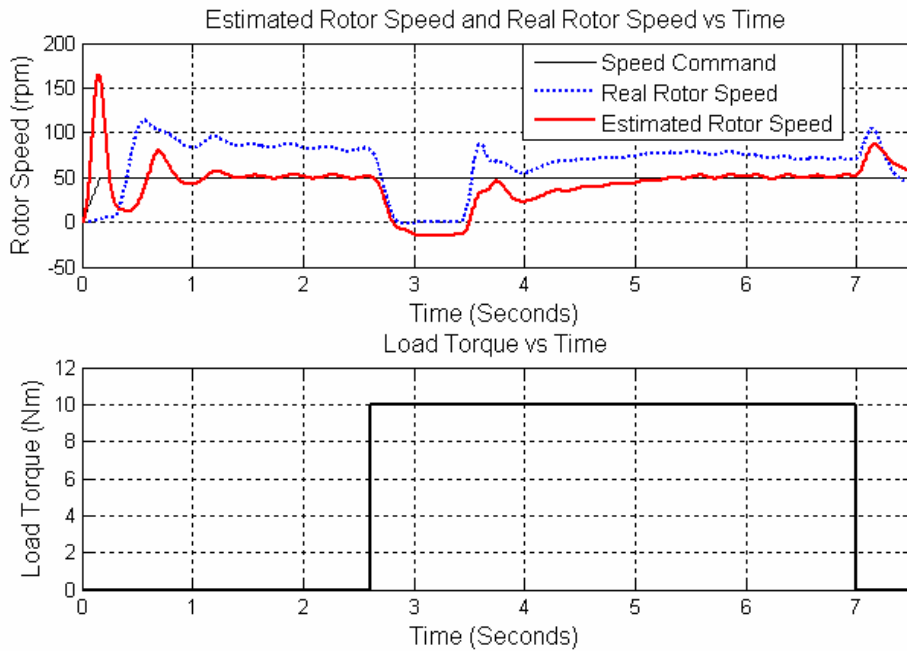
Figure 4-44 50 rpm speed reference, motor speed estimate under switched loading-2

111

As it is observed from Figure 4-43 and Figure 4-44, there isn't proper speed control at 50 rpm. So, closed-loop speed control could not be achieved at 50rpm by enabling Kalman filter state observer.
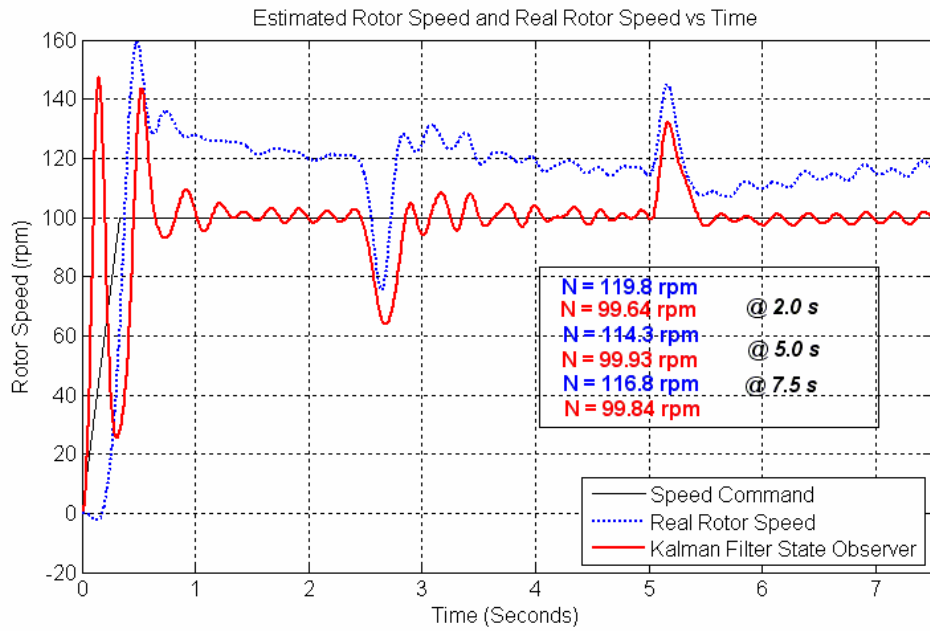
Figure 4-45 100 rpm speed reference, motor speed estimate under switched loading-1
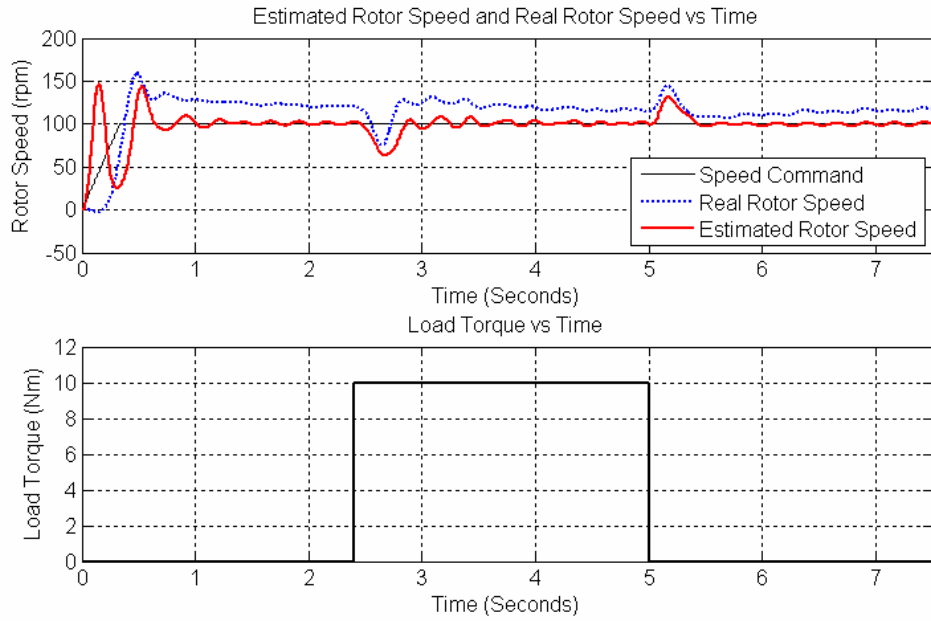
Figure 4-46 100 rpm speed reference, motor speed estimate under switched loading-2
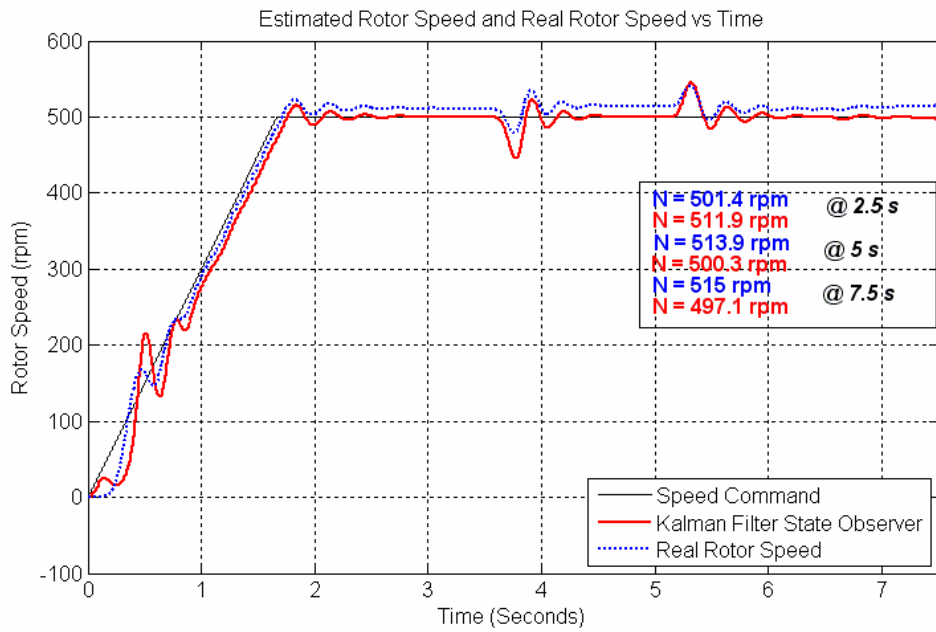
Figure 4-47 500 rpm speed reference, motor speed estimate under switched loading-1
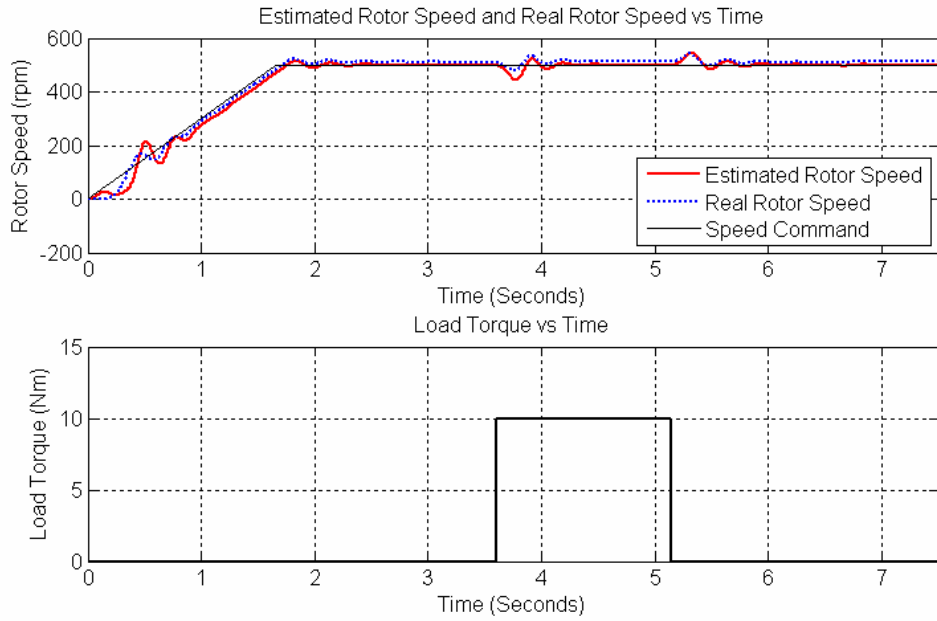
Figure 4-48 500 rpm speed reference, motor speed estimate under switched loading-2
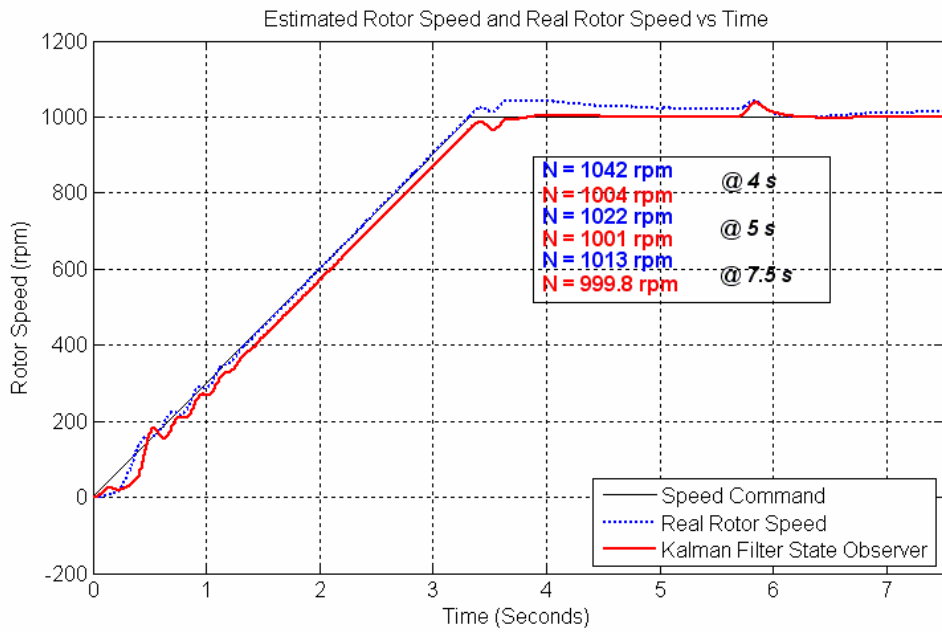
Figure 4-49 1000 rpm speed reference, motor speed estimate under switched loading-1
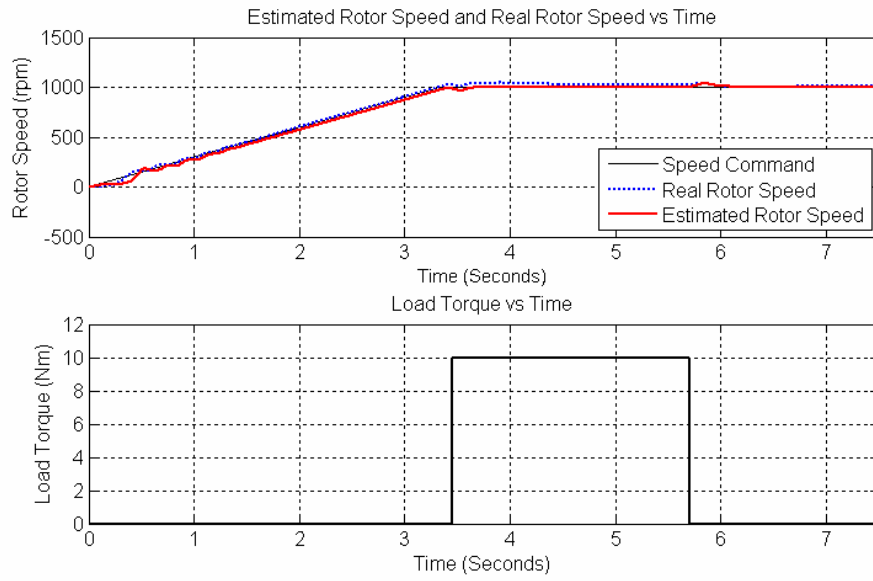
Figure 4-50 1000 rpm speed reference, motor speed estimate under switched loading-2
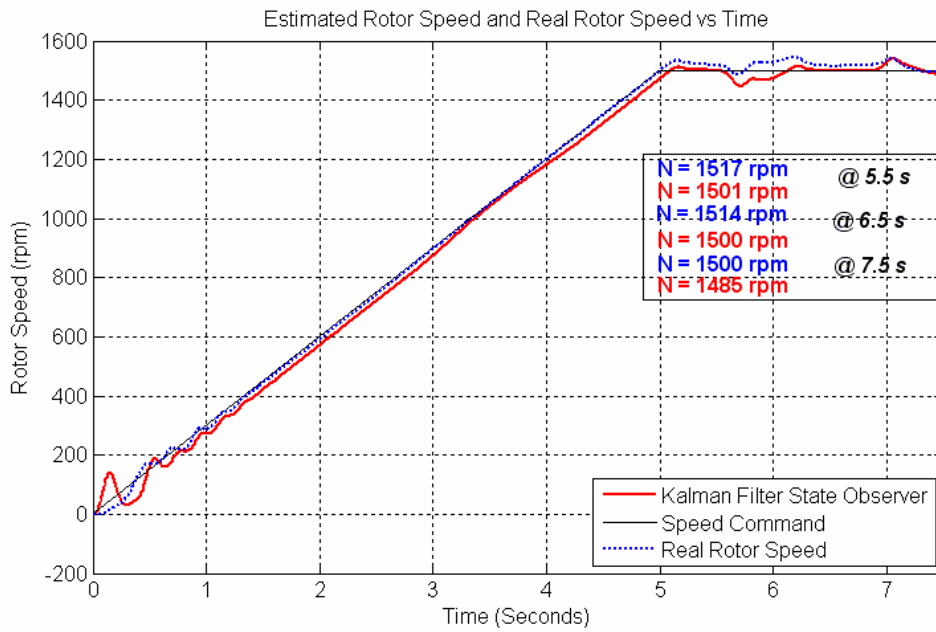
Figure 4-51 1500 rpm speed reference, motor speed estimate under switched loading-1
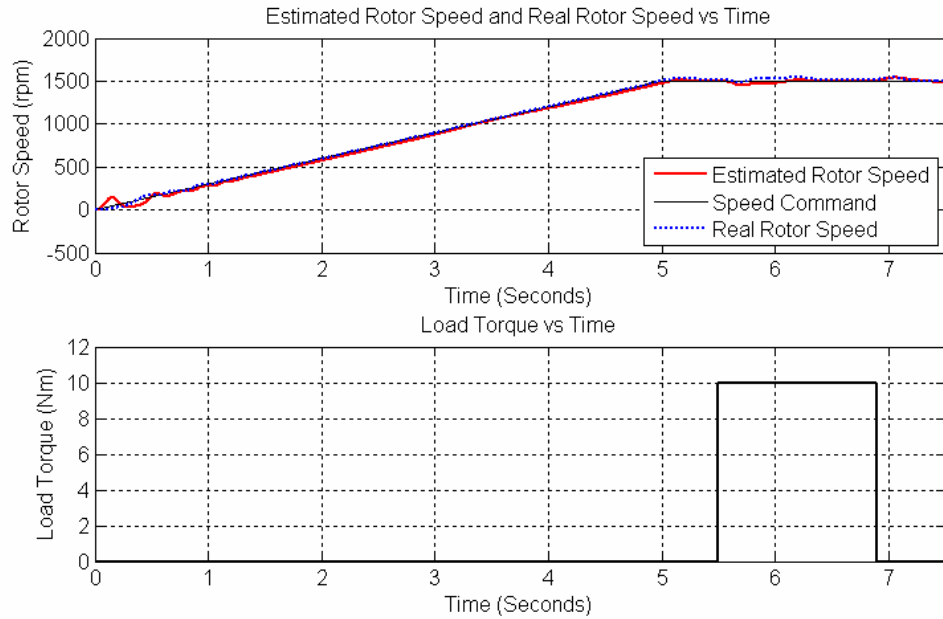
Figure 4-52 1500 rpm speed reference, motor speed estimate under switched loading-2

No connection could be established between the speed estimator performance and loading. It seems that loading do not have any dominant effect on the speed estimation characteristics of Kalman filter state observer. It is hard to conclude from the experimental result that loading and speed estimator performances have a correlation. Closed-loop operation could be achieved at speeds higher than 50 rpm.

4.1.4.3.   The Kalman Filter for Speed Estimation Performance under Accelerating Load

The section investigates the performance of the Kalman filter state observer for speed estimation under accelerating torque. The aim in this investigation is to ensure sensorless vector drive performance while accelerating under loading. Note that Kalman filter used for the speed estimation does not include the dynamics of the system. Although this corresponds to infinite inertia, actually this is not true, but the

required correction is realized by the Kalman filter as the system noise, which also takes account of the computational inaccuracies.

Speed command, real rotor speed and estimated rotor speed for 100rpm to 250rpm, 500 rpm to 750rpm and 1000 to 1250 rpm cases are represented at Figure 4-53, Figure 4-55 and Figure 4-57.respectively. The load profiles are added to speed response at Figure 4-54, Figure 4-56 and Figure 4-58.
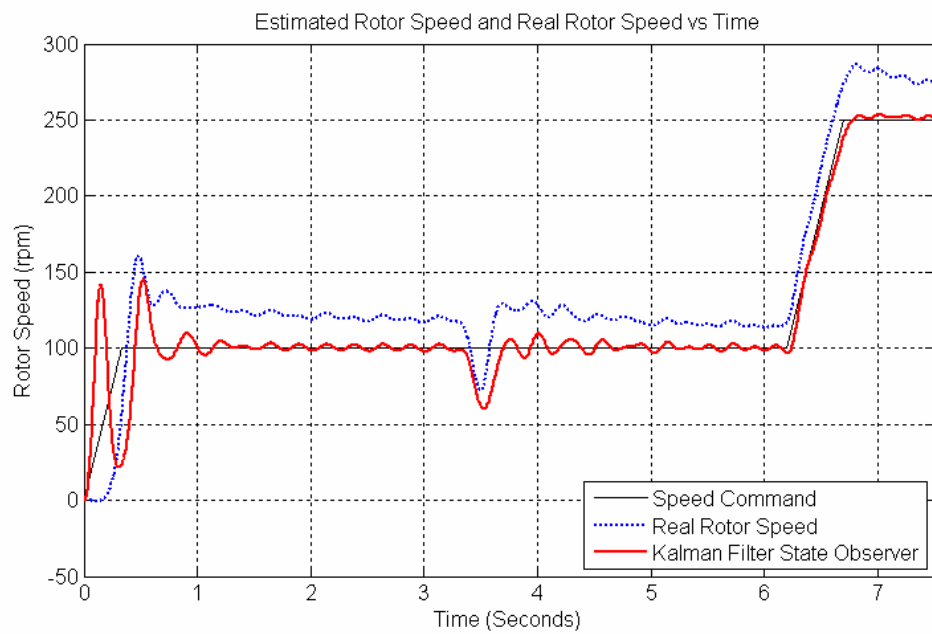
Figure 4-53 100 rpm to 250 rpm speed reference, motor speed estimate under accelerating load-1
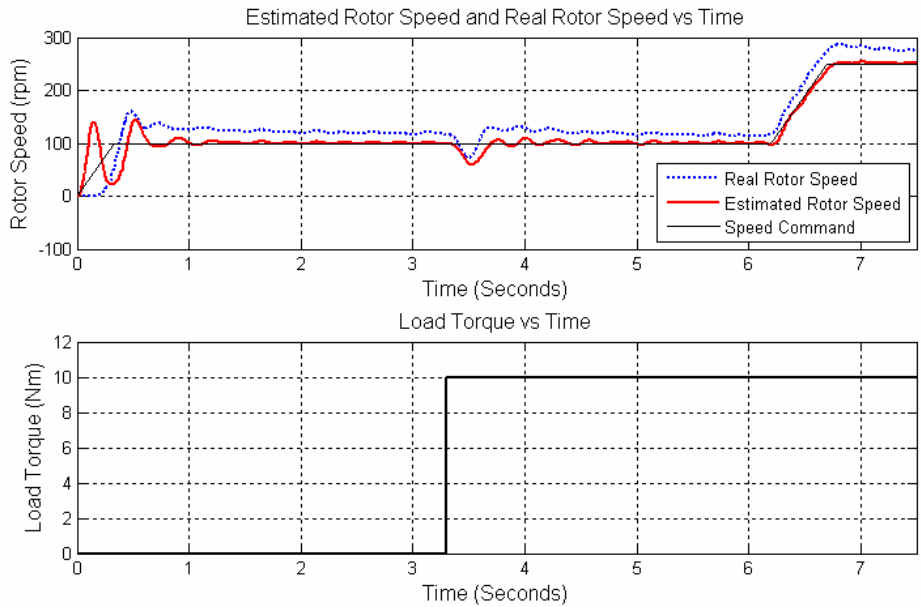
Figure 4-54 100 rpm to 250 rpm speed reference, motor speed estimate under accelerating load-2
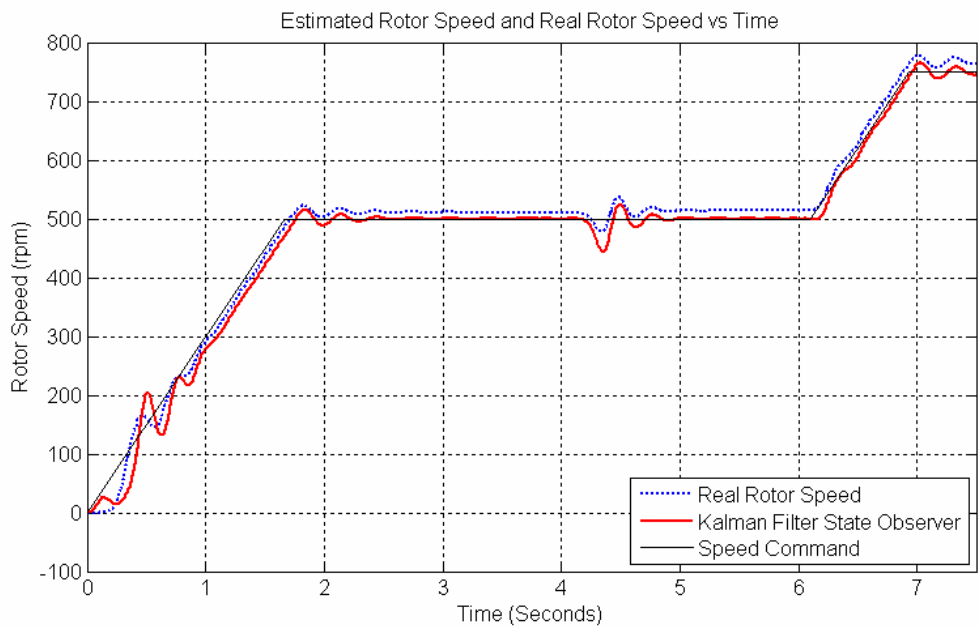
Figure 4-55 500 rpm to 750 rpm speed reference, motor speed estimate under accelerating load-1

118
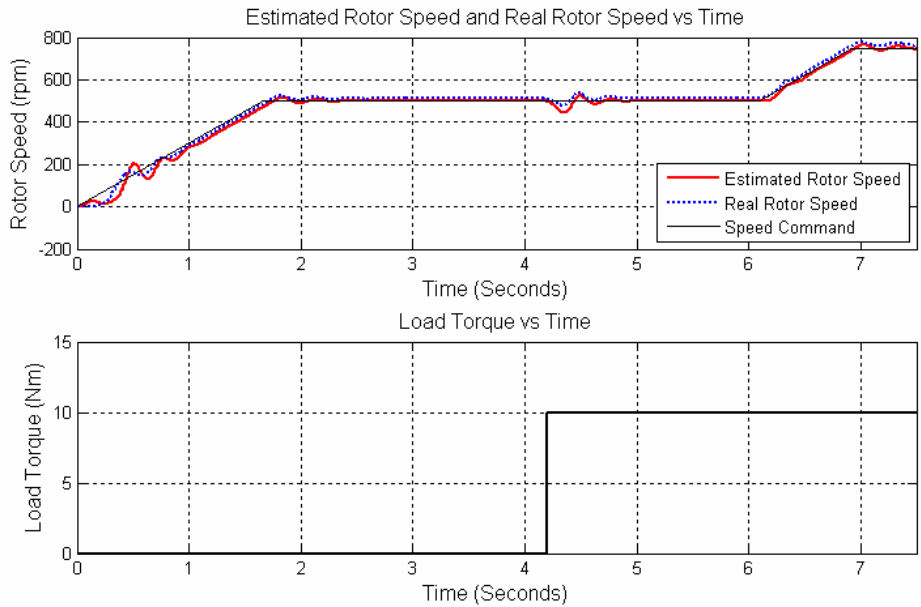
Figure 4-56 500rpm to 750rpm speed reference, motor speed estimate under accelerating load-2
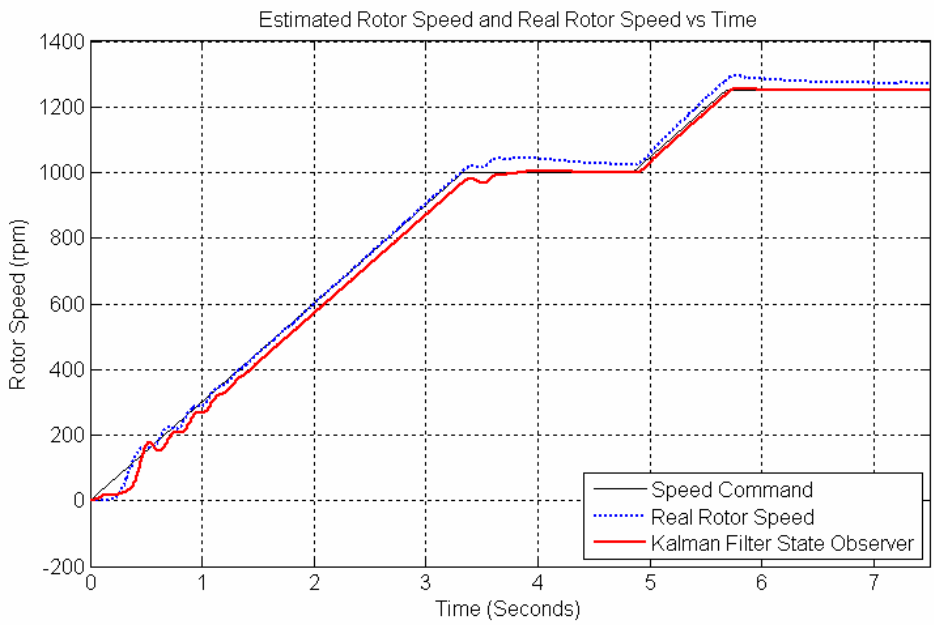
Figure 4-57 1000 rpm to 1250 rpm speed reference, motor speed estimate under accelerating load-1
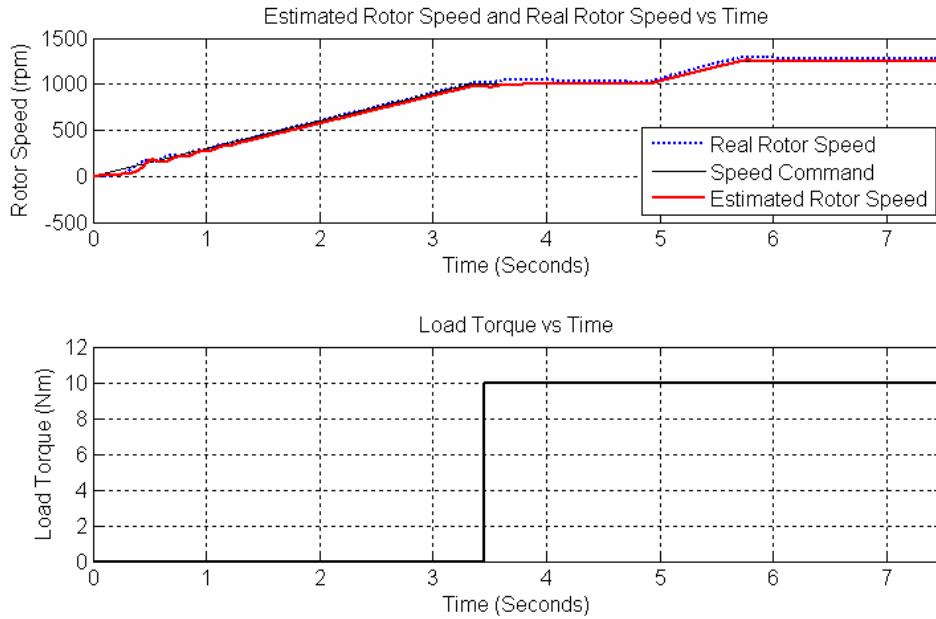
Figure 4-58 1000 rpm to 1250 rpm speed reference, motor speed estimate under accelerating load-2

It can be deduced from Figure 4-53 to Figure 4-58 that the acceleration under loading could be achieved by using Kalman filter state observer. The system noise is corrected to some extent but the speed estimator performance under loading is worse than the speed estimation performance speed adaptive flux observer.

4.1.4.4. The Kalman Filter for Speed Estimation Performance under No-Load Speed Reversal

The speed estimator performance of the Kalman filter state observer is observed under no-load speed reversal. The aim of this section is to determine the speed estimator performance at zero speed crossing and low speed range.

Speed command, real rotor speed and estimated rotor speed for 100rpm to -100rpm, 500 rpm to -500 rpm and 1000 rpm to -1000 rpm cases are represented at Figure 4-31, Figure 4-32 and Figure 4-33 respectively.
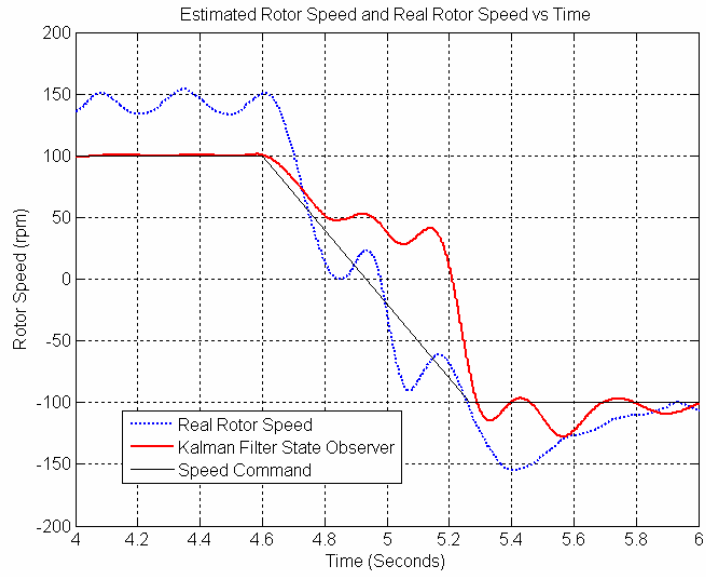
Figure 4-59 100 rpm to -100 rpm speed reference, motor speed estimate under no-load speed reversal
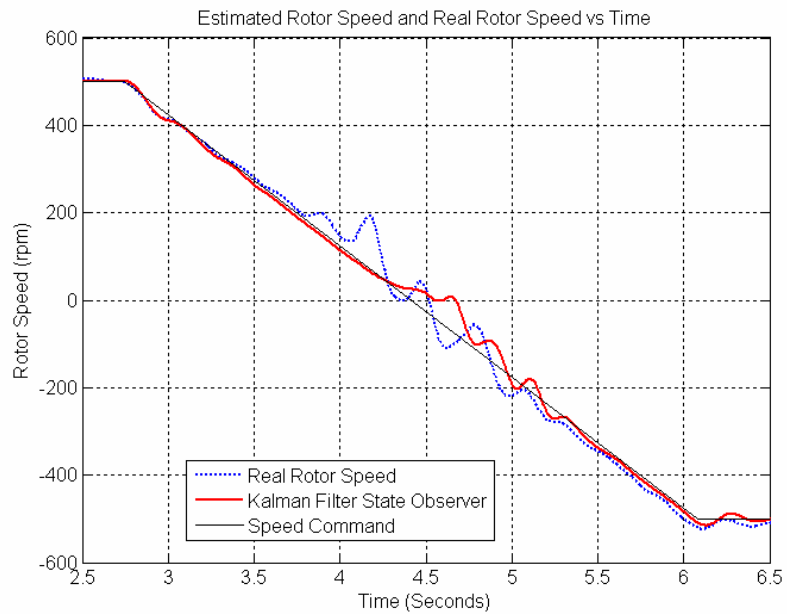
Figure 4-60 500 rpm to - 500 rpm speed reference, motor speed estimate under no-load speed reversal
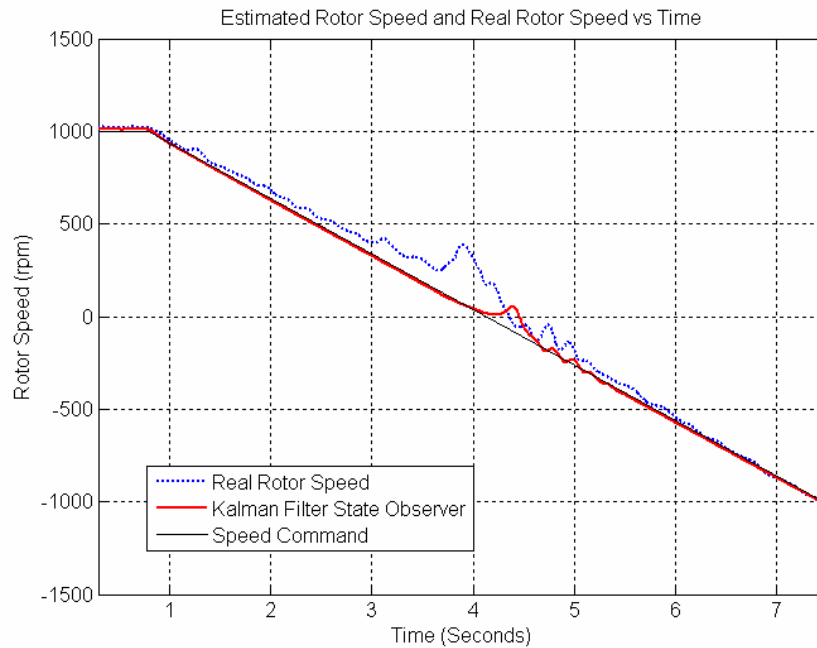
Figure 4-61 1000 rpm to -1000 rpm speed reference, motor speed estimate under no-load speed reversal

As it can be seen from Figure 4-59, Figure 4-60 and Figure 4-61 both at low speeds and the zero speed crossing, system performance decreases. It is difficult to conclude whether speed adaptive flux observer or Kalman filter for speed estimation has better estimation performance at zero speed crossing.

The experiments of Kalman filter for speed estimation show that speed estimation based on Kalman filter for speed estimation has limited tracking capability for whole speed range and for no-load and with load cases. In general, Kalman filter state observer has no superiority with respect to speed adaptive flux observer.

The main reason for poorer speed estimation performance to occur is that adaptive scheme is internally corrected by speed estimation of flux observer; there is no coupling between speed adaptive flux estimation scheme and Kalman filter for speed estimation. So, closed-loop adaptive scheme is broken.

4.1.5 Experimental Results of Parallel Run of Speed Adaptive Flux Observer and Kalman Filter for Speed Estimation

The induction motor parameters at Table 4-2 is used at the experimental stage of both parallel run of speed adaptive flux observer and Kalman filter for speed estimation.

In these experiments, motor is run in the closed- loop speed mode and the quadrature encoder coupled to the shaft of the motor is utilized in order to verify the estimated speed. The output of speed adaptive flux observer is utilized as speed feedback. Also, the Kalman filter for speed estimation is running in order to verify its performance when the adaptive scheme is enabled.

Both speed estimators designed with speed adaptive flux observer have been tested experimentally for satisfactory operation at different speeds of motor.

The control parameters used at the speed adaptive flux observer experiments are listed at Table 4-4

4.1.5.1. No-Load Experiments of Parallel Run of Speed Adaptive Flux Observer and Kalman Filter for Speed Estimation

In these no-load experiments, motor is run in the closed- loop speed mode and the quadrature encoder coupled to the shaft of the motor is utilized in order to verify the estimated speed. The output of speed adaptive flux observer is utilized as speed feedback.

Log of the mechanical rotor angle, the estimated speed, and the actual speed are taken for 500rpm, 1000rp and, 1500rpm, constant speed request. The speed estimate derived from actual rotor (quadrature encoder) position is given as dotted line.
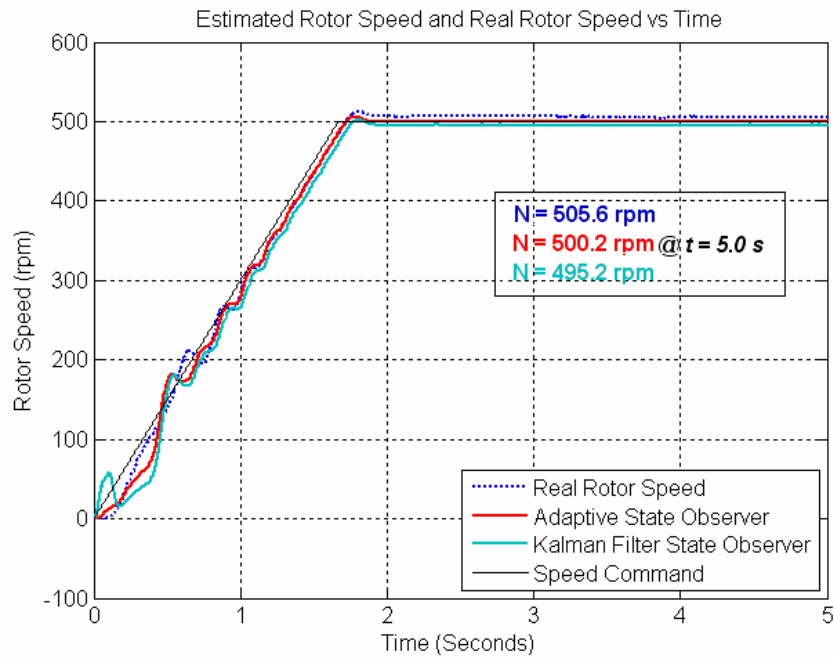
Figure 4-62 500 rpm speed reference, motor speed estimate
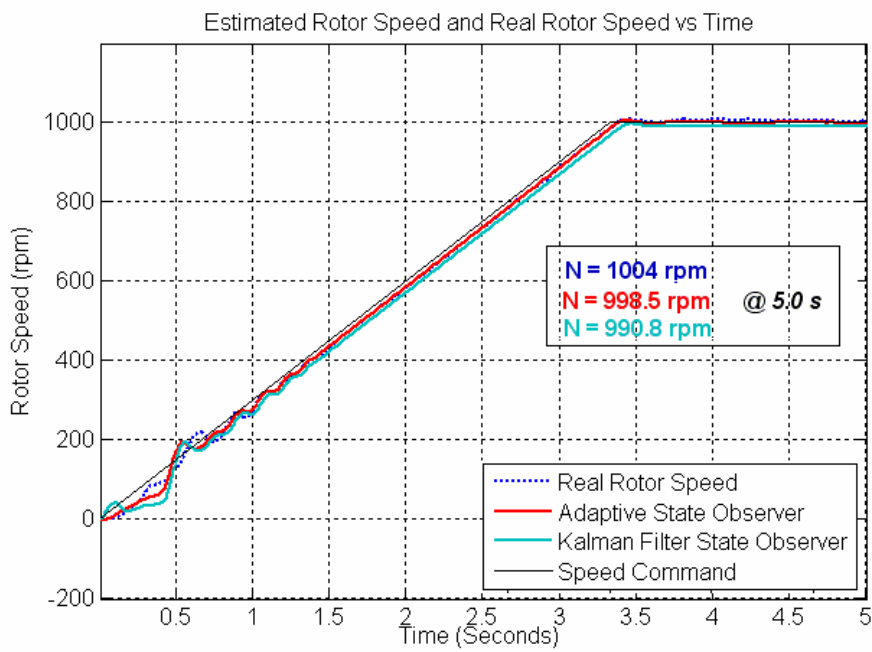
Figure 4-63 1000 rpm speed reference, motor speed estimate
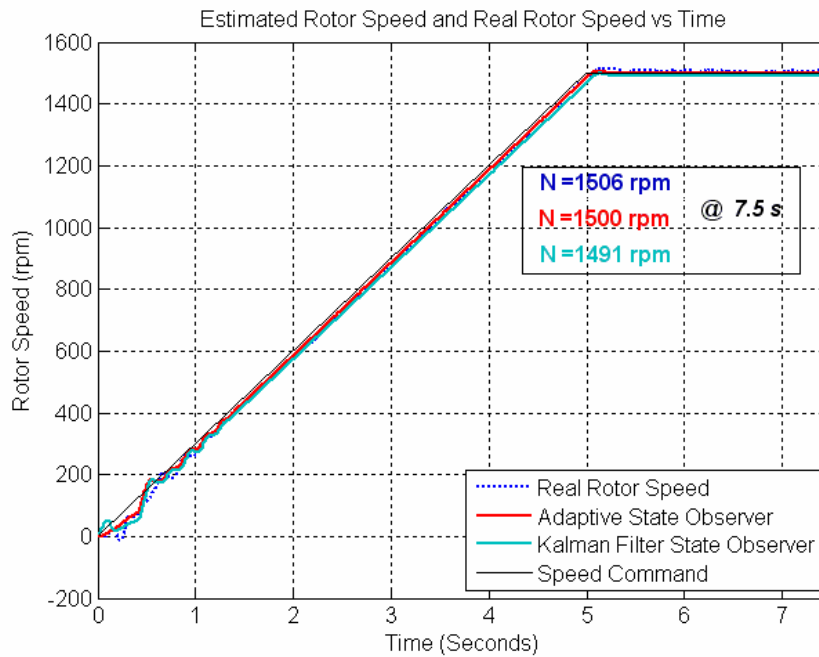
Figure 4-64 1500 rpm speed reference, motor speed estimate

It can be seen from Figure 4-62 to Figure 4-64 that no-load speed estimation performance of Kalman filter state observer is enhanced. It is observed that the measured percentage speed estimator error of Kalman filter state observer is less than 1.5 %. At steady-state, there is a speed offset about 10 rpm with respect to Adaptive state observer. When adaptive scheme is enabled, the performance of Kalman state observer is improved.

4.1.5.2. Parallel Run of Speed Adaptive Flux Observer and Kalman Filter for Speed Estimation under Switched Loading

This section gives a comparative the performance analysis of the Kalman state observer under switched loading while the output of speed adaptive flux observer being utilized as speed feedback. The loading is obtained by using the Magtrol dynamometer coupled to the shaft of the induction motor.

Speed command, real rotor speed and estimated rotor speed for 500 rpm 1000 rpm and 1500 rpm cases are given in Figure 4-65, Figure 4-67, andFigure 4-69, respectively. The load profiles are added to speed response at Figure 4-66, Figure 4-68 and Figure 4-70.
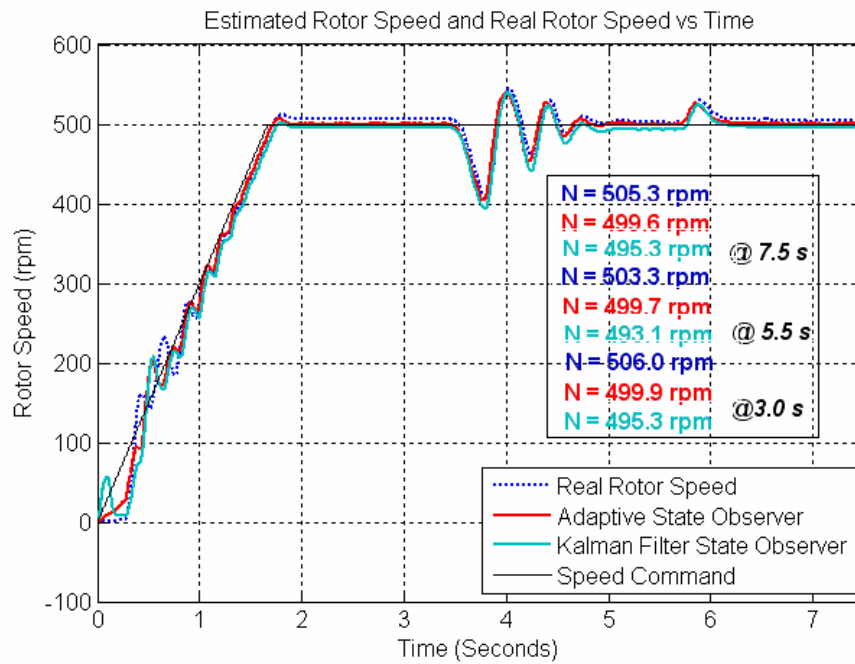
Figure 4-65 500 rpm speed reference, motor speed estimate under switched loading-1
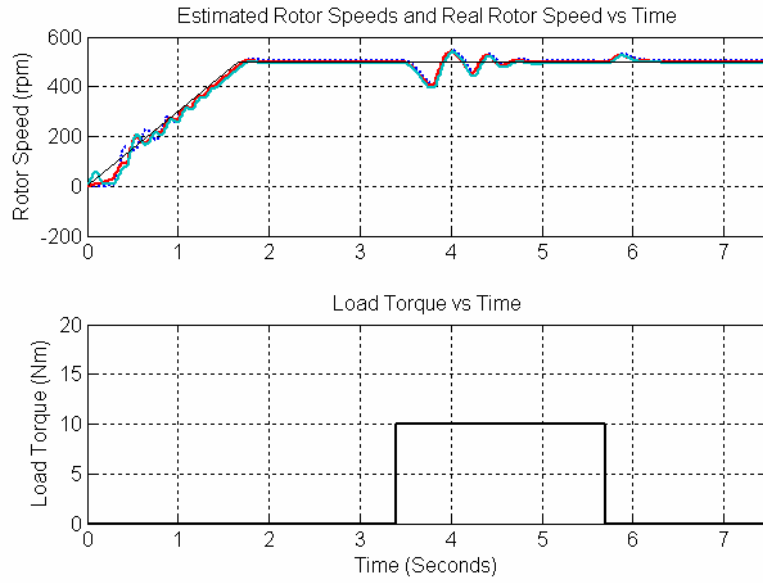
Figure 4-66 500 rpm speed reference, motor speed estimate under switched loading-2
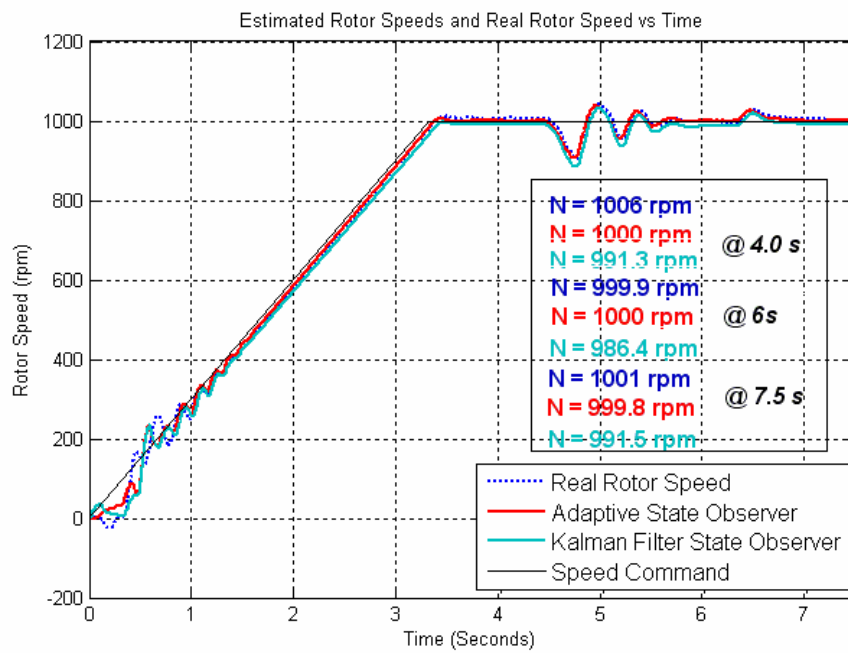
Figure 4-67 1000 rpm speed reference, motor speed estimate under switched loading-1
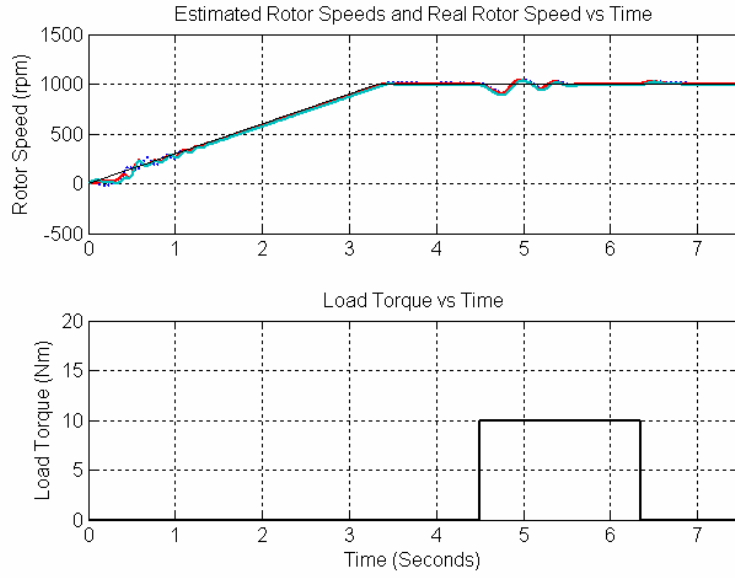
Figure 4-68 1000 rpm speed reference, motor speed estimate under switched loading-2
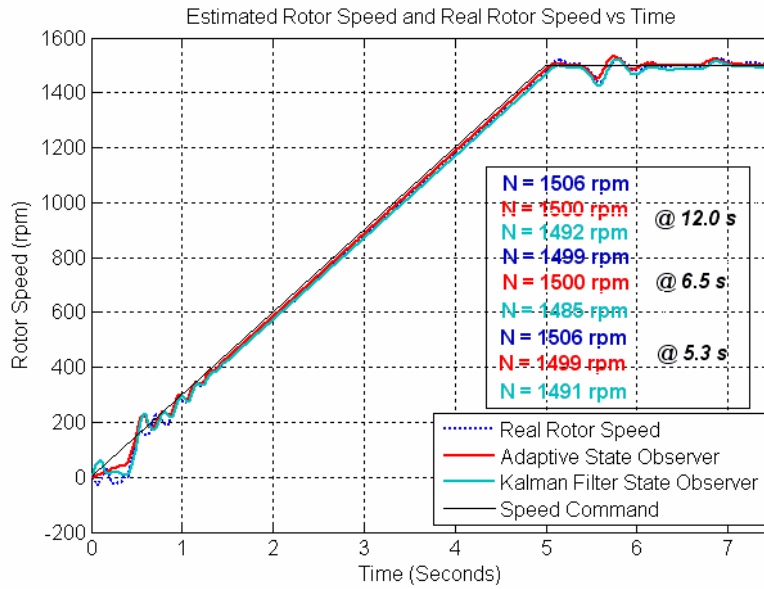
Figure 4-69 1500 rpm speed reference, motor speed estimate under switched loading-1
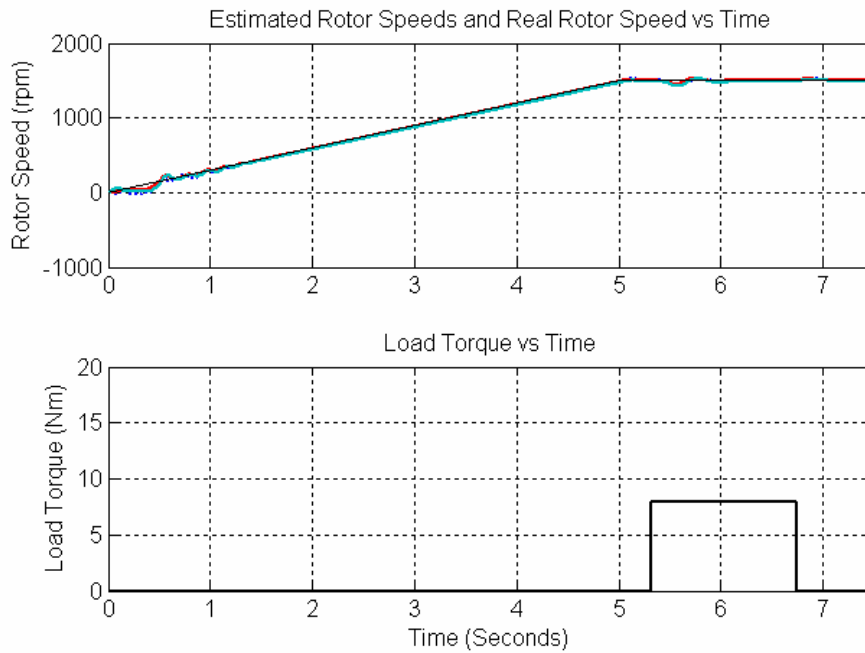
Figure 4-70 1500 rpm speed reference, motor speed estimate under switched loading-
2

The experiments in this section show that when adaptive scheme is enabled, the performance of Kalman state observer is improved. Tracking capability for whole speed range and for no-load and with load cases are getting better. It is observed that both at no-load and load cases, there is a speed offset about 10 rpm which worsen steady-state performance.

4.1.5.3. Parallel Run of Speed Adaptive Flux Observer and Kalman Filter for Speed Estimation under Accelerating Load

The speed estimator performance of the Kalman filter state observer is investigated under accelerating torque. The aim of this section is to ensure sensorless vector drive performance while accelerating load while the output of speed adaptive flux observer is utilized as speed feedback.

Kalman filter for speed estimation model does not include dynamics of system. Although this corresponds to infinite inertia, actually this is not true, but the required correction is performed by the Kalman filter by the system noise, which also takes account of the computational inaccuracies.

Speed command, real rotor speed and estimated rotor speed for 500 rpm to 750rpm and 1000 to 1250 rpm cases are represented at Figure 4-71 and Figure 4-73 respectively. The load profiles are added to speed responses in Figure 4-72 and Figure 4-74.
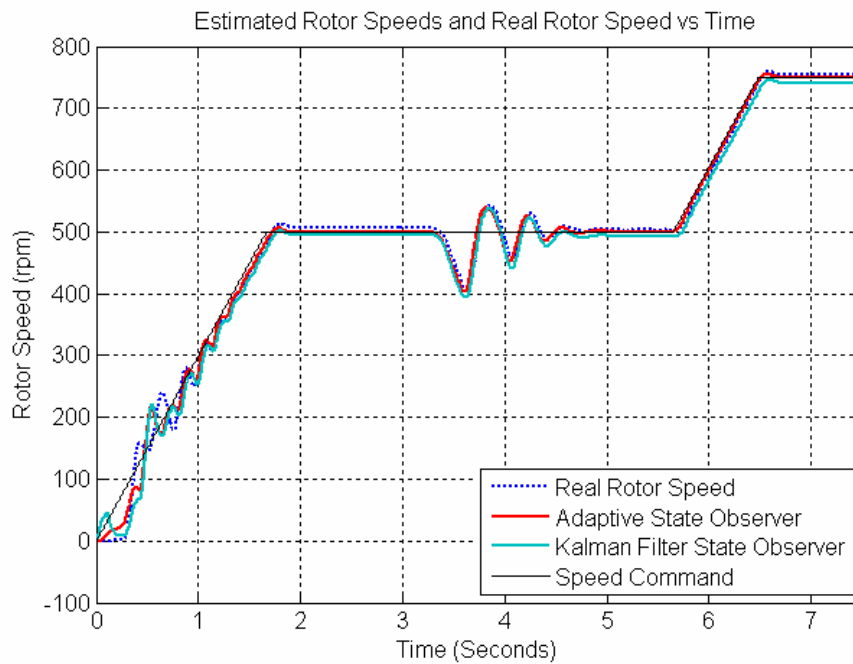
Figure 4-71 500 rpm to 750 rpm speed reference, motor speed estimate under accelerating load-1
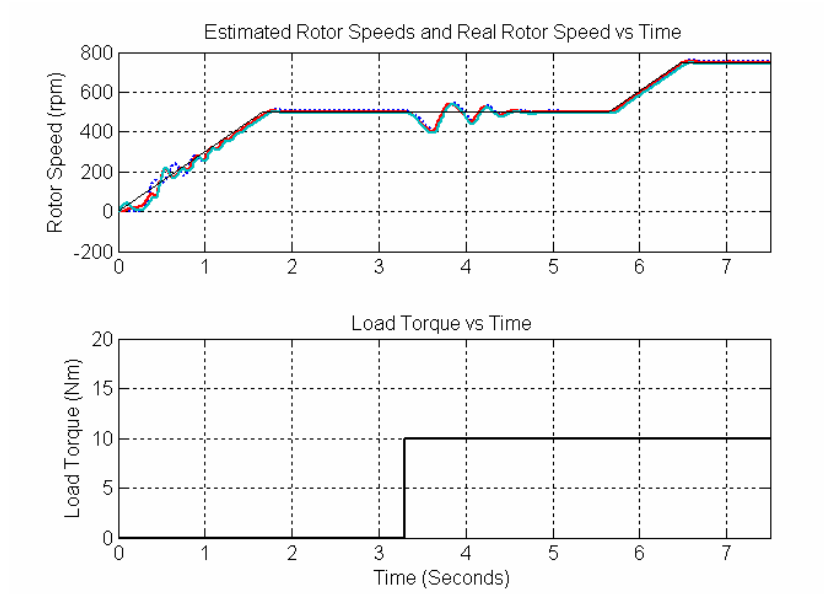
Figure 4-72 500 rpm to 750 rpm speed reference, motor speed estimate under accelerating load-2
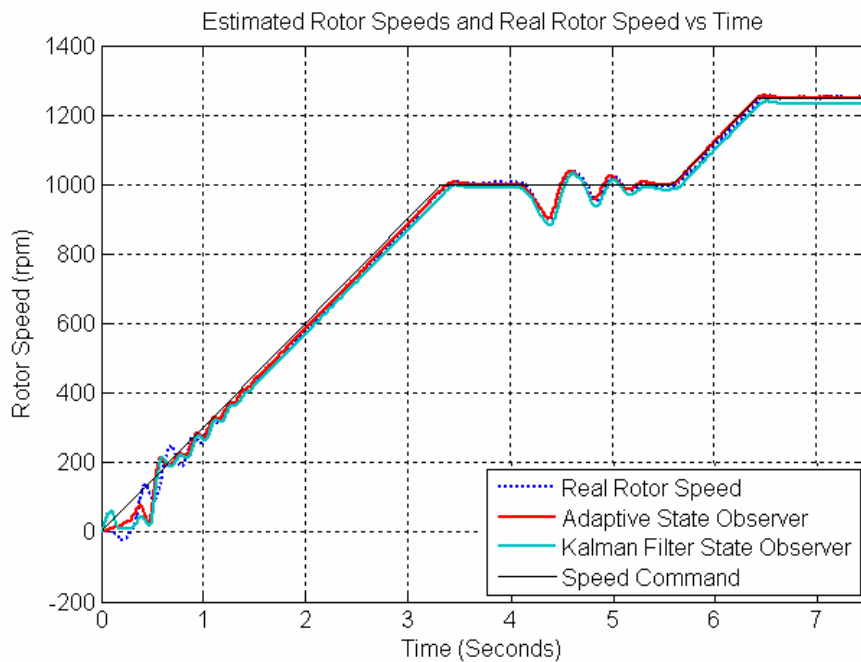
Figure 4-73 1000 rpm to 1250 rpm speed reference, motor speed estimate under accelerating load-1

131
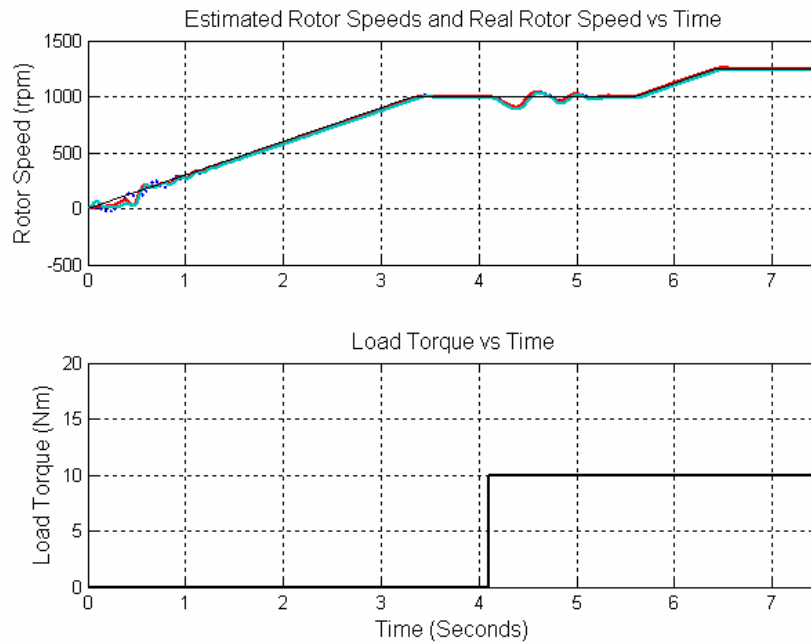
Figure 4-74 1000 rpm to 1250 rpm speed reference, motor speed estimate under accelerating load-2

It can be deduced from Figure 4-71 and Figure 4-73 that the acceleration under loading could be achieved by using Kalman filter state observer. The system noise is corrected to some extent, but the speed estimator performance under loading is worse than the speed estimation performance speed adaptive flux observer.

4.1.5.4. Parallel Run of Speed Adaptive Flux Observer and Kalman Filter for Speed Estimation under No-load Speed Reversal

The speed estimator performance of Kalman filter state observer is observed under no-load speed reversal. The aim of this section is to determine the speed estimator performance at zero speed crossing and low speed range.

Speed command, real rotor speeds and estimated rotor speed for, 500 rpm to -500 rpm and 1000 rpm to -1000 rpm cases are given at Figure 4-75 and Figure 4-76.
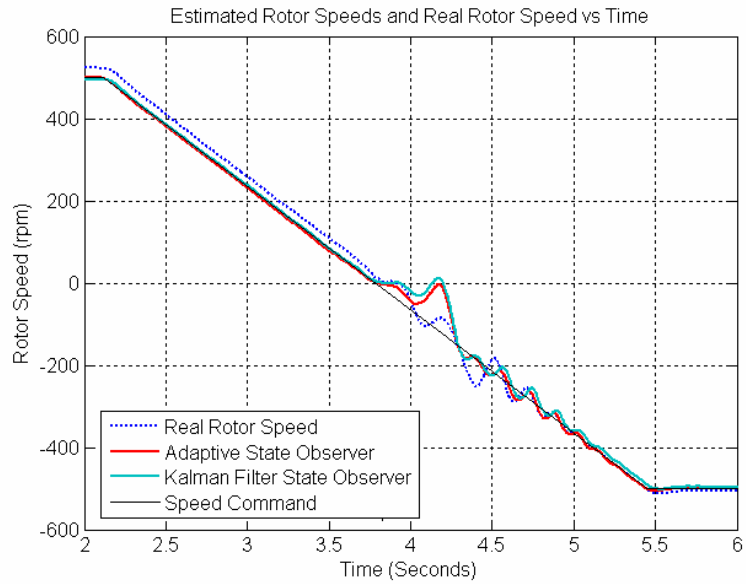
Figure 4-75 500 rpm to -500 rpm speed reference, motor speed estimate under no-load speed reversal
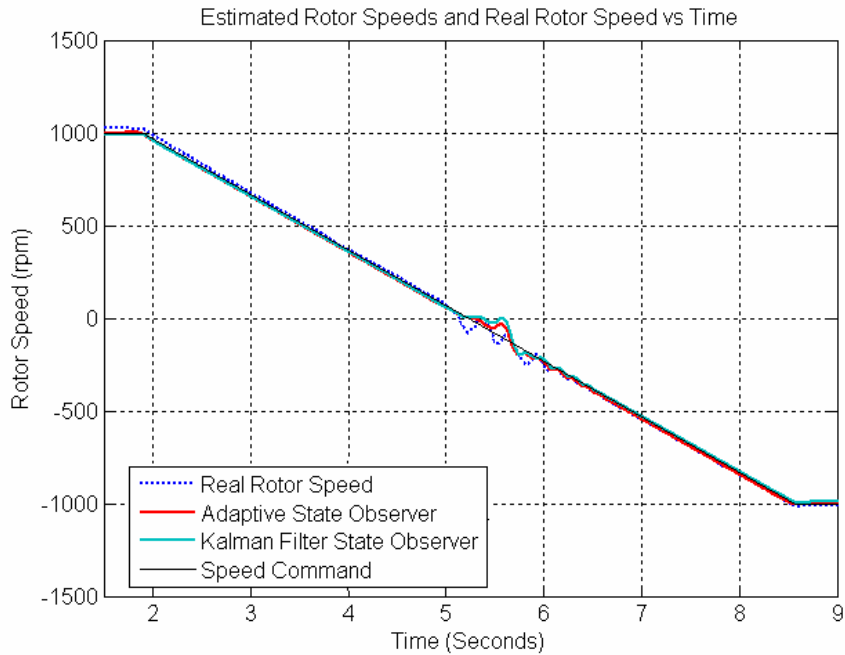
Figure 4-76 1000 rpm to -1000 rpm speed reference, motor speed estimate under no-load speed reversal

4.2   Simulations of Extended Kalman Filter

Although, the low speed estimation performance of EKF is focused throughout study, due to intense calculations in real-time in order to determine EKF states such that rotor flux and stator currents and rotor speed, some overloading problems occurred while performing real time EKF experiments on DSP. So, simulations of EFK are performed. It is deduced from EKF simulations that EKF is convenient for low speed operation and its performance could be increased by compansating voltage errors caused by dead-time effects inverter switches, voltage drop in the power electronic devices and the fluctuations of the dc link line voltage. Unfortunatelly, those effects are not compansated at experiments and simulations for all the estimation algorithms.

Simulations were performed in order to investigate effectiveness of the derived algorithms for the extended Kalman filter (EKF) observer and to tune the covariance matrices of it. The EKF observer is tuned by optimizing the entries of the

measurement noise covariance R matrix and the process noise covariance Q matrix. In order to obtain fast and dynamic response and estimation accuracy MATLAB Simulink is used as simulation tool. Convariance matrices, Q and R, are tuned by the help of Matlab Response Optimization Toolbox.

The inputs of the EKF simulations are reconstructed phase voltages and logged phase current outputs of the induction machine. Log of the mechanical rotor angle, reconstructed phase voltages and phase currents are are taken from various experiments in order to use them at simulations. Motor parameters at Table 4-2 are used at the simulations of EKF observer.

The simulations are realized using phase voltages and phase current data obtained from drive system by closed-loop speed control with encoder speed.

4.2.1.   Tuning of EKF Covariance Matrices

In order to tune the covariance matrices of EKF, Matlab Response Optimization Toolbox is used. The encoder, stationary reference frame variables i^s_{ds}, i^s_{qs}, V^s_{ds} and V^s_{qs} are logged from real-time experiments. The encoder signal is set as desired waveform and entries of Q and R matrices are selected as tuned parameters, multiple trials are performed to get an optimized speed estimator performance. Especially, performance at lower speeds is focused. Thus, EKF speed estimatator experiments at 50 rpm, 100 rpm and 150 rpm are investigated.

4.2.2.   Simulations at Lower Speeds

In this section, the performance of EKF is simulated under switched loading while encoder is utilized as speed feedback. The loading is obtained by using the Magtrol dynamometer coupled to the shaft of the induction motor. Encoder, stationary reference frame i^s_{ds}, i^s_{qs}, V^s_{ds} and V^s_{qs} variables are logged from real-time experiments and they are inputted to EKF simulation.

Real rotor speed and estimated rotor speed are represented for 50 rpm, 100 rpm, and 150 rpm cases
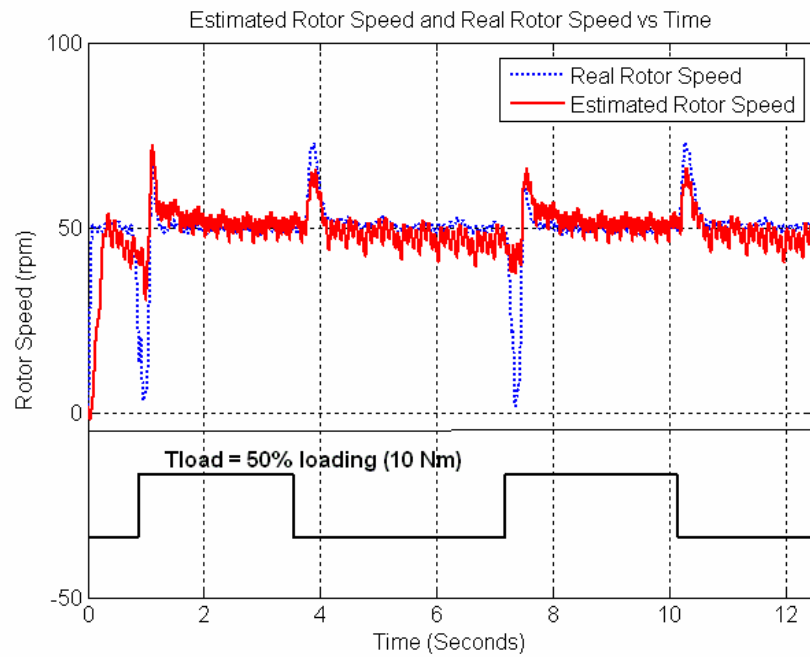
Figure 4-77 50 rpm speed reference, motor speed estimate under switched loading

Since EKF estimates the stationary reference frame i^s_{ds}, and i^s_{qs} currents. Real and Estimated stationary reference frame currents are given at Figure 4-78 and Figure 4-79 for 50 rpm speed command.
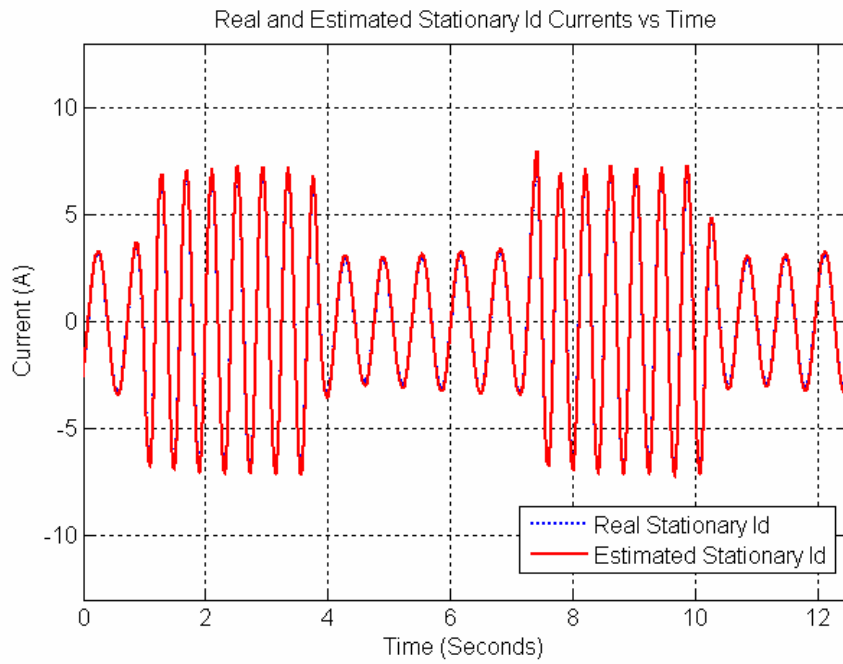
Figure 4-78 50 rpm speed reference, stationary reference frame i^s_{ds} current
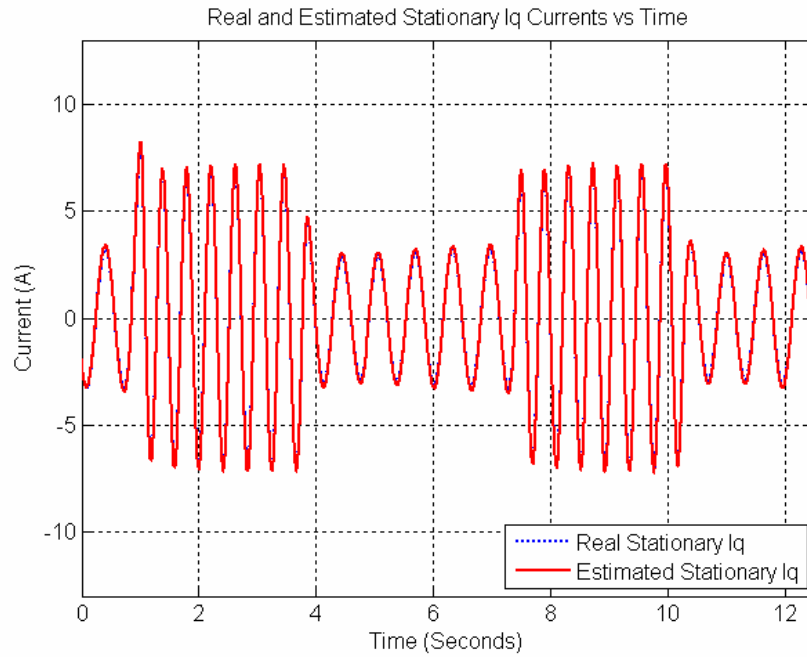
Figure 4-79 50 rpm speed reference, stationary reference frame, i^s_{qs} current

As it can be seen from Figure 4-77, the speed estimation performance of EKF is better than speed adaptive state observer and Kalman filter state observer. The EKF speed output at 50 rpm is oscillating which is due to some noise on stationary reference frame voltages V^s_{ds} and V^s_{qs}. Since voltages are low, noise on voltages become dominating on speed estimation.

The estimated i^s_{ds} and i^s_{qs} currents are exactly matched at the simulation for 50 rpm speed command.
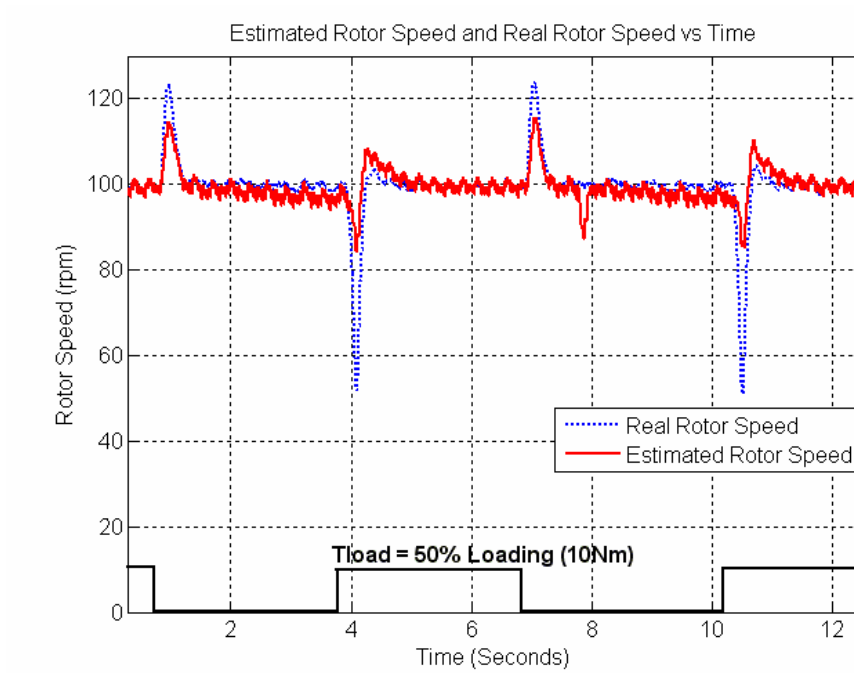
Figure 4-80 100 rpm speed reference, motor speed estimate under switched loading
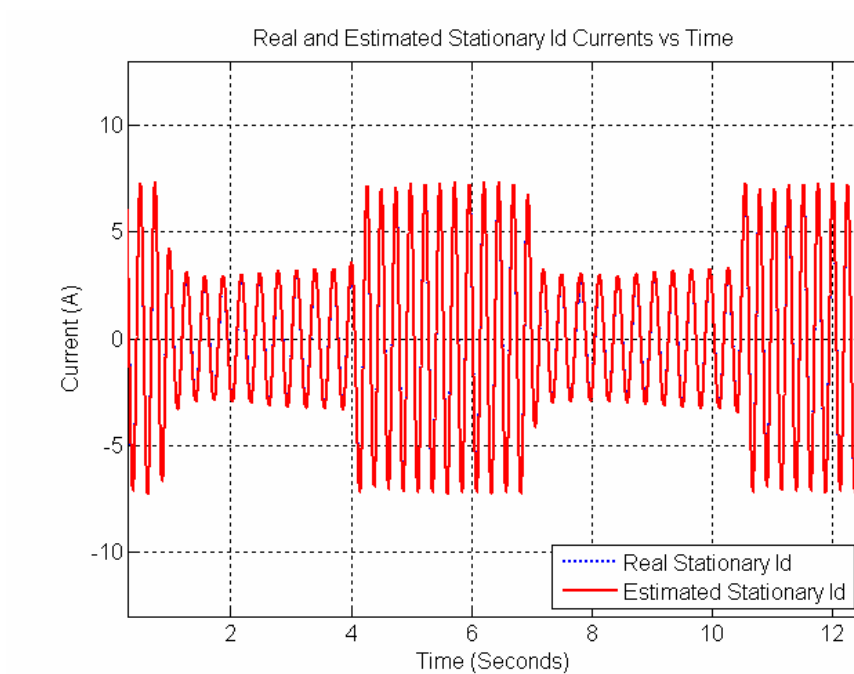
Figure 4-81 100 rpm speed reference, stationary reference frame, i^s_{ds} current

139
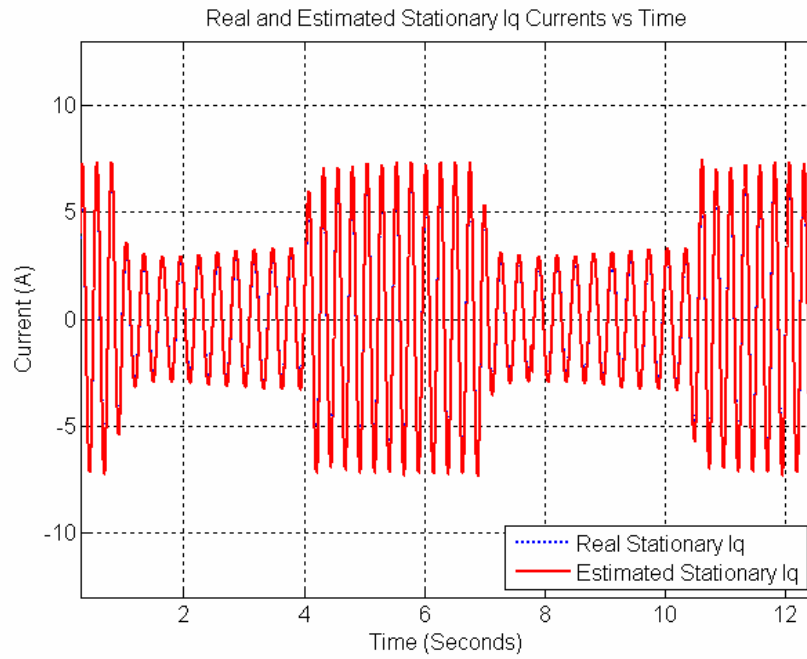
Figure 4-82 100 rpm speed reference, stationary reference frame, i^s_{qs} current
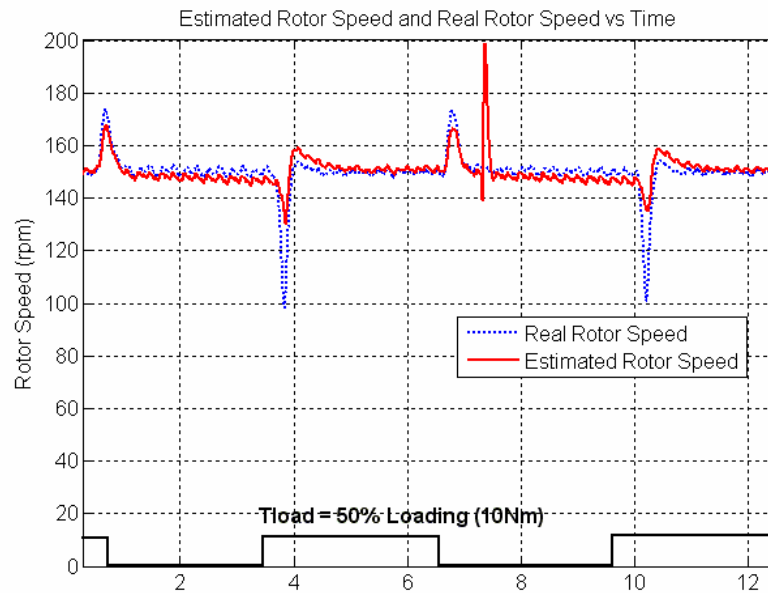
Figure 4-83 150 rpm speed reference, motor speed estimate under switched loading

140
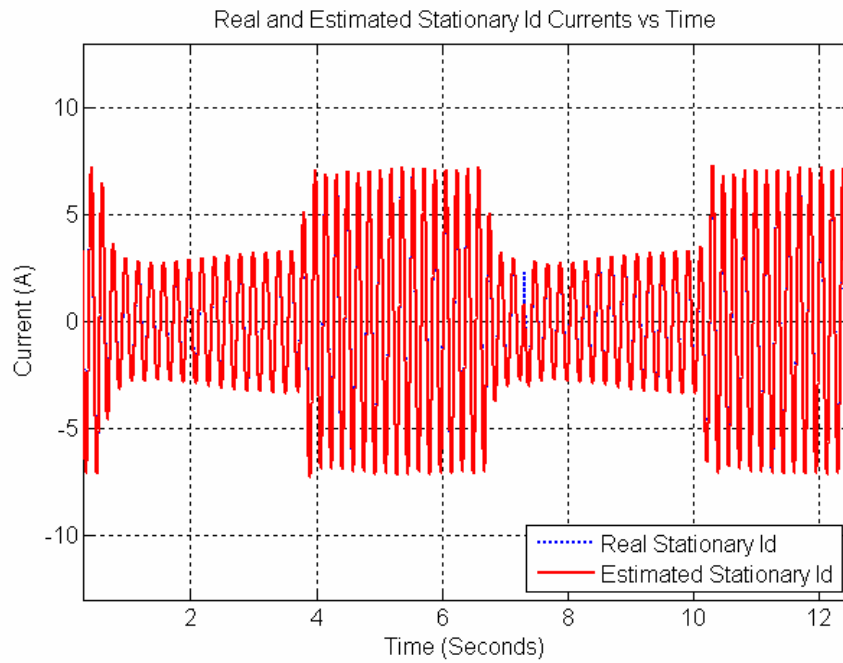
Figure 4-84 150 rpm speed reference, stationary reference frame, i^s_{ds} current
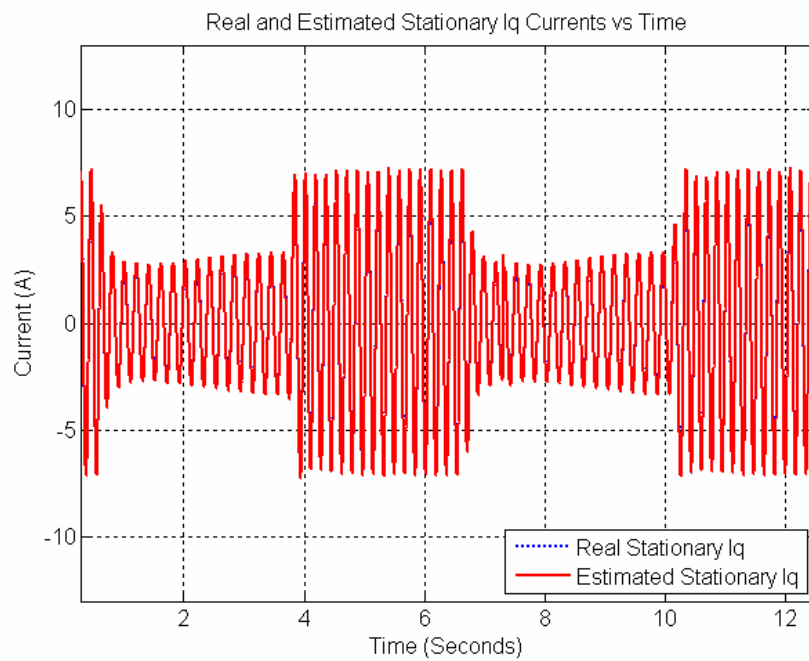
Figure 4-85 150 rpm speed reference, stationary reference frame, i^s_{qs} current

141

As it can be seen from Figure 4-77 - Figure 4-85 that the estimation performance at low speed is better than the other two methods. The magnitute and frequency of oscillations on speed estimate decreased when speed command is increased. In other words, noise on the voltage terms becomes negligible when speed is increased

The estimates of current components are very well matched with direct and quadrature axis currents derived with measured current terms.

CHAPTER 5

CONCLUSION

This work mainly includes implementation and experimental investigation of flux and speed estimators for sensorless closed-loop speed control of induction motor. The performance of observers is investigated in terms of steady-state and dynamic speed response. The performance of speed estimators are compared based on experimantal results and simulations.

Induction motor model based speed adaptive flux observer, Kalman filter state observer and induction motor model based extended Kalman filter are implemented throughout the study. In order to provide coherent control structure, mathematical model of the induction motor has been derived both in stationary and synchronously rotating dq axes system. In addition to that, space vector PWM and field orientation concepts are introduced at the control system.

The response of the system against step loading has been tested on an experimental set-up. Closed-loop speed control is enabled by utilizing closed-loop speed feedback of sensorless speed estimation The test results are satisfactory in terms of accurary of speed estimation and speed sensorless closed-loop vector control.

It has been deduced that adaptive state observer can be used for both speed estimation and rotor flux estimation and it has ability to adapt itself to its speed parameter which is estimated internally. Its speed estimation performance is investigated under no-load, constant load and switched load cases. It performed well at motor speeds greater than 100 rpm in terms of steady-state and dynamic behaviour. The percentage speed estimation accuracy is measured lower than 1% at speeds greater than 100 rpm. However, adaptive state observer is affected by the motor parameter variations at 50 rpm and 100 rpm. The results obtained from the adaptive speed observer tests are comparative to those reported in the literature

A Kalman filter state observer has been considered as the speed estimation scheme for the motor speed in the study. The application requires the use of another estimator for the estimation of the flux components and the rotor flux angle. So, The output performance of the Kalman filter state observer is linked with the accuracy of flux estimation and accuracy of speed observer. Complementary observer has been chosen as speed adaptive flux observer algorithm. Since, speed adaptive flux observer algorithm has ability to adapt itself to its speed parameter which is estimated internally, flux observer becomes independent of closed-loop speed feedback which leads to poorer performance compared with the estimated speed output of speed adaptive flux observer. Closed-loop speed control based on Kalman filter state observer percentage speed estimation accuracy is measured lower than 3% at speeds greater than 250 rpm. It is observed that steady-state and dynamic performance of Kalman filter state observer is poorer than speed adaptive state observer. Also, it is more complex to implement it compared to speed adaptive state observer.

Another estimator considered in the thesis work is the extented Kalman filter (EKF) algorithm. The algorithm is introduced in the form of computer simulations and script code for DSP implementation. The algorithm, however, could not have been experimentally tested in the study. It is deduced from EKF simulations that EKF is convenient for low speed operation and its performance could be improved by compensating; voltage errors caused by dead-time effects in inverter switches, voltage drop in the power electronic devices, and the fluctuations of the dc link line voltage. The covariance matrices are optimized in order to ensure satisfactory low speed performance by computer simulations. The percentage speed estimation accuracy is calculated that EKF has estimated the rotor speed with $\leq 5\%$ for the speeds 50 rpm, 100 rpm and 150 rpm at steady state. When EKF simulation results are compared with the results of the two other methods, EKF is convenient for low speed operation.

The simulations and experiments conducted in the study have illustrated that it is possible to increase the performance at low speeds at the expense of increased computational burden on the processor. However, in order to control the motor at zero speed, other techniques such as high frequency signal injection technique may probably be used as well as a different electronic hardware.

For future work, the estimation accuracy and the dynamic response of the estimators may be improved by compansating voltage errors caused by dead-time effects inverter switches, voltage drop in the power electronic devices and the fluctuations of the dc link line voltage. Also variations of stator and rotor resistances could be modelled.

The estimators can be designed by other techniques, such as, extended Kalman filter (EKF) technique, neural networks based estimators, sliding mode estimators. Furthermore, more advanced control structures can be investigated for better control of both motor current loop and speed loop. Some hardware upgrades together with high frequency signal implementation could be done to control the motor at zero speed.

REFERENCES

[1]   S. Campbell, H. A. Toliyat "DSP-based electromechanical motion control", CRC Press, 2004

[2]   F. Blaschke, Das Verfahren der Feldorientierung zur Regelung der Drehfeldmachine. PhD thesis, TU Braunsdcweiq, 1974,

[3]   K. Hasse, Zur Dynamik Drehzahlgeregelter Antriebe mit Stromrichtergespeisten Asynchron-Kurzschlusslaufermachinen. PhD thesis, TH Darmstadt, 1969.

[4]   Takahashi and T. Noguchi, "A new quick-response and high-efficiency control strategy of an induction motor," IEEE Trans. Ind. Applicat., vol. 22, pp.820-827, Sep./Oct. 1986.

[5]   H. Kubota, K. Matsuse, and T. Nakano, "DSP-based speed adaptive flux observer of induction motor," IEEE Trans. Ind. Appl., vol. 29, no. 2, pp. 344-348, Mar./Apr. 1993.

[5]   H. Kubota and K. Matsuse "Flux observer of induction motor with parameter adaptation for wide speed range motor drives," in Proc. IPEC'90, Tokyo, Japan, 1990, pp. 1213-1218.

[6]   P. L. Jansen and R. D. Lorenz, "Transducerless position and velocity estimation in induction and salient ac machines," IEEE Trans. Ind. Appl., vol. 31, no. 2, March/April 1995, pp. 240- 247.

[7]   P. L. Jansen and R. D. Lorenz, "Transducerless field orientation concepts employing saturation-induced saliencies in induction machines," Proc. IEEE Industry Applicat. Soc. Annual Mtg., Lake Buena Vista, FL, October 1995, pp. 174-181.

[8]   D. Holliday, J. E. Fletcher, and B. W. Williams, "Noninvasive rotor position and speed sensing of asynchronous motors," Proc. European Conf. on Power Electron. and Applicat.,Sevilla, Spain, September 1995, pp. 1.333-1.337.

[9]   P.L. Jansen and R.D. Lorenz "Transducerless position and velocity estimation in induction and salient ac machines", IEEE Tran. IA, vol. 31, no.2, pp.240-247, Mar/April, 1995

[10] B. Peterson, "Induction machine speed estimation: Observations on observers," Ph.D. Thesis, Dept. of Industrial Electrical Engineering and Automation, Lund University, Lund, Sweden, 1995.

[11] G. C. Verghese and S. R. Sanders, "Observers for flux estimation in induction machines," IEEE Trans. Ind. Electron., vol.35, no. 1, February 1988, pp. 85-94.

[12] P. L. Jansen and R. D. Lorenz, "A physically insightful approach to the design of and accuracy assessment of flux observers for field oriented induction machine drives," IEEE Trans. Ind. Appl., vol. 30, no. 1, January/February 1994, pp 101-110.

[13] R. J. Kerkman, B. 3. Seibel, T. M. Rowan, and D. Schlegel, "A new flux and stator resistance identifier for ac drive systems," Proc. IEEE Industry Applicat. Soc. Annual Mtg., Lake Buena Vista, FL, October 1995, pp. 310-318.

[14] D. Hurst and T. G. Habetler, "Sensorless speed measurement using current harmonics spectral estimation in induction machine drives," IEEE Trans. Pouter Electron., vol. 11, no. 1, January 1996, pp. 66-73.

[15] P. L. Jansen and R. D. Lorenz, "Transducerless position and velocity estimation in induction and salient ac machines," IEEE Trans. Ind. Appl., vol. 31, no. 2, March/April 1995, pp. 240 247.

[16] P. L. Jansen and R. D. Lorenz, "Transducerless field orientation concepts employing saturation-induced saliencies in induction machines," Proc. IEEE Industry Applicat. Soc. Annual Mtg., Lake Buena Vista, FL, October 1995, pp. 174-181.

[17] D. Holliday, J. E. Fletcher, and B. W. Williams, "Noninvasive rotor position and speed sensing of asynchronous motors," Proc. European Conf. on Power Electron. and Applicat., Sevilla, Spain, September 1995, pp. 1.333-1.337.

[18] C. Schauder, "Adaptive speed identification for vector control of induction motors without rotational transducers," IEEE Trans. Ind. Appl., vol. 28, no. 5, September/October 1992, pp.

[19] M. VClez-Reyes, K. Minami, and G. C. Verghese, "Recursive speed and parameter estimation for induction machines," Proc. IEEE Ind. Appl. Conf., San Diego, CA, 1989, pp. 607-611.

[20] H. Bmrsting and P. Vadstrup, "Robust speed and parameter estimation in induction motors," Proc. European Conf. on Power Electron. and Applicat., Sevilla, Spain, September 1995, pp.1054-1061.1.089-1.093.

[21] D.W. Novotny and T.A. Lipo, "Vector Control and Dynamics of AC Drives", Oxford University Press Inc., Oxford, New York, 1997.

[22] E. Clarke, Circuit Analysis of AC Power Systems, Vol. I- Symmetrical and Related Components, John Wiley and Sons, New York, 1943

[23] M. Ertek, "Speed Estimation Techniques For Sensorless Vector Controlled Induction Motor Drive" M.S Thesis EE Dept. Metu, December 2005

[24] R. H. Park, "Two-reaction theory of synchronous machines – Generalized method of analysis- Part I," AIEE Trans., Vol. 48, July 1929, pp.716-727

[25] N. Mohan, W. Sulkowski, P. Jose and T. Brakken, "Including voltage space vectors PWM in undergraduate courses"

[26] P. Vas, Sensorless Vector and Direct Torque Control, Oxford University Press, New York, 1998.

[27] H. Kubota, K. Matsuse, and T. Nakano, "New adaptive flux observer of induction motor for wide speed range motor drives" in Conf. Rec. IEEE IECON'90 pp. 921-926.

[28] H. Kubota, I. Sato, Y. Tamura, K. Matsuse, H. Ohta and Y. Hori "Regenerating-mode low-speed operation of sensorless induction motor drive with adaptive observer" IEEE Transactions on Industry Applications, vol. 38, no. 4, pp. 1081-1086, July/August 2002.

[29] G. Welch and G. Bishop, "An Introduction to the Kalman Filter", April 5 2004.